University Of Cyprus
Faculty of Pure and Applied Sciences
Department Of Biological Sciences

Laboratory of Developmental Biology and BioImaging Technology
(Assistant Professor, Paris A. Skourides)

MOLECULAR CLONING AND FUNCTIONAL CHARACTERIZATION OF XENOPUS LAEVIS NUCLEOTIDE BINDING PROTEIN 1 (xNUBP1) DURING EARLY EMBRYONIC DEVELOPMENT

Ph.D. THESIS

ANDRIANI IOANNOU

NICOSIA, MAY 2013

Πανεπιστήμιο Κύπρου
Σχολή Εφαρμοσμένων και Θετικών Επιστημών
Τμήμα Βιολογικών Επιστημών

Εργαστήριο Αναπτυξιακής Βιολογίας
και Βιοαπεικόνισης
(Επίκουρος Καθηγητής Πάρης Α. Σκουρίδης)

ΜΟΡΙΑΚΗ ΚΛΩΝΟΠΟΙΗΣΗ ΚΑΙ ΛΕΙΤΟΥΡΓΙΚΟΣ ΧΑΡΑΚΤΗΡΙΣΜΟΣ ΤΗΣ xNUBP1 ΚΑΤΑ ΤΗΝ ΠΡΩΙΜΗ ΕΜΒΡΥΙΚΗ ΑΝΑΠΤΥΞΗ ΤΟΥ *XENOPUS LAEVIS*

ΔΙΔΑΚΤΟΡΙΚΗ ΔΙΑΤΡΙΒΗ

ΑΝΤΡΙΑΝΗ ΙΩΑΝΝΟΥ

ΛΕΥΚΩΣΙΑ, ΜΑΙΟΣ 2013

MEMBERS OF THE EXAMINING COMMITTEE

Dr. Paris Skourides, Assistant Professor, Department of Biological Sciences (Research Advisor), University of Cyprus

Dr. Niovi Santama, Associate Professor, Department of Biological Sciences (Committee president), University of Cyprus

Dr. Chrysoula Pitsouli, Assistant Professor, Department of Biological Sciences, University of Cyprus

Dr. Efthimios Skoulakis, Associate Investigator,Institute of Cellular and Developmental Biology BSRC Alexander Fleming, Greece

Dr. Stavros Malas, Head, Developmental and Functional Genetics Group, Cyprus Institute of Neurology and Genetics

Acknowledgments

Two roads diverged in a wood, and I took the one less travelled by, and that has made all the difference. – Robert Frost

Nothing worth having comes easy! I can honestly say that this definitely holds true for a Ph.D. This dream of mine has been an uphill climb; one in which the finish line always seemed to be out of reach. Yet here I am; at the end of a very long journey, which I could not have completed without the help of many special people.

My first debt of gratitude must go to my advisor, Dr. Paris Skourides, for giving me the opportunity to realize one of the biggest goals of my life. His motivational words and nicknames will never be forgotten.

The best and worst moments of my doctoral journey have been shared with all the members of the lab; past and present. We've all been there for one another and have taught ourselves and each other many things along the way. Without them, it would have just been a lab, and not the second home it became. I thank each and every one of them for all their help and support; they will always share a place in my heart. Thank you Dr. Panayiota Stylianou, Maria Andreou, Ioanna Antoniades, Nicoletta Petridou, Neophytos Christodoulou, Iro Eleftheriou, Dr. Sara Zanardelli, Anna Eleftheriou, Georgia Hatzilambi and Katerina Othonos (mini me). I would also like to thank Dr. Annita Charalambous for all her help and support, all the members of the PG lab, where I spent the first two years of my time at UCY and my friends Pam and Christina for being there for me though the good and the bad times.

My family has been my rock. Without them, the young girl with unattainable goals and the entire world against her would have never reached as far as she did. I would like to thank my parents for all their support, especially my mom, for always being there for me. You are the strongest woman I know, and I appreciate all the sacrifices you have made for me. I owe a huge debt of gratitude to my number one fan and best friend, my sister Cleo. Who always believed in me, stood by me, and pushed me to keep on fighting. I would also like to thank my brother in law Chris. I honestly cannot put into words how thankful I am to both of you for your ceaseless support and guidance throughout every stage of my education. I would also like to thank my two little munchkins Vivi and Paul; whose presence always put a smile on my face.

A good support system is important to surviving and staying sane in graduate school. I would like to emphasize how much I appreciate all of these people for believing in me, even when I didn't.

Thank you!!

Dedication

This thesis is dedicated to my sister Cleo and my brother-in-law Chris. Without you, this would not have been possible.

Abstract

Nucleotide binding protein 1 (Nubp1) is a highly conserved phosphate loop (P-loop) ATPase involved in diverse processes including iron-sulfur protein assembly, centrosome duplication and lung and limb development. Research conducted concerning the function of Nubp1 has focused mainly on its role as a scaffold in the cytosolic iron-sulfur protein assembly process. Previous research has clearly shown that Nubp1 is indispensible for normal cellular function; however, most of the studies conducted have been *in vitro*. In order to answer the important questions of how and why Nubp1 is so important, it is not enough to look *in vitro* at the cellular level; we must examine the role of Nubp1 *in vivo* at the level of the organism.

The general aim of this project was the molecular cloning, expression and functional characterization of *Xenopus laevis* Nubp1. By using *Xenopus laevis*, a model organism which has paved the way for the identification of transcription factors, gene regulatory networks and inter- and intracellular signaling pathways that control early development, we have been able to observe xNubp1 localization live using sophisticated imaging systems, manipulate xNubp1 expression levels by overexpression and loss-of-function experiments, and have slowly begun to piece together the puzzle of the function of Nubp1 *in vivo* during vertebrate development.

We show that xNubp1 is expressed maternally, is associated with actin and microtubule cytoskeletons, displays elevated expression in neural tissues and is essential during several key processes during development. Our data reveal that xNubp1 is required for convergent extension and apical constriction movements during neural tube closure and for Rohon-beard sensory neuron peripheral axon elongation. In addition, xNubp1knockdown leads to aberrant ciliogenesis of the multi-ciliated cells of the epidermis as well as the monociliated cells of the gastrocoel roof plate. Specifically, xNubp1 is required for basal body migration, spacing and docking in multi-ciliated cells and basal body positioning and axoneme elongation in monociliated gastrocoel roof plate cells.

Live imaging of basal body migration and the different pools of actin during the process of ciliated cell intercalation revealed that two independent pools of actin are present from the onset of cell intercalation; an internal network surrounding the basal bodies, anchoring them to

the cell cortex and an apical pool of punctate actin which eventually matures into the characteristic apical actin network.

We show that xNubp1 colocalizes with the apical actin network of multiciliated cells and that problems in basal body transport in xNubp1 morphants are associated with defects of the internal network of actin, while spacing and polarity issues are due to a failure of the apical and sub-apical actin pools to mature into a network. These effects of xNubp1 knockdown on the actin cytoskeleton are independent of RhoA localization and activation, suggesting that xNubp1 may have a direct role in the regulation of the actin cytoskeleton.

Περίληψη

Η Nubp1 (Nucleotide binding protein 1) είναι μια συντηρημένη ATPάση (τύπου P-loop) που συμμετέχει σε διάφορες διαδικασίες όπως το σχηματισμό των πρωτεϊνών σιδήρου-θείου, το διπλασιασμό του κεντροσωματίου και την ανάπτυξη των πνευμόνων και των άκρων. Προηγούμενες μελέτες έχουν δείξει ξεκάθαρα ότι η Nubp1 είναι απαραίτητη για τη φυσιολογική λειτουργία του κυττάρου. Εντούτοις, οι περισσότερες μελέτες έχουν διεξαχθεί *in vitro*. Για την απάντηση σημαντικών ερωτημάτων που αφορούν το πώς και γιατί η Nubp1 είναι τόσο σημαντική, δεν αρκεί η *in vitro* μελέτη σε κυτταρικό επίπεδο αλλά απαιτούνται *in vivo* μελέτες σε επίπεδο οργανισμού.

Ο βασικός στόχος αυτής της μελέτης ήταν η κλωνοποίηση, έκφραση και χαρακτηρισμός της λειτουργίας της Nubp1 στον *Xenopus laevis* (xNubp1). Η χρήση του *Xenopus laevis*, σαν οργανισμό μοντέλο, είναι ιδανική για την ταυτοποίηση μεταγραφικών παραγόντων, δικτύων ρύθμισης της γονιδιακής έκφρασης καθώς και διακυτταρικών και ενδοκυτταρικών σηματοδοτικών μονοπατιών υπεύθυνων για τη την πρώιμη ανάπτυξη. Επομένως, έγινε δυνατή η παρατήρηση του εντοπισμού της xNubp1 σε επίπεδο ζωντανού οργανισμού χρησιμοποιώντας εξελιγμένα συστήματα απεικόνισης και η τροποποίηση των επιπέδων έκφρασης της xNubp1 (με πειράματα κέρδους και απώλειας της λειτουργίας) πετυχαίνοντας τη κατανόηση της λειτουργίας της xNubp1κατά την ανάπτυξη των σπονδυλωτών *in vivo*.

Έχουμε δείξει ότι η xNubp1 εκφράζεται μητρικά, συνδέεται με τους κυτταροσκελετούς ακτίνης και μικροσωληνίσκων, παρουσιάζει αυξημένα επίπεδα έκφρασης σε νευρικούς ιστούς και είναι απαραίτητη σε σημαντικές διεργασίες κατά την εμβρυογένεση. Τα δεδομένα μας προτείνουν ότι η xNubp1 απαιτείται για τις κινήσεις της συγκλίνουσας επέκτασης και της κορυφαίας συστολής οι οποίες επιτελούνται κατά τη διάρκεια του κλεισίματος του νευρικού σωλήνα αλλά και για την επιμήκυνση των περιφερικών αισθητικών νευρώνων Rohon-beard. Επιπρόσθετα, η μείωση των επιπέδων έκφρασης της xNubp1 οδηγεί σε ανωμαλίες κατά τη δημιουργία των βλεφαρίδων στα πολυ-βλεφαριδοφόρα κύτταρα της επιδερμίδας καθώς και στα μονο-βλεφαριδοφόρα κύτταρα της οροφής του γαστρόκοιλου. Συγκεκριμένα, η xNubp1 απαιτείται για τη μετανάστευση, την αγκυροβόληση και τη σωστή τοποθέτηση των βασικών σωματίων στα πολυ-βλεφαριδοφόρα κύτταρα. Επιπλέον, είναι απαραίτητη για τη σωστή τοποθέτηση των βασικών σωματίων και την επιμήκυνση των αξονηματίων στα μονο-βλεφαριδοφόρα κύτταρα της οροφής του γαστρόκοιλου.

Ζωντανή απεικόνιση της μετανάστευσης των βασικών σωματίων και των διαφορετικών πληθυσμών ακτίνης κατά τη διάρκεια της παρεμβολής των βλεφαριδοφόρων κυττάρων, έδειξε ότι δύο ανεξάρτητοι πληθυσμοί ακτίνης υπάρχουν από την έναρξη της παρεμβολής των κυττάρων: ένα εσωτερικό δίκτυο που περιβάλλει τα βασικά σωμάτια και τα αγκυροβολεί στον κυτταρικό φλοιό και ένας ανοργάνωτος πληθυσμός στην κορυφαία επιφάνεια του κυττάρου ο οποίος τελικά ωριμάζει δίνοντας το χαρακτηριστικό κορυφαίο δίκτυο ακτίνης.

Τα αποτελέσματα μας δηλώνουν ότι η xNubp1 συνεντοπίζεται με το κορυφαίο δίκτυο ακτίνης των πολυ-βλεβαριδοφόρων κυττάρων και πώς τα προβλήματα μεταφοράς των βασικών σωματίων που παρουσιάζονται κατά την απώλεια της xNubp1 από τα κύτταρα (morphants) σχετίζονται με ανωμαλίες του εσωτερικού δικτύου ακτίνης. Από την άλλη, προβλήματα στην τοποθέτηση και πολικότητα των βασικών σωματίων οφείλονται στην αποτυχία του κορυφαίου και υπο-κορυφαίου πληθυσμού ακτίνης να ωριμάσουν σε οργανωμένα δίκτυα. Οι επιπτώσεις της μείωσης των επιπέδων της xNubp1 στον κυτταροσκελετό ακτίνης είναι ανεξάρτητες από τον εντοπισμό και την ενεργότητα της RhoA, υποδηλώνοντας ότι η xNubp1 πιθανών να έχει ένα άμεσο ρόλο στη ρύθμιση του κυτταροσκελετού

Table of Contents

I. List of Figures

II. List of Tables

III. List of movies (CD)

- **Movie 1- xNubp1 localizes to the perinuclear space during interphase and mitotic spindle during mitosis**. This video shows the localization of xNubp1-GFP in the XL-177 Xenopus cell line.
- **Movie 2- xNubp1 localizes to the mitotic spindle during mitosis**. This video shows the localization of xNubp1-GFP on the spindle and cleavage membrane during mitosis in the XL-177 Xenopus cell line.
- **Movie 3- *Xenopus* tailbuds are sensitive to light touch.** Video showing stage 31/32 control embryos twitching and swimming away after being lightly poked with a hair knife.
- **Movie 4- xNubp1 morphant embryos do not respond to light touch.** Video showing stage 31xNubp1 morphant embryo injected with 13ng SpMO at the animal hemisphere of each blastomere at the two cell stage. The embryo fails to react after being lightly poked with a hair knife.
- **Movie 5- Fluid flow across *Xenopus* epidermis using QDs.** Video showing the flow of Quantum dots over the epidermis of a stage 31/32 control Xenopus embryo.
- **Movie 6- Decreased fluid flow across xNubp1 morphant *Xenopus* epidermis using QDs.** Video showing the decreased flow of Quantum dot containing media over the epidermis of a stage 31/32 xNubp1 morphant Xenopus embryo.
- **Movie 7- Beating of Cilia on control multi-ciliated epidermal cell.** Cilia on a multi-ciliated epidermal cell of a stage 31 control embryo all beat in a synchronized and polarized whip-like manner.

- **Movie 8- Beating of Cilia on xNubp1 morphant multi-ciliated epidermal cell**. The Synchronized polarized beating of multiciliated epidermal cells is severely affected in xNubp1 morphant stage 31 embryos. The cilia beat in a more rigid manner and are not coordinated.
- **Movie 9- Beating of Cilia on xNubp1 morphant multi-ciliated epidermal cell.** The Synchronized polarized beating of multiciliated epidermal cells is severely affected in xNubp1 morphant stage 31 embryos. The cilia beat in a more rigid manner and some barely beat at all.
- **Movie 10- Actin dynamics on ciliated and non-ciliated apical cell surface.** Time-lapse movie of a ciliated and non-ciliated neighboring cell of a stage 29 embryo expressing mKate-actin. The actin network of the ciliated cell is stable and shows almost no remodeling within the acquisition period. Whereas the apical actin network in the neighboring non-ciliated cell is quite dynamic.
- **Movie 11- Actin dynamics on ciliated and non-ciliated apical cell surface of xNubp1 morphant.** Time-lapse movie of a ciliated and non-ciliated neighboring cell of a stage 29 xNubp1 morphant embryo expressing mKate-actin. The actin network of the ciliated cell is extremely unstable and is completely remodeled within the acquisition period. The apical actin network in the neighboring non-ciliated cell is dynamic and shows no change compared to control non-ciliated cells.

1 Introduction

1.1 Nucleotide Binding Protein 1 (Nubp1)

Nucleotide binding protein 1 (Nubp1) is a phosphate loop (P-loop) ATPase which is highly conserved from yeast to humans, thus indicating an important role for this protein *in vivo*. P-loop NTPases make up one of the largest protein families. They are found in all three kingdoms of life and comprise 10 to 18% of all gene products (1). P-loop protein subgroups perform an array of functions, examples of which include; translation, signal transduction, protein transport and localization, chromosome partitioning and cell division, metal ion insertion and membrane transport (1, 2). These NTPases are characterized by an N-terminal Walker A motif and a distal Walker B motif (3). The Walker A motif consists of a hydrophobic β-strand followed by a glycine-rich region with the following consensus sequence; GxxxxGK[ST], and then an α–helical region. This flexible loop interacts with the phosphate moiety of the NTP substrate (1, 2). The walker B motif contains a conserved residue (aspartate or glutamate) that binds a Mg^{2+} ion which is an important cofactor for catalysis of the phosphate moiety.

Sequence analysis has revealed structural homology between Nubp1 and a family of bacterial ATPases involved in the cell division process and chromosome partitioning (4-6), thus raising the possibility that Nubp1 may be involved in cell division. In addition, a recent study has implicated murine Nubp1 in the cell division process (7). Nubp1 shares extensive sequence similarity to the prokaryotic MinD ATPase. MinD is a member of a group of bacterial proteins (NifH-ArsA-ParA-MinD subgroup) containing a "deviant" Walker A-motif (contain 2 lysine residues instead of one (G<u>K</u>GGVG<u>K</u>ST), which are involved in a diverse range of functions including transport, nitrogen fixation, DNA segregation and spatial regulation of cell division (8, 9). MinD and ParA members have also been characterized as bacterial cytoskeletal proteins (10, 11). Proteins of the MinD subgroup are involved in placement of the bacterial division sites, whereas proteins of the ParA subgroup are involved primarily in DNA partitioning (11). In prokaryotes, in addition to being important for the proper placement of the cell division machinery, MinD proteins also interestingly show motor protein-like behavior (12). Min proteins organize in membrane associated coils and undergo a rapid pole-to-pole oscillation

movement *in vivo* (7, 9, 11). ParA proteins work together with the DNA-binding proteins ParB and the cis-acting DNA sequence ParS to segregate bacterial chromosome and plasmids (10). A recent study by Ptacin et.al using the bacterium *Caulobacter crescentus* demonstrated that these bacteria (and others) segregate their chromosome using a partitioning (Par) apparatus that has surprising similarities to eukaryotic spindles. ATP bound ParA can oscillate between poles and forms narrow linear structures along the long axis of the cell *in vivo* and as a result of ParB stimulated depolymerization of these structures, moves the centromeres to opposite poles (13).

Another member of the ParA subfamily are the bacterial ApbC/Mrp proteins. These prokaryotic proteins have the highest homology with Nubp1 (roughly 30-40% identity with Nubp1 eukaryotic orthologs) (4). These proteins, in addition to archaeal ApbC proteins, have been shown to be involved in iron-sulfur cluster metabolism, specifically acting as iron-sulfur cluster carrier proteins (14, 15).

Nubp1 proteins are evolutionary well conserved among eukaryotes (Table 1 & Figure1) and are ubiquitously expressed throughout embryogenesis and in many adult organs (6). Mouse, human, *Xenopus*, and *Zebrafish* Nubp1 share a sequence identity ranging from 77-90%. Northern blot analysis of murine Nubp1 showed additional transcripts, suggesting that alternatively spliced forms of the protein may exist (6), however, this observation has not been studied further. Nubp1 and the Yeast (*S.cereviciae*) homolog, Nucleotide binding protein of 35kDa (Nbp35), have been shown to localize within the nucleus (4, 16) and the cytoplasm (2, 4, 17, 18). Nbp35 has roughly a 51-57% sequence identity with Nubp1 of the above mentioned species.

The *in vivo* role of the Nubp1 homolog in yeast (Nbp35) has been analyzed using gene disruption methods, and Nbp35 was shown to be essential for cell viability (4). In addition, site directed mutagenesis experiments have shown that the conserved P-loop ATPase motif and the conserved N-terminal cysteine cluster ($C\text{-}X_{13}\text{-}C\text{-}X_{2}\text{-}C\text{-}X_{5}\text{-}C$) are both required for Nbp35 function (4).

SeqA	Name	Length	SeqB	Name	Length	Score
1	XL-N1a	315	2	XTN1	320	94.0
1	XL-N1a	315	3	HumN1	320	81.0
1	XL-N1a	315	4	mouse-N1	320	80.0
1	XL-N1a	315	5	zebfish-N1	321	82.0
1	XL-N1a	315	6	Yeast-N1	328	55.0
1	XL-N1a	315	7	drosophila-N1	311	53.0
1	XL-N1a	315	8	XL-N1b	315	96.0
2	XTN1	320	3	HumN1	320	78.0
2	XTN1	320	4	mouse-N1	320	77.0
2	XTN1	320	5	zebfish-N1	321	81.0
2	XTN1	320	6	Yeast-N1	328	55.0
2	XTN1	320	7	drosophila-N1	311	53.0
2	XTN1	320	8	XL-N1b	315	94.0
3	HumN1	320	4	mouse-N1	320	89.0
3	HumN1	320	5	zebfish-N1	321	74.0
3	HumN1	320	6	Yeast-N1	328	51.0
3	HumN1	320	7	drosophila-N1	311	53.0
3	HumN1	320	8	XL-N1b	315	80.0
4	mouse-N1	320	5	zebfish-N1	321	75.0
4	mouse-N1	320	6	Yeast-N1	328	53.0
4	mouse-N1	320	7	drosophila-N1	311	53.0
4	mouse-N1	320	8	XL-N1b	315	79.0
5	zebfish-N1	321	6	Yeast-N1	328	57.0
5	zebfish-N1	321	7	drosophila-N1	311	55.0
5	zebfish-N1	321	8	XL-N1b	315	82.0
6	Yeast-N1	328	7	drosophila-N1	311	47.0
6	Yeast-N1	328	8	XL-N1b	315	55.0
7	drosophila-N1	311	8	XL-N1b	315	54.0

Table 1. Alignment of the Nubp1(N1) orthologs.

ClustalW (19) alignment of the various Nubp1(N1) orthologs. XT and XL stand for *Xenopus tropicalis* and *Xenopus laevis* respectively. The length column depicts the number of amino acids making up the protein and the score column shows the percent identity between the two sequences.

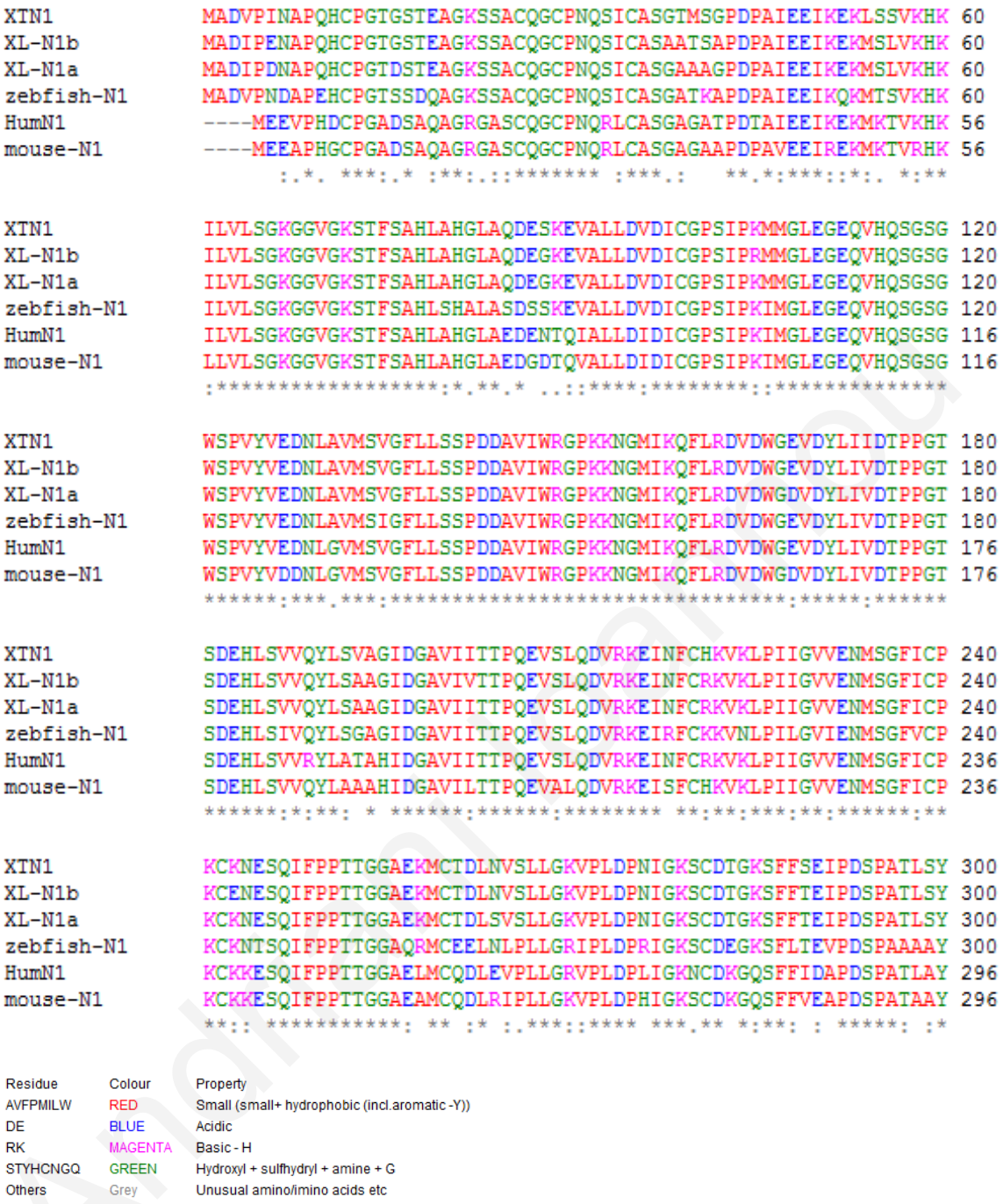

Figure 1. Amino acid sequence alignment of Nubp1 orthologs.

ClustalW (19) alignment of several Nubp1 orthologs. Xenopus tropicalis Nubp1(XTN1), Xenopus laevis Nubp1a and b (XL-N1a, XL-N1b respectively), Zebrafish Nubp1 (zebrafish-N1), Human Nubp1 (HumN1) and mouse Nubp1 (mouse-N1). Amino acids are color coded according to their physicochemical properties. Asterisks represent conserved amino acids.

Research conducted concerning the function of Nubp1/Nbp35 and the closely related Nubp2 (termed Cfd1in yeast) has focused mainly on their role as scaffolds in the cytosolic iron-sulfur protein assembly process (2, 17, 18), where they are involved in the transfer of iron-sulfur clusters (cofactors) to many proteins involved in electron transfer, enzymatic catalysis and regulation of gene expression (17, 20). Depletion of human Nubp1 in HeLa cells by RNA interference (RNAi) suggest an essential role for Nubp1, in complex with human Nubp2, for cell growth, the maturation of cytosolic iron-sulfur proteins and for cellular iron regulation (18).

Nubp2 is another nucleotide-binding protein which is related to the Mrp/MinD proteins of prokaryotes. Nubp1 and 2 proteins share roughly 50% identity at the amino acid level. Nubp2 lacks the cysteine rich N-terminal region present in Nubp1(Figure 2), however, it contains the other conserved regions found in nucleotide binding proteins, including the walker A (P-loop) and B motifs (6) and the Cysteine rich region in the C-terminal domain (17). In yeast, mouse and humans, Nubp2 has been shown to interact with Nubp1 (2, 7, 17, 18) and in yeast, both were shown to be necessary for survival. However, even though they share high sequence similarity they cannot functionally replace each other (2). In mammalian cell lines, Nubp2 knockdown by RNAi failed to produce a spindle assembly phenotype, whereas Nubp1 knockdown led to supernumerary centrosomes at interphase and mitosis, leading to multipolar spindles and tri-nucleated cells (7). In the study by Christodoulou et. al, murine Nubp1 and Nubp2 were found to interact with Kinesin 5A (KIFC5A), a minus-end directed kinesin-like protein of the kinesin-14 family, which localize to the centrosomes at spindle poles and has the ability to bundle microtubules. The findings from this paper suggest that Nubp1 and KIFC5A are involved in a common pathway controlling centrosomes duplication in mammalian cells.

A very recent study has shown that murine Nubp1 is essential for normal embryonic development (21). Schnatwinkel and Niswander (2012) show that transgenic mice expressing a mutated form of Nubp1, which differs only in two highly conserved amino acids at its C-terminus, develop lung hypoplasia leading to death shortly after birth, (21). The transgenic mice also presented syndactyly and eye cataracts. Therefore, since studies have shown that Nubp1 has several different, but essential roles during development, it is important to further

examine the role of this protein in higher eukaryotes. The African clawed frog *Xenopus laevis* is an ideal organism for this type of study.

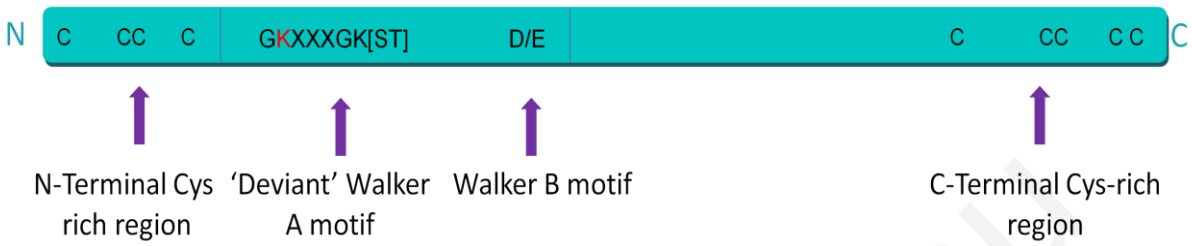

Figure 2. Schematic of Nubp1 domains

1.2 Xenopus laevis as a model organism

The African clawed frog *Xenopus laevis*, like other amphibians are tetrapods, so they have all of the fundamental features of land-dwelling vertebrates. Their embryos are large (1 to 1.4 mm in diameter), robust, develop rapidly (Figure 3) externally in a simple salt solution (22) and therefore can be observed and manipulated relatively easily. *Xenopus laevis* females can lay large numbers of eggs repeatedly by means of a simple hormone injection (22, 23) and can be fertilized *in vitro* by adding *Xenopus laevis* sperm to the oocytes (23). *Xenopus* embryos have the ability to heal well after surgery, making grafting and tissue explants experiments possible. Another very important advantage of using *Xenopus* embryos as a model, is that gain-of-function experiments can be carried out by overexpression of injected mRNA encoding a protein of interest. In addition, loss of function experiments using dominant negative forms of a protein, antisense RNA (24), oligonucleotides (25), and morpholino oligos (MO's) (26-29), which have become one of the most widely used methods for gene knock-down in *Xenopus* and other model systems, are well established and standard practice in *Xenopus*. All these features allow for micromanipulation, microinjection, microdissection and labeling of the *Xenopus* embryo and thus make *Xenopus laevis* an excellent organism for the functional characterization of genes and proteins and for Molecular and Developmental biology research in general.

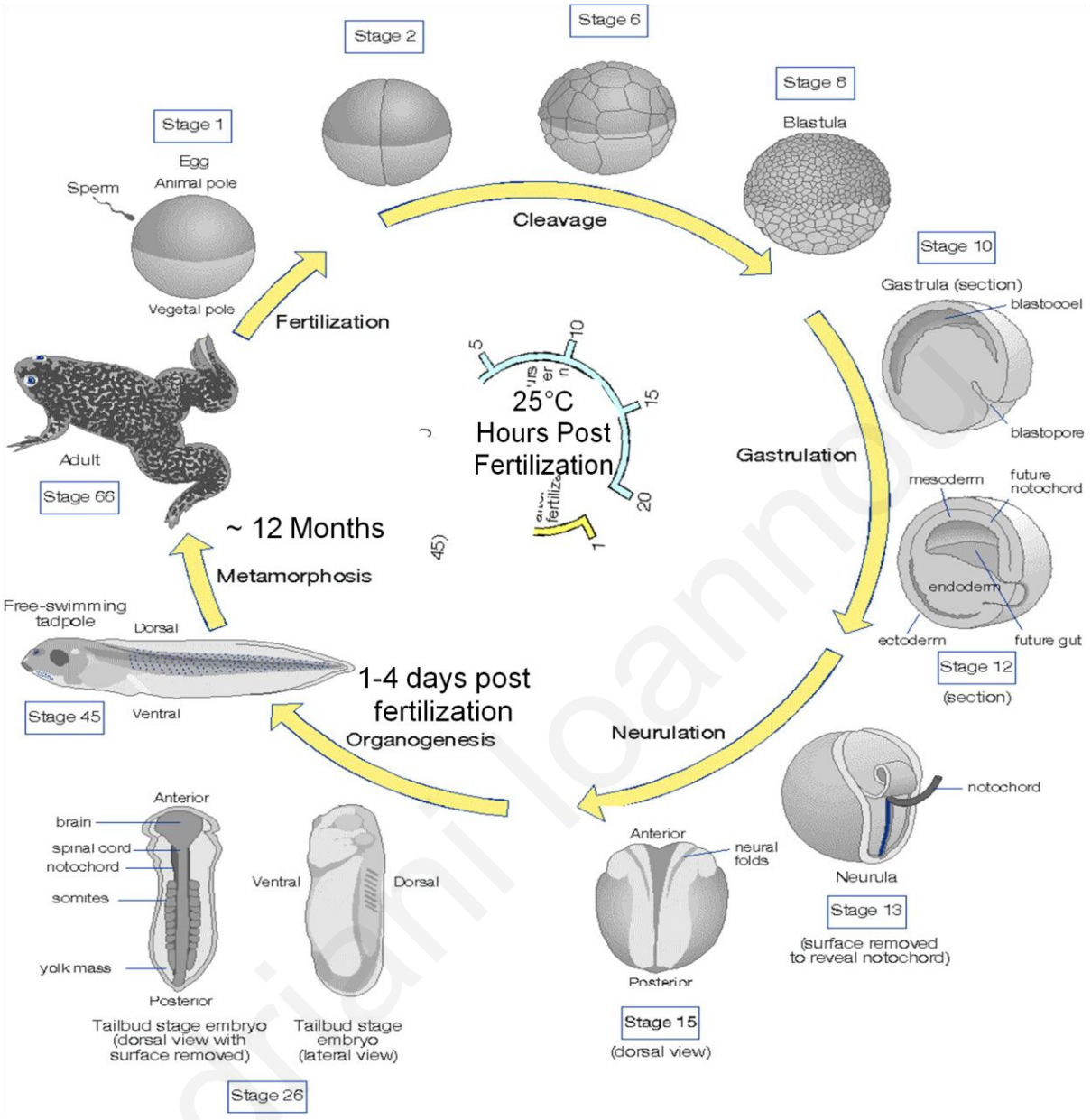

Figure 3. Xenopus laevis developmental stages adapted from (30).

1.3 Normal development of *Xenopus laevis*

1.3.1 Fertilization, cleavage and blastula stages

During oogenesis, the animal – vegetal (A-V) axis of the embryo is established by the restriction of RNAs to either the animal (darker top half) or the vegetal (lighter bottom half) pole. This creates a radially-symmetrical egg (31). The second axis to form is the dorsal-ventral axis, which is determined by the site of sperm entry. The entry point marks the future ventral side of the embryo and this axis determination occurs via a process known as cortical rotation, in which the cortical cytoplasm rotates 30° leading to the translocation of material previously located in the vegetal pole, to the prospective dorsal side of the embryo. This movement requires the assembly of a parallel array of microtubules which nucleate from the sperm centrosome (31-33) (Figure 4).

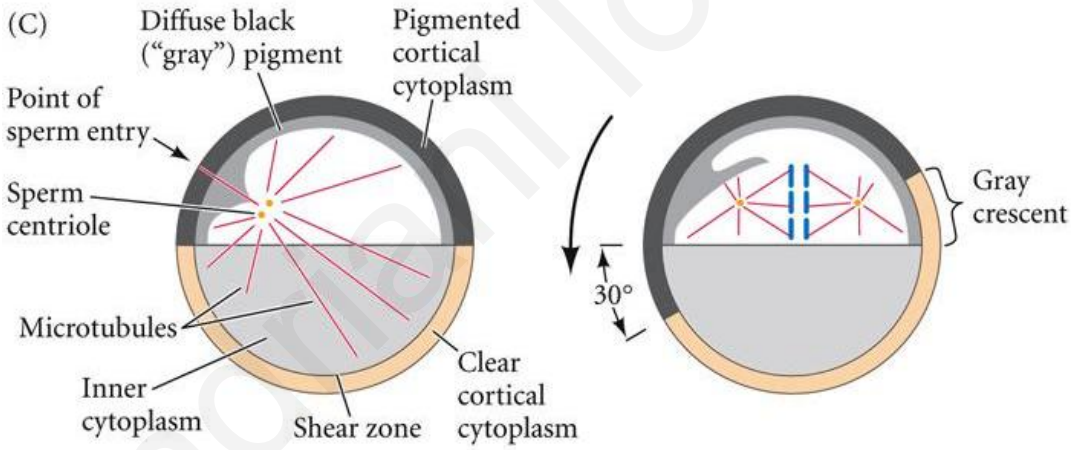

Figure 4. Reorganization of the Xenopus egg cytoplasm by cortical rotation.

On the left is a schematic cross section of an egg midway through the first cleavage cycle, before cortical rotation has occurred. On the right, is a schematic showing an egg about 80% of the way into the first cleavage. The cortical cytoplasm rotates 30 degrees relative to the internal cytoplasm. Gastrulation will begin in the gray crescent, the region opposite the point of sperm entry. Adopted from reference (32).

Within approximately 90 minutes of fertilization, the first cleavage is observed along the A-V axis (Figure 5A). This divides the embryo into equal halves. The next 11 cleavages occur at intervals of about 20 minutes with no G- phases. Therefore, the size of the cells (termed blastomeres) decreases and only the blastomere number increases (Figure 5B-H) (32, 34). At the 128-cell stage, a fluid-filled cavity, the blastocoel, develops at the animal hemisphere, and the embryo is then referred to as a blastula (32) (Figure 5H). After the twelfth cell cycle, zygotic transcription is activated. This is termed the mid-blastula transition (MBT) and prepares the embryo for gastrulation (32, 35).

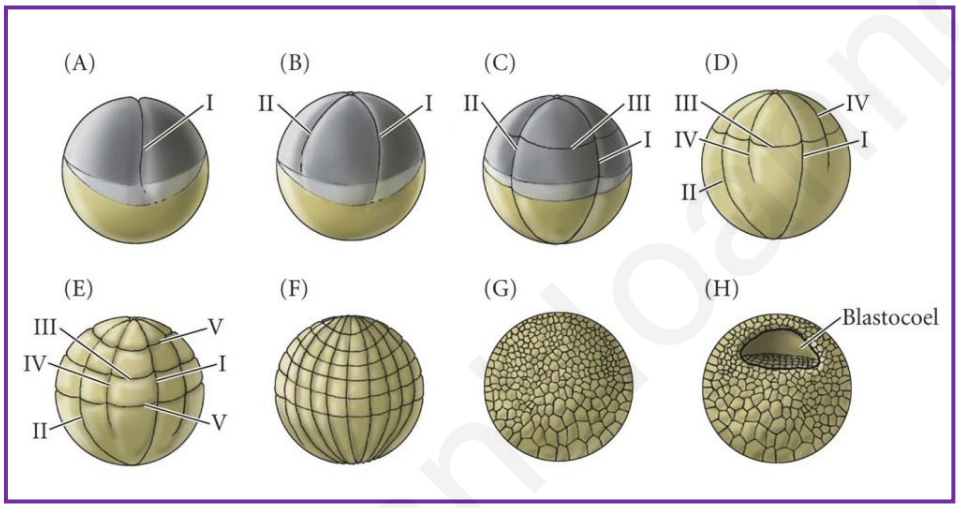

Figure 5. Cleavages of a frog egg.

(A,B) Due to impediment from the vegetal yolk, the second cleavage occurs in the animal hemisphere before the first cleavage is completed. (C) The third cleavage is equatorial towards the animal pole. (D-H) The vegetal hemisphere ultimately contains fewer and larger blastomeres than the animal pole. H depicts a cross-section through a mid-blastula stage embryo. Adopted from reference (32).

1.3.2 Gastrulation

Gastrulation is the morphogenetic process which transforms a group of cells which make up the animal at the blastula stage of development into the three-layered gastrula (36). The three germ layers; the endoderm, mesoderm and ectoderm are shaped into a characteristic body plan and the definitive anteroposterior (AP) and dorsoventral (DV) axes are established (34) during

gastrulation. The process of gastrulation involves highly integrated and regulated cell movements such as epiboly, mesoderm migration, convergent extension, and signaling events, which together result in the correct placement of tissues and the formation of the basic body plan of the embryo (Figure 6). As a result of the movements of gastrulation, cells are brought into new positions, allowing them to interact with cells that were initially not near them. This paves the way for inductive interactions, which are the hallmark of neurulation and organogenesis. The ectoderm, the most exterior germ layer, forms the skin, the nervous system, and other external tissues. Mesoderm, the middle germ layer, forms muscle, the skeletal system, and the circulatory system and the most internal germ layer, the endoderm, forms the lining of the gut and other internal organs (32).

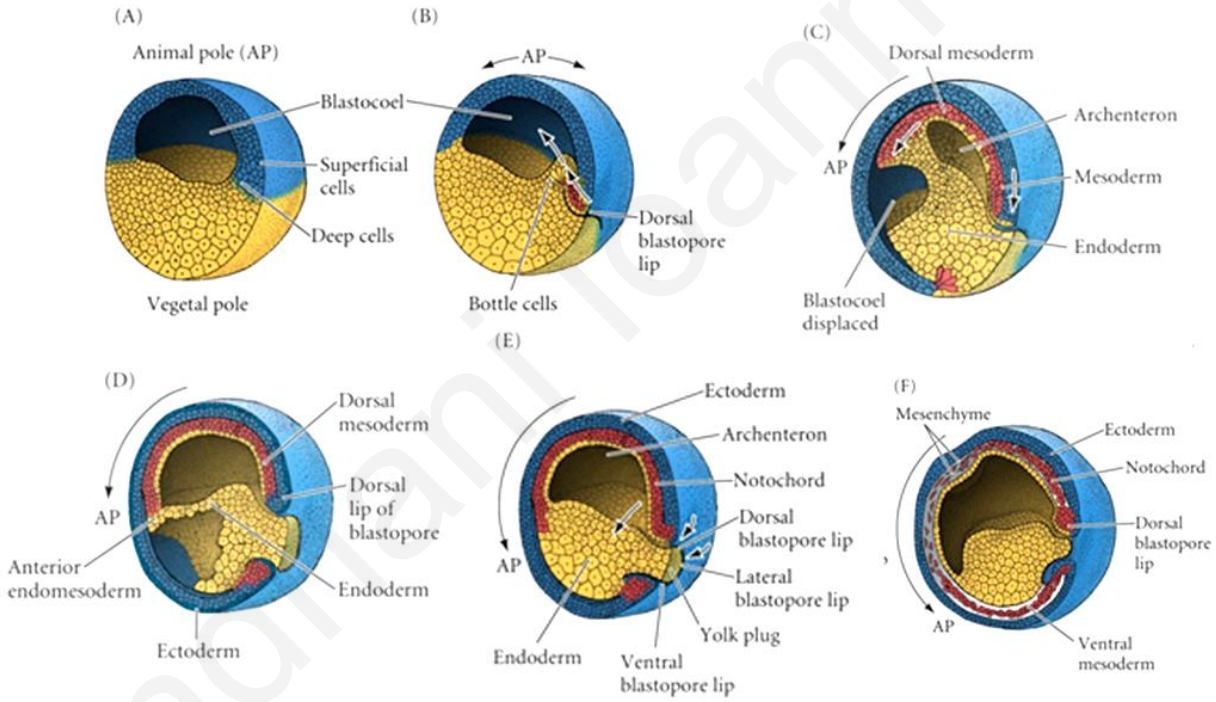

Figure 6. Cell movements during *Xenopus* gastrulation.

(A, B) Early gastrulation. The bottle cells of the margin move inward to form the dorsal lip of the blastopore, and the mesodermal precursors involutes under the roof of the blastocoels. AP marks the position of the animal pole, which will change as gastrulation continues. (C, D) Mid-gastrulation. The archenteron forms and displaces the blastocoel and the cells migrate down toward the vegetal region. (E, F) Toward the end of gastrulation, the embryo becomes surrounded by ectoderm, the endoderm has been internalized and the mesodermal cells have been positioned between the ectoderm and the endoderm. Adopted from (32).

1.3.3 Spemann's Organizer and neural induction

In 1924, Hans Spemann and Hilde Mangold showed that at the dorsal lip of the blastopore, where gastrulation begins in amphibians, a group of cells known as the Spemann organizer, regulates the formation of all embryonic axes (37, 38). The cells which make up the organizer migrate into the embryo during gastrulation and go on to form the notochord (32) The morphogenetic and inductive properties of the Spemann organizer are essential for the establishment of the early vertebrate body plan (38). The organizer secretes a variety of zygotic proteins that act as antagonists to various members of the BMP and Wnt families of ligands, which are secreted by ectodermal cells (37). BMP4 for example, is a powerful ventralizing factor. However, the organizer secretes proteins such as Chordin, Noggin and Follistatin, which block the action of BMP4 leading to the induction of the neural character. This process is called neural induction (32, 39). Thus, ectodermal cells on the dorsal side of the embryo cannot bind BMP4 and thus are induced to form neural tissues instead of epidermis (39) (Figure 7).

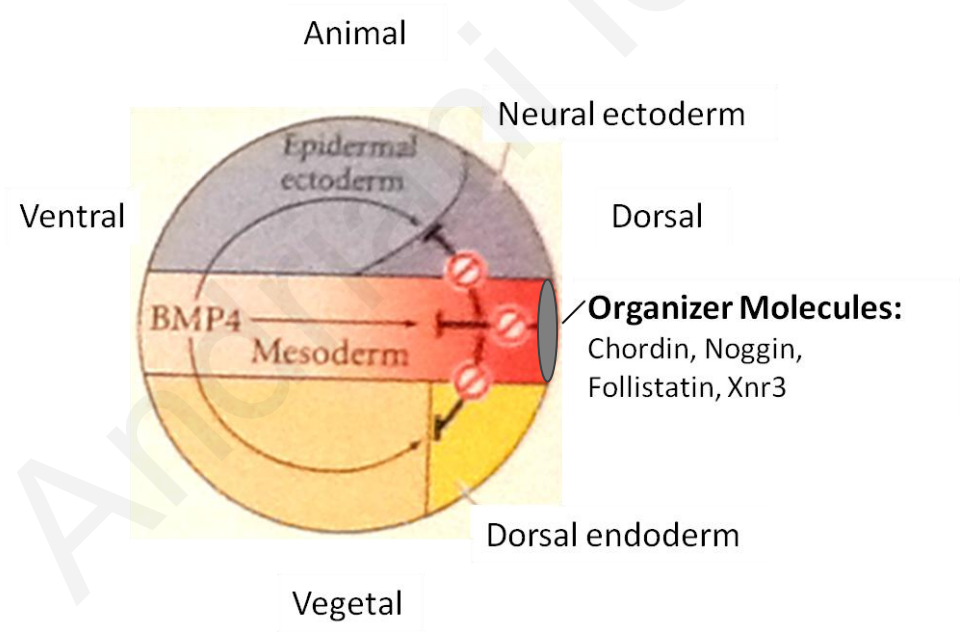

Figure 7. Model for the action of the Spemann organizer

Schematic showing the three prospective germ layers of the *Xenopus* embryo. Factors secreted from the Spemann organizer on the dorsal side of the embryo inhibit ventralizing signals such ad BMP4 which are secreted from the ventral side of the embryo. This inhibition of BMP4 in the ectoderm leads to neural induction in the dorsal ectoderm.

1.3.4 Neurulation and organogenesis

Like gastrulation, neurulation is comprised of an orchestrated combination of signaling events, cell shape changes and cell movements which make possible the emergence of patterns and distinct embryonic structures. Neurulation is a process which results in the formation of the neural tube, which ultimately gives rise to the brain and spinal cord (Figure 8). Neural crest cells, which migrate away from the neural tube and give rise to a large array of cell types such as melanocytes, cartilage and peripheral neurons, are also created during neurulation (32). Neurulation is initiated when the underlying dorsal mesoderm signals to the overlying ectoderm to elongate into columnar neural plate cells. The neural plate lengthens and narrows along the AP axis by convergent extension movements and bending of the neural plate form the neural groove which then closes to form the neural tube (32).

During the tailbud and tadpole stages, we begin to recognize the main vertebrate features. During organogenesis, groups of cells splits into several independent populations, which migrate to different locations and are therefore exposed to different combinations of signaling molecules, which allow the cells to acquire different fates. After organogenesis is completed, the mature tadpole begins to swim and feed. Later, the tadpole larva will undergo metamorphosis to give rise to the adult frog (Figure 3) (32).

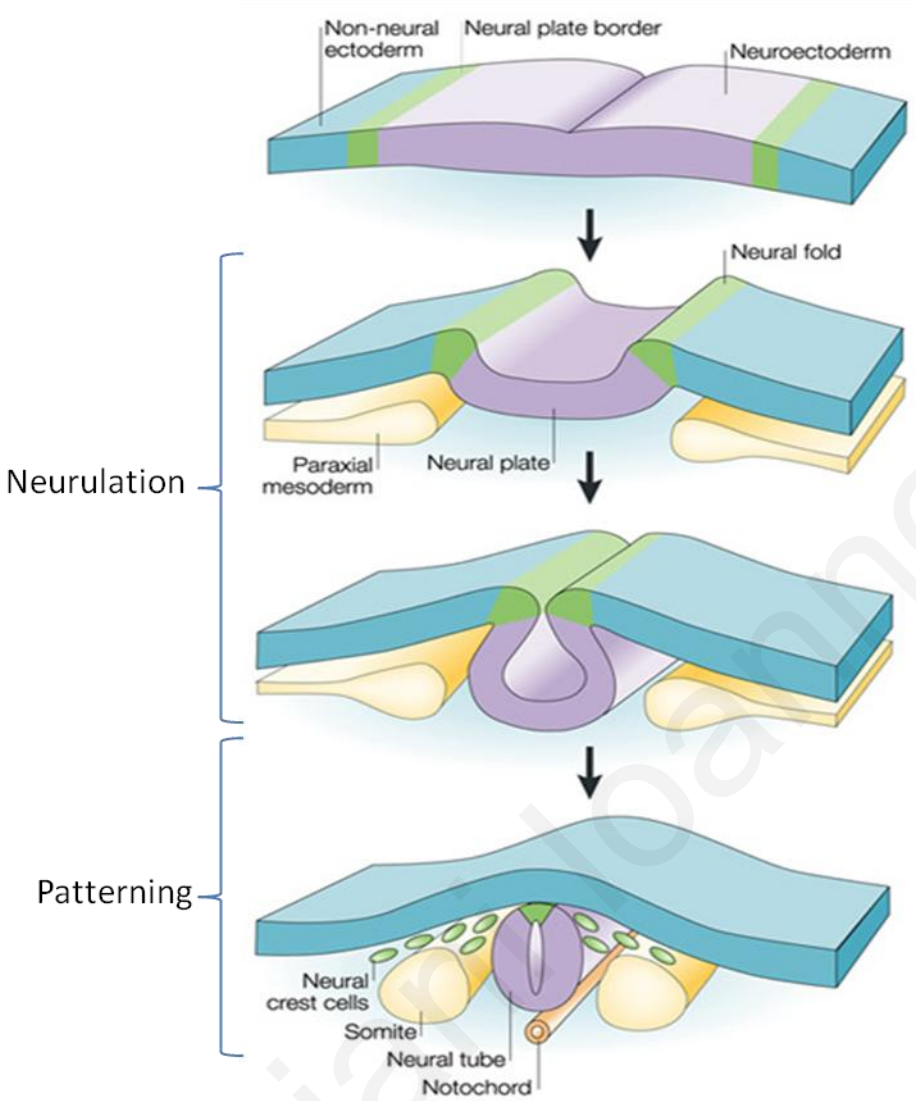

Figure 8. Schematic representation of neural tube closure.

The sides of the neural plate (purple) buckles, rolls up and fuses to form the neural tube. Neural plate border (green) is induced by signals from the neurectoderm (purple) and non-neural ectoderm (blue). Adopted from (40).

1.4 Neural tube closure

In birds, mammals and amphibians, the formation of the neural tube, the brain and all but the most caudal region of the spinal cord occurs through primary neurulation (41-43). During normal vertebrate development, the flat precursor to the central nervous system (CNS), the neural plate, elevates, rolls up towards the dorsal midline and then fuses to form a hollow tube which will eventually become the brain and spinal cord. For neural tube closure (NTC) to occur properly, several autonomous and region-specific morphogenetic events, including neural fold elevation, neural plate bending and convergent extension (CE), which require cell shape changes and polarized cell migration, must be coordinated (44, 45). Defects in NTC are the second most common birth defect in humans (46, 47). Experimentation using animal models has revealed that failure of neural tube closure is due to either defects in cell fate or in cell movement (47).

1.4.1 Convergent extension

The morphogenetic process of convergent extension (CE) during NTC specifically acts in the hindbrain and spinal cord (47). Cells undergoing CE movements narrow along one axis and elongate along a perpendicular axis (Figure 9). During early embryogenesis, CE movements occur during gastrulation and neurulation, axis elongation and organogenesis (48). During gastrulation, mesodermal cells located in the dorsal region of the equatorial region converge and extend toward the dorsal midline (49). This process is driven by mediolaterally oriented, bipolar protrusions which exert traction on neighboring cells, resulting in mediolateral intercalation (50-52) (Figure 10A). During neurulation, presumptive hindbrain and spinal cord undergo CE movements in parallel to similar events occurring in the underlying mesoderm. CE movements in the posterior neural plate involve different behaviours than those in mesodermal cells. Intercalation of more lateral cells in the posterior neural plate involves medially oriented, monopolar protrusions and more medial cells of the notoplate display randomly oriented motility (51) (Figure 10B). Disruption of CE during NTC can lead to the neural tube defects such as; Spina bifida (opening of the caudal region of the neural tube) and craniorachischisis (opening along the entire length of the neural tube) (45, 47). At the

molecular level, experiments performed in *Xenopus* and *Zebrafish* have demonstrated that the non-canonical Wnt pathway or planar cell polarity (PCP) pathway, mediated by Dishevelled, plays a crucial role in the establishment of cell polarity (53-55) and convergent extension.

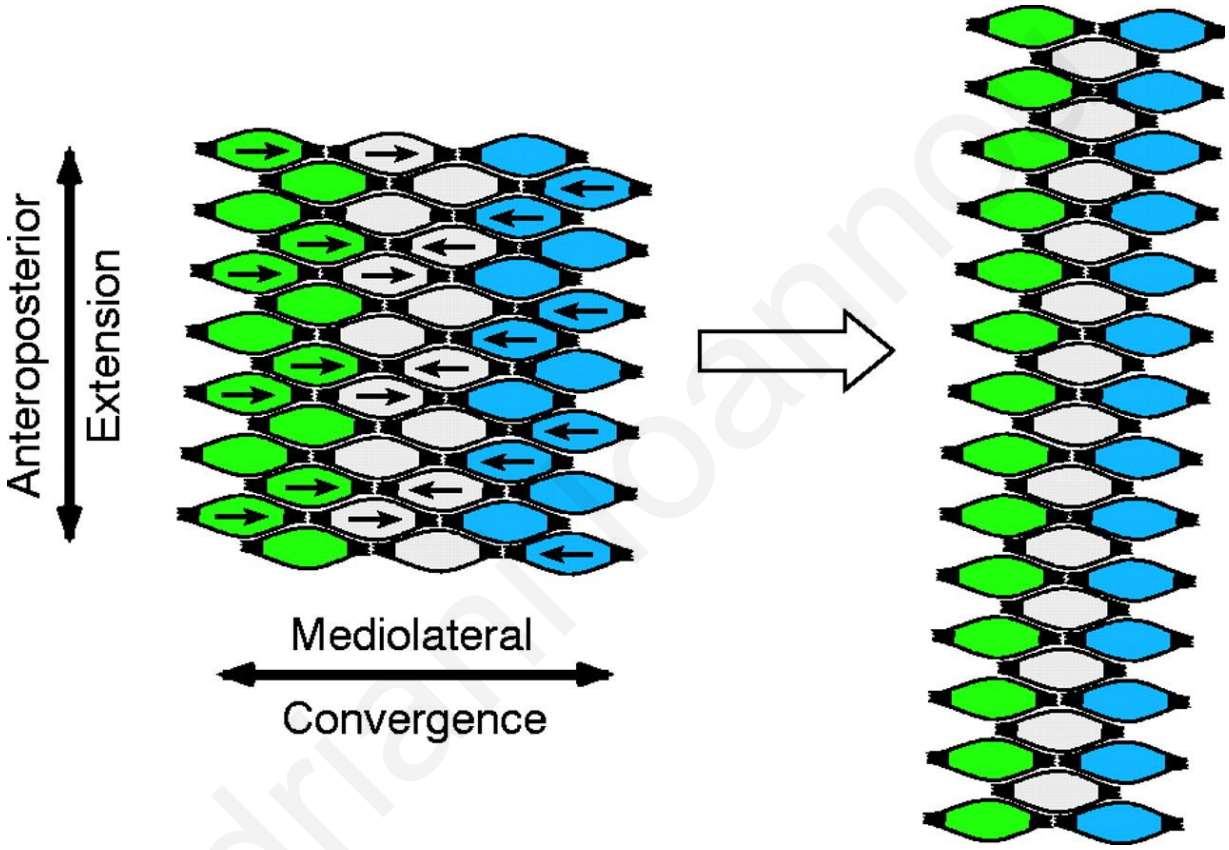

Figure 9. Mediolateral intercalation during convergent extension.

Simplified scheme of convergent extension in the mesoderm of *Xenopus* during gastrulation. Cells converge together on the mediolateral axis and the tissue extends on the anteroposterior axis. Adopted from (56).

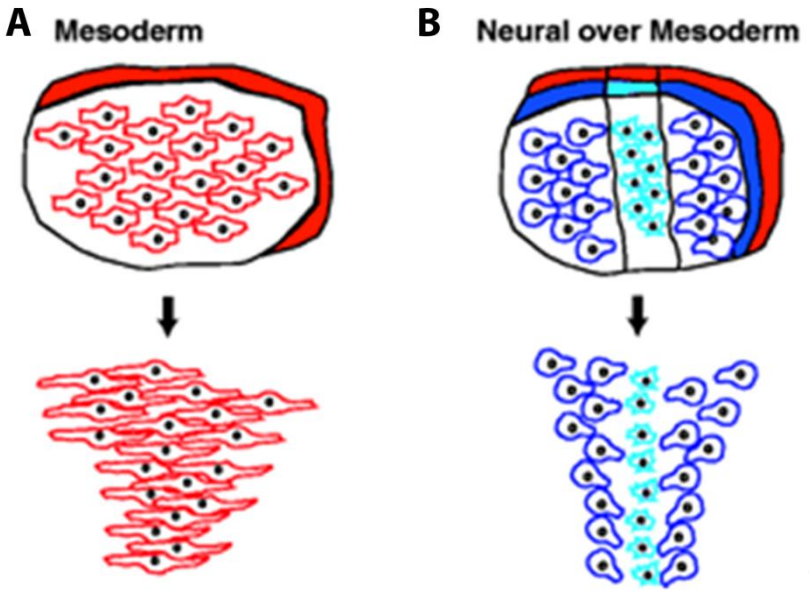

Figure 10. Convergent extension.

(A) Mesodermal cells undergoing CE form bipolar protrusions. (B) Cells in the neural plate undergoing CE, form monopolar protrusions oriented toward the midline. Adopted from (51).

1.4.2 Apical constriction

During apical constriction, the apical meshwork of filamentous actin (F-actin) in certain cells, driven by the molecular motor myosin, contracts, causing the cells to adopt a wedged shape (Figure 11). Apical constriction is most important in the anterior neural tube (future brain) and in the caudal-most region of the spinal cord (43, 47). Disruption of genes controlling apical constriction are associated with anencephaly (open anterior neural tube) and caudally restricted spina bifida (45). During anterior NTC, neuroepithelial cells also undergo apicobasal elongation and apical constriction in order to promote neural plate bending (42, 43, 57). Apical constriction in medial and dorsolateral cells of the neural plate creates hinge points (Figure12). The medial hinge point forms the neural groove and the more lateral neural plate on each side elevates around it forming the neural folds (43, 58). In the region of the future brain, a pair of dorsolateral hinge points form, and lead to further bending of the neural folds.

The medial hinge points and dorsolateral hinge points always form a region where the neural plate is anchored to adjacent tissue (43).

Studies have shown that the actin and microtubule cytoskeleton play important roles in neural tube closure. Pharmacological disruption of either actin or microtubules disrupts neural tube closure (59-61). Actin binding proteins and their regulators, including Shroom3, RhoA, ROCKs, Rap1, Xena and MIM and cell adhesion molecules such as N-cadherin and Nectin contribute to apical constriction by regulating myosin activity or regulating actin assembly (44, 62-67). Microtubules have also been shown to be important for cellular morphogenesis required for neural tube closure (59). Shroom3 regulates the re-distribution of γ-tubulin and in turn the assembly of apically localized parallel microtubule arrays required to drive apicobasal elongation of neural tube cells (68). In addition, Mid1 and Mid2 are essential for neural tube closure through their stabilization of microtubules, which is required for cell elongation and apical constriction (69).

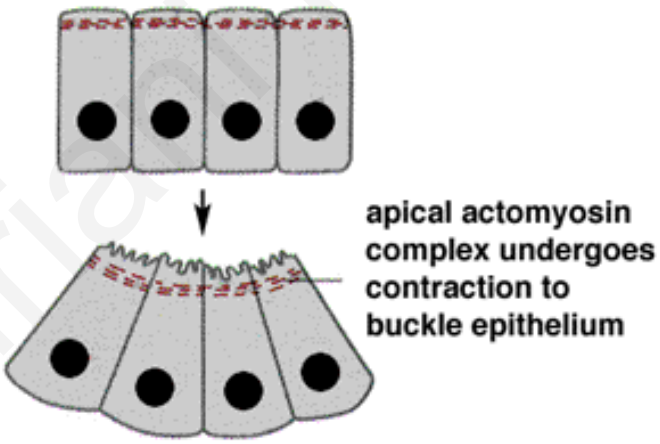

Figure 11. Apical constriction.

Schematic of apical constriction caused by acto-myosin contraction. Adopted from (70).

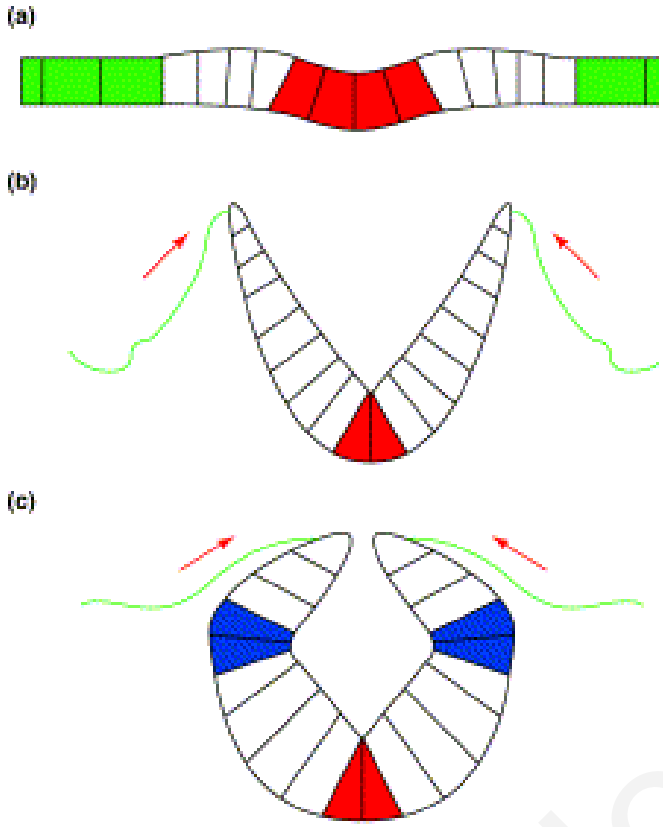

Figure 12. Morphogenic events during neural tube closure.

(a) Cells in the medial region of the neural plate undergo an apical constriction that results in formation of the medial hinge point (red). (b) Folding of the neural plate around the medial hinge point occurs as the neural folds form at the edges of the neural plate and elevate. Epidermal cells rearrange to force the neural folds to converge in the dorsal midline (red arrows). (c) Dorsal–lateral hinge points (blue) form as neural folds come in contact with the epidermis, which continues to drive convergence of the neural folds towards the dorsal midline. Adopted from reference (41)

1.5 Patterning of the neural tube

The vertebrate CNS is patterned along it antero-posterior (AP), dorsal-ventral (DV) and left-right axes (LR) (71). Signals along the AP axis divide the neural tube into four main regions: forebrain, midbrain, hindbrain and spinal cord (71). During and after neural tube closure two opposing signalling pathways lead to cell fate determination along the DV axis. Experiments in the chick and subsequently in amphibians has shown that the notochord, which acts as an organizing center for the overlying neural tissues, is the source of the signal (Sonic Hedgehog (Shh)), which is involved in the specification of the floor plate (71, 72). BMP signalling dorsally from the boundary of the neural and non-neural ectoderm form the roof plate (71). The secreted factor Shh act as a long-range morphogen which acts by regulating the expression of transcription factors and directs the pattern of neurogenesis by conferring positional information to ventral neural progenitors (72) (Figure 13). Patterning of the LR axis occurs concomitantly with AP and DV patterning during gastrulation and is initiated by activin which is regulated by Nodal and Lefty (71).

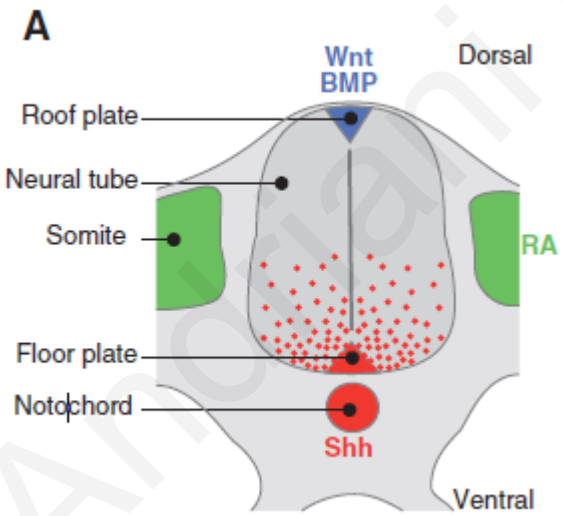

Figure 13. Neural tube patterning.

Schematic of a transverse section of an amniote embryo. The key signals include Shh (red), secreted by the notochord and floor plate; retinoic acid (RA, green), produced by the somites that flank the neural tube; and BMP and Wnt family members (blue), which are produced dorsally. The spread of Shh from ventral to dorsal establishes a gradient of activity within the ventral neural tube (red dots). Adopted from (72)

1.6 Neurogenesis

The secreted signals, such as Shh, establish the DV pattern of progenitor domains in the neural tube by spatial regulation of the expression of transcription factors (72) (Figure 14). The differential expression of genes in the different domains of the neural tube along the DV axis determines the neural subtype progeny. BMP signalling dorsally combined with Shh signalling ventrally, results in the differential expression of genes such as Pax7, Pax3, Msx1 and Msx2 in the dorsal spinal cord and leads to the differentiation of a different set of neurons to those found in the ventral neural tube (71) (Figure 15). A specific subset of neurons formed in the dorsal neural tube, are the Rohon-Beard (RB) sensory neurons.

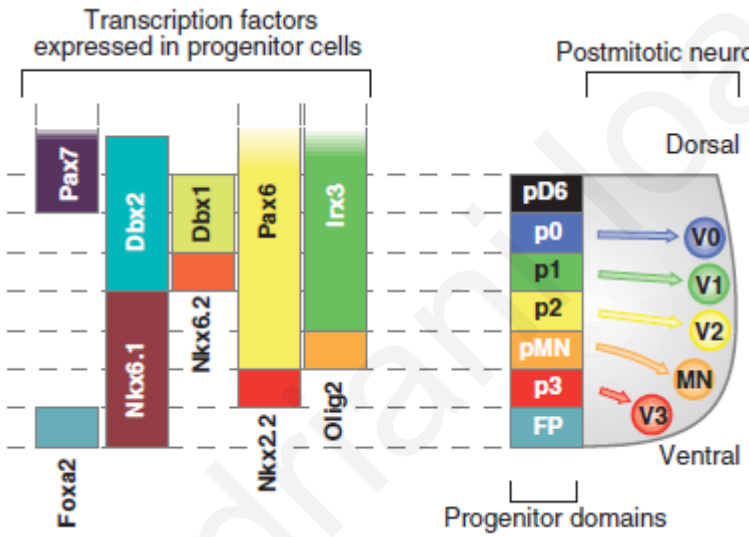

Figure 14. dorsal-ventral pattern of progenitor domains in the ventral neural tube.

Schematic of the ventral half of the neural tube, where the ventral gradient of Shh activity controls position identity by regulating the expression, in neural progenitors, of a set of transcription factors which require Shh signaling for their expression. The differential response of these genes to graded Shh signaling establishes distinct dorsal and ventral boundaries of expression for each factor and defines domains of progenitors (p). Each progenitor domain generates different ventral (V) interneuron subtypes (V0-V3) or motor neurons (MN). Consequently, the spatially segregated production of distinct neuronal subtypes is determined by the DV pattern of transcription factor expression in progenitors. The ventral boundary of the progenitor domain for dorsal interneurons dI6 (pD6) illustrates the range of Shh signaling in the ventral neural tube. Adopted from (72).

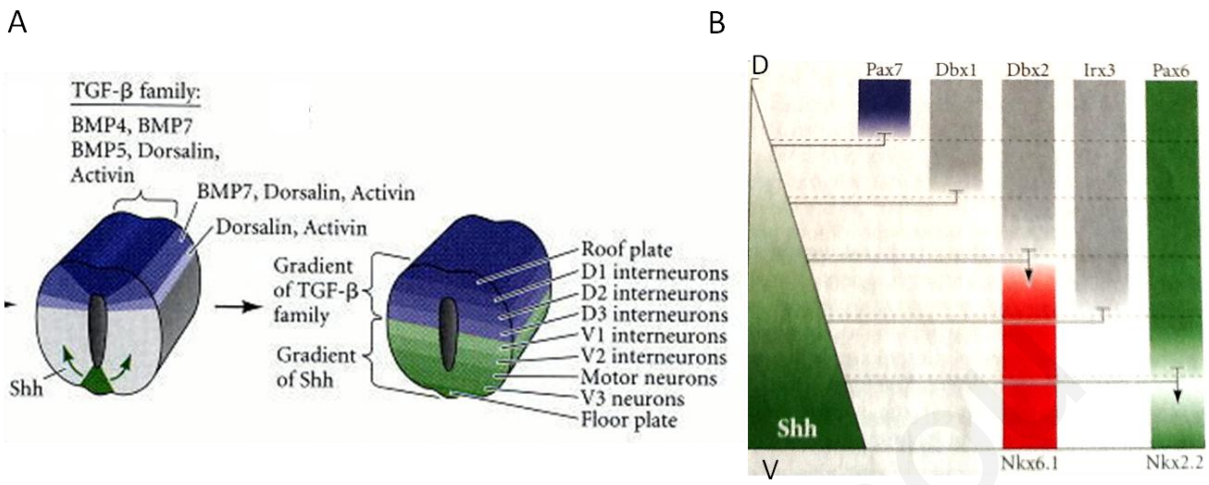

Figure 15. Dorsal-ventral patterning of the neural tube.

(A) From the roof plate, BMP4 establishes a cascade of TGF-β factors, spreading ventrally into the neural tube. Shh diffuses dorsally as a gradient from the floor plate cells. The neurons of the spinal cord are given their identities by their exposure to these gradients. (B) Depiction of the expression patterns of several factors along the DV neural tube. Adapted from (32)

1.6.1 Rohon-Beard Sensory Neurons

At the onset of neurulation, the ectoderm of vertebrate embryos transforms to three cell types: the neural plate, which will form the central nervous system, the non-neural ectoderm, which forms the epidermis, and at the borders of these two populations, the neural plate border (NPB) arises (Figure 8) due to BMP activity gradient. These gradients are established in the ectoderm by an interaction between BMPs produced in the ectoderm and BMP inhibitors such as, noggin, chordin and follistatin, secreted from the mesoderm (73-75). In addition to the neural crest and pre-placodal ectoderm, which the NPB gives rise to, in anamniotes such as *Xenopus laevis*, the NPB also gives rise to the hatching gland and Rohon-Beard (RB) mechanosensory neurons which mediate a tactile response at larval stages (76). RB neuron precursor cells are localized to the most posterior region of the NPB. Bmp, canonical Wnt, Fgf and Notch signaling have all been found to be implicated in the induction of RB progenitors (76, 77). By the end of neurulation, RB neuron cell bodies lie in two bilateral rows in the dorsal spinal cord on either side of the dorsal midline (Figure 16C). Their ascending and descending central axons extend anteriorly and posteriorly within the dorsal spinal cord (Figure 16A) and they extend highly branched peripheral axons subcutaneously (Figure16B, D), which transmit sensory stimuli to the CNS (78-81). These neurons help promote an escape response caused by touch. In *Xenopus laevis*, RB neurons begin undergoing apoptosis from stage 46 and their function is eventually taken over by dorsal root ganglia neurons (76, 82, 83).

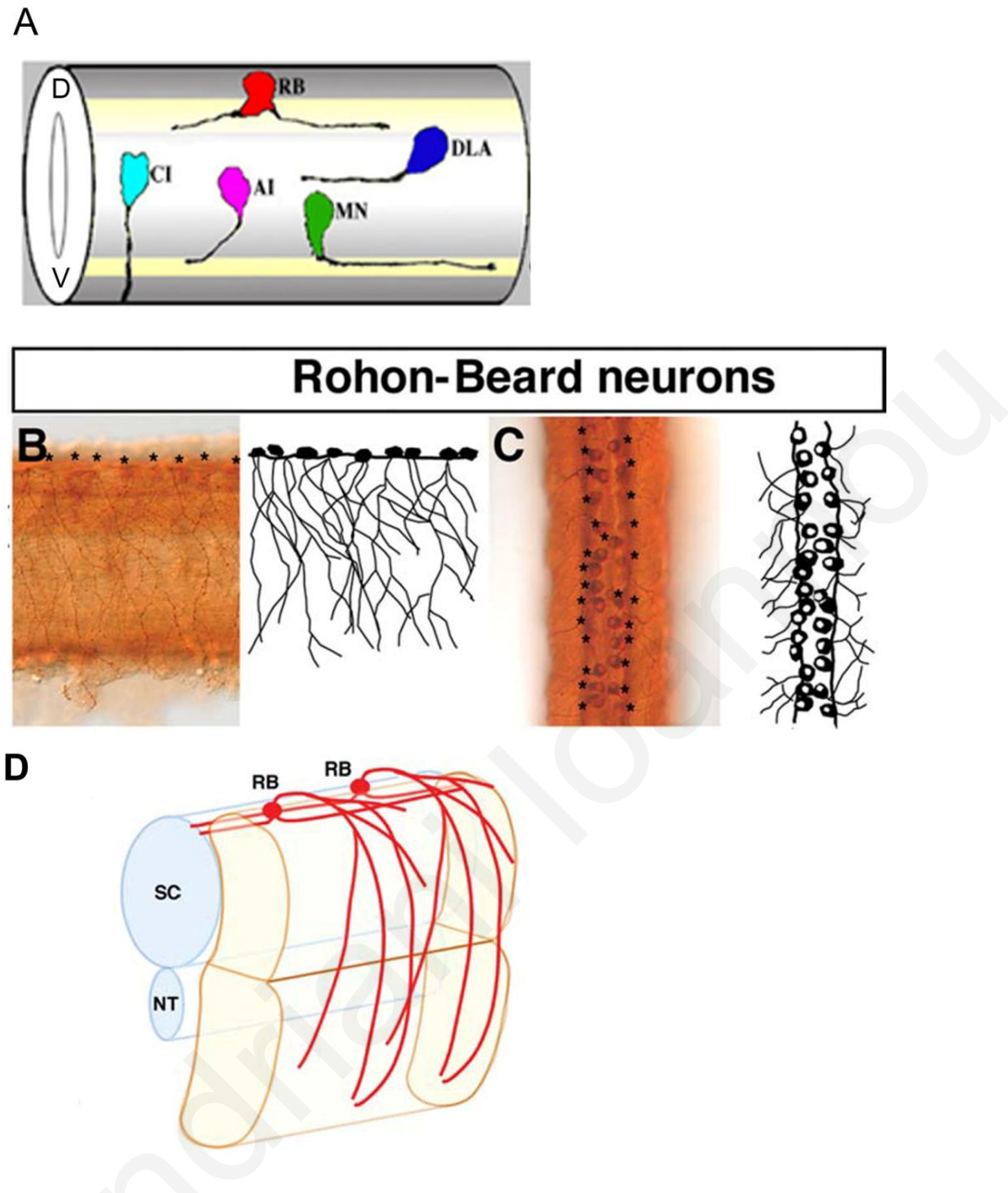

Figure 16. Rohon-Beard neurons.

(A) Schematic of Xenopus neural tube showing RB neuron (Red) cell body found in the dorsal neural tube. The axon runs along longitudinally along the neural tube. Adopted from (84). (B, C) Images to the left are RB neurons in Zebrafish embryo stained by anti-acetylated α-tubulin. Images to the right are schematic depictions of left-hand images. (B) Lateral view with anterior to the left showing peripheral axons innervating the skin. (C) Dorsal view with anterior at top showing RB neuron cell bodies (asterisks) in bilateral rows on the dorsal spinal cord. (D) Schematic views of the axial structure of Zebrafish embryos. NT, notochord; RB, Rohon-Beard neuron; SC, spinal cord. B-D adapted from (81).

1.7 Ciliogenesis

1.7.1 Types of cilia and ciliated epithelia

Cilia are microtubule-based organelles, extending from basal bodies (centriole-based structures) on the surface of certain cells. There are two main types of cilia; primary cilia and motile cilia (Figure 17A, C). Primary cilia have a 9+0 arrangement of microtubules making up the axoneme, and due to the fact that they lack dynein arms (Figure 17B), are usually non-motile. Primary cilia, which have a sensory role, are found in almost every cell type and are important for normal tissue homeostasis (85, 86). Motile cilia are found in specialized tissues such as the respiratory tract, the oviducts of mammals and the epidermis of the *Xenopus* epidermis. Motile cilia are usually found in multiple copies and are characterized by the typical 9+2 arrangement of microtubules, with nine outer microtubule doublets and a central pair of microtubules (Figure 17D). In addition to the two main classes, there is also a class which has features of both primary and motile cilia. These are motile monocilia. These cilia have a 9+0 microtubule arrangement with dynein arms. Motile monociliated cells are found for example, in the mouse node and the *Xenopus* gastrocoel roof plate (GRP) , they produce a clock-wise rotational movement (87) and are important for left-right asymmetry in the embryo.

Mucociliary epithelia are essential for the proper physiology of many organ systems (88). These epithelia are predominately made up of two cell types; multi-ciliated cells and mucus-secreting goblet cells (88, 89) and are essential in the vertebrate respiratory tract, across the surface of the *Xenopus* epidermis (Figure 18) (89, 90) and for the transport of the ovum from the ovary to the uterus in mammals (91). Disruption of cilia function or ciliogenesis can lead to a variety of respiratory diseases and infertility (92, 93). The *Xenopus* epidermis has recently become a popular model for studying ciliogenesis due to the similarities it shares with the vertebrate airway (90) and most importantly, due to its accessibility. Motile cilia have also been implicated in symmetry breakage (87, 94, 95). In Xenopus, motile cilia on the GRP, a structure related to the mouse node, produce a leftward flow of extracellular fluid which is important for the establishment of left-right asymmetry (87, 96).

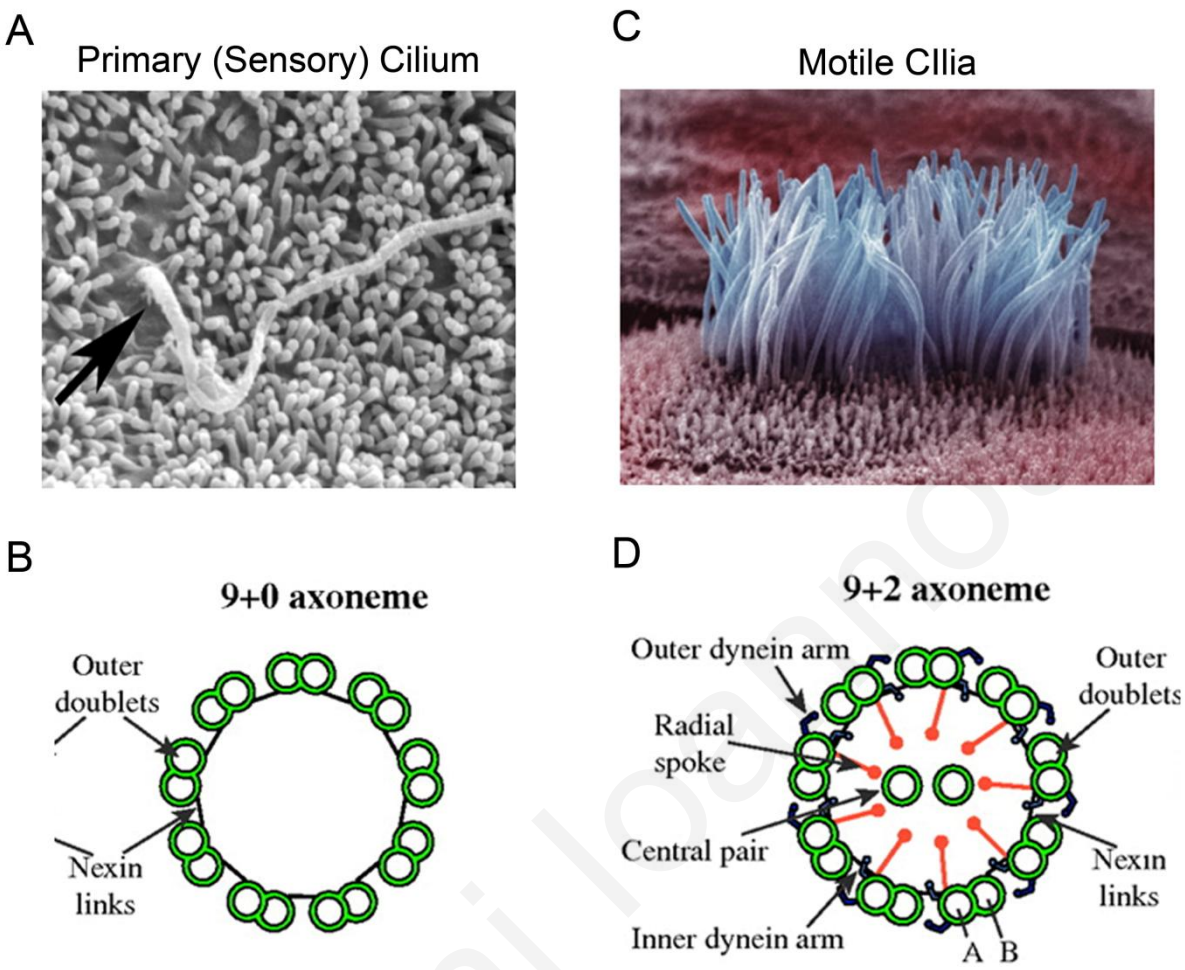

Figure 17. Primary and motile cilia and axoneme structure.

(A) Scanning electron micrograph of a primary cilium (97). (B) The structure of the canonical immotile 9+0 axoneme (86). (C) Image of a multiciliated cell in lung bronchiole (98). (D) The structure of the canonical motile 9+2 axoneme the immotile 9+0 axoneme (86).

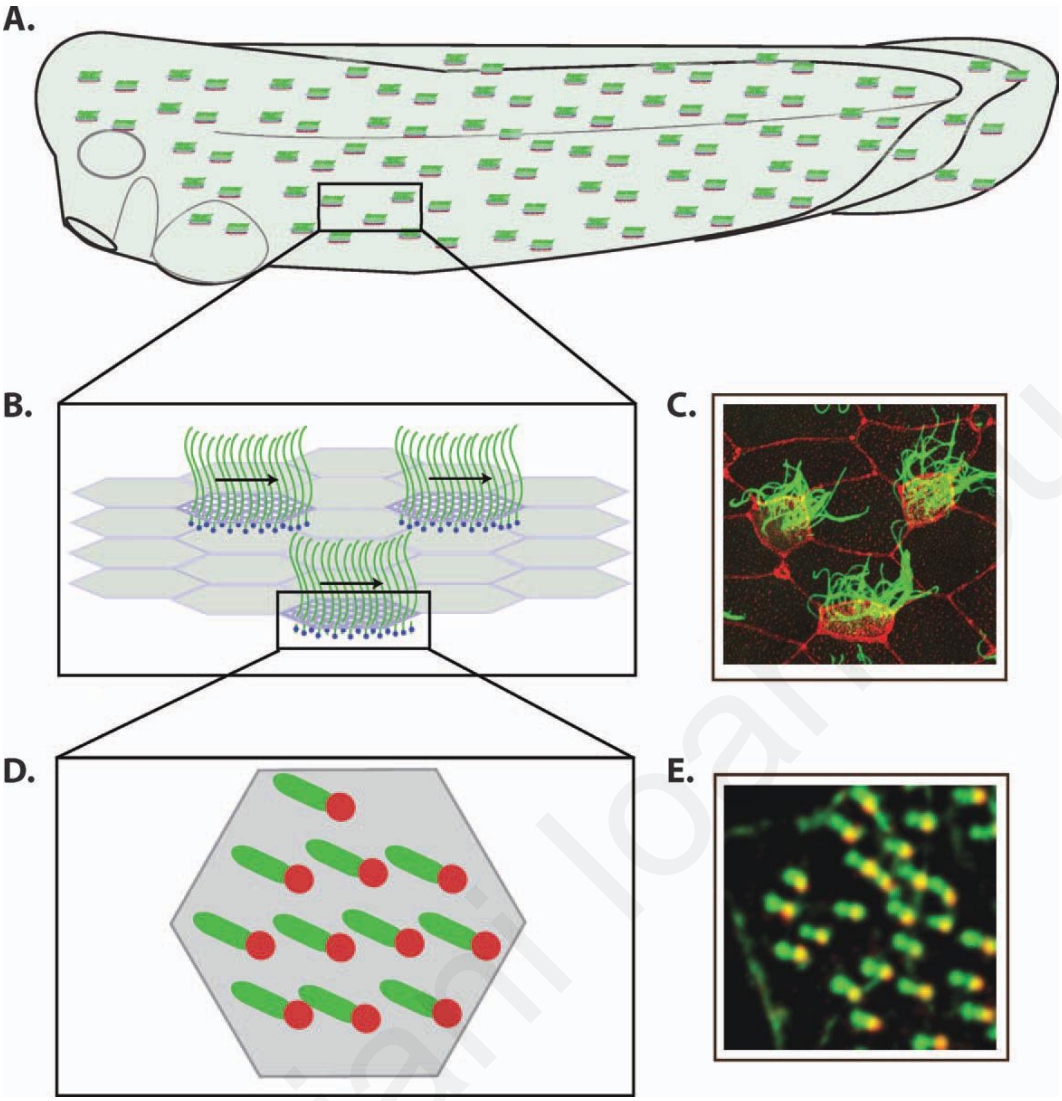

Figure 18. Xenopus multiciliated epidermis.

(A) Image of a Xenopus embryo showing the punctate pattern of ciliated cells that cover the surface. (B) Enlarged inlay of (A) indicating that individual ciliated cells must be coordinately polarized. (C) Multiciliated epidermal cells of Xenopus embryo stained with anti Beta-tubulin antibody to mark the cilia (green) and Rhodamine labeled phalloidin to mark actin (Red). (D) Enlarged inlay of (B) indicating the polarization of basal bodies in a ciliated cell. Basal bodies are shown in red and striated rootlets are shown in green. (E) Portion of a cell from a Xenopus embryo injected with the basal body marker, Centrin-RFP (red) and the rootlet marker GFP-CLAMP (green) which is used to score the orientation of individual cilia. Adopted from (99).

1.7.2 Basal bodies, planar polarization and the actin cytoskeleton in multiciliated cells

The basal body is a modified centriole, which has acquired several accessory structures during its formation (100). In primary cilia, the basal body develops from one of the two centrioles (101). In multi-ciliated cells basal bodies form de novo deep within the cytoplasm (100). Once multiple centrioles form, they become basal bodies by acquiring accessory structures such as the rootlet, the basal foot and the transition fibers (Figure 19) while they are deep within the cell body (102). The transport of these basal bodies to the apical surface and their subsequent docking occurs via an acto-myosin based mechanism (86, 103-105) which is not yet completely understood. The apical surface of multi-ciliated cells is enriched with a dense meshwork of actin. The actin regulators RhoA and Ezrin, in addition to planar cell polarity (PCP) pathway proteins Dishevelled, Inturned and Fuzzy, have been shown to be important for apical enrichment of actin and basal body docking (88, 106-109). In *X.laevis* ciliated epidermal cells, this network of actin is comprised of two distinct but interconnected pools; the apical and sub-apical pool of actin (110). Loss of the apical actin network leads to problems with basal body localization and polarity and appears to be necessary for basal body docking (88, 103, 106, 110). The formation of the apical actin network is temporally linked to basal body docking and is dependent on RhoA (107, 111). Once basal bodies dock at the apical surface they must be planar polarized in order to beat in a polarized manner and create directional fluid flow. Sub apical actin has been shown to be important for spacing as well as cell wide polarity (110, 112-114). The planar polarization of ciliary beating is initially weak and becomes refined by a flow mediated positive feedback mechanism (115). In ciliated *X.laevis* epidermal cells, the basal bodies are polarized along the anterior-posterior axis in the direction of the effective stroke; which is posterior with a ventral bias (88, 112, 115). The basal foot, an accessory structure of the basal body points in the direction of ciliary beat (the effective stroke) (116, 117) and the striated rootlet points in the opposite direction (88, 112, 115, 117) (Figure 18 B, D and Figure 19). Although much has been discovered concerning ciliogenesis in multiciliated epithelia, the precise mechanisms involved in basal body migration, docking and polarity are not yet completely clear.

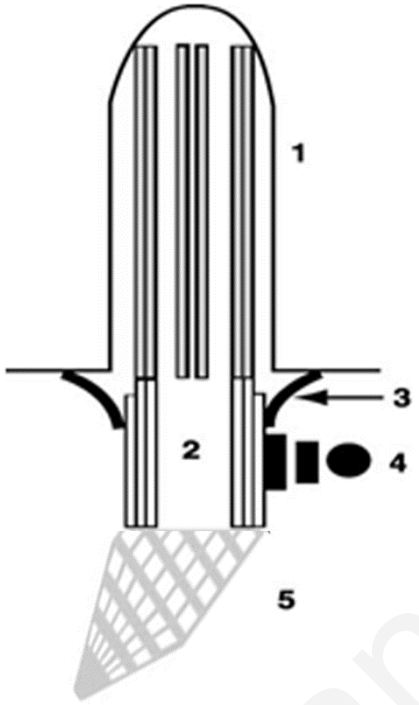

Figure 19. Schematic representation of the structure of a cilium.

(1) Ciliary axoneme covered by the ciliary membrane. (2) Basal body. (3) Transition fiber (distal appendage). (4) Basal foot (subdistal appendage). (5) Striated rootlet pointing in the opposite direction of the basal foot. Image adapted from (118).

2 Project Objectives

The general scientific hypothesis of this project was that xNubp1 has an important role during vertebrate development. In order o address this hypothesis we had four specific scientific objectives:

Objective 1: Clone the *Xenopus laevis* Nubp1 gene and construct various tagged versions of the protein.

Objective 2: Determine the temporal and spatial expression of xNubp1.

Objective 3: Examine the intracellular localization of xNubp1 *in vitro* and in the context of the embryo.

Objective 4: Functionally characterize the role of xNubp1during embryonic development by performing gain-of-function and loss-of-function studies via targeted mRNA or antisense morpholino oligonucleotide injections respectively.

3 Methodology

3.1 Obtaining, housing and maintenance of *Xenopus laevis* frogs

Adult frogs were obtained from several international suppliers, such as NASCO (United States) and Xenopus express (France/UK). Frogs were shipped in peat moss during the spring and autumn in order to avoid the extreme temperature conditions of winter and summer months. New frogs were kept separately from the older ones, and a recovery/resting period of two weeks was allowed after receiving each new shipment of frogs. This resting period was crucial and helped to increase the quality of oocytes obtained and used for the experiments (23).

Male and female frogs were housed in separate tanks. Approximately 20 females or 30 males (males are much smaller than females) were housed in each tank of the aquarium, which was a partially self-cleaning system (12 tanks of 90L each, Figure 20). This particular setup was very effective due to the large number of frogs we house in our lab. The system has a holding capacity of approximately 300 frogs and contains about 1700 liters of water. The system drips fresh water in and out continuously and prevents accumulation of wastes. The toxic waste is therefore kept low and solid waste is drained continuously.

The quality of the ingoing water was monitored to ensure it was optimal for the frogs. Several parameters were measured once a week. These included: pH (6.5 to 7 is optimal for *Xenopus*), conductivity (hardness of the water), gH, kH, NO_3, NH_4 and NO_2. We monitored the system with the help of Aquacontroller (system observation online). In order to keep the conductivity stable at 1200µS (119), a salt solution (NaCl and Ocean salt) was gradually dispensed (in a drip wise fashion) into the incoming water sump of the aquarium system. High water quality is essential for the health of the frogs and the quality of the oocytes produced. High concentration of calcium and high gH values result in higher survival rates and normal development of *Xenopus* embryos. The hardness of the water improves the firmness of the oocytes and the survival and normal development of embryos (119). In addition, the water was pumped through biological filter to remove ammonia, nitrites and fine particles and across four high capacity UV lights to kill bacteria and other pathogens, before being pumped back to the tanks. The frogs were kept on a regular light-dark cycle of 12 hours light and 12 hours dark (controlled system of light cycle in the animal facility). The temperature of the room and

the water in the aquarium was kept at 18^{o}C, which is optimal for the frogs and for all the stages of embryonic development (120). The frogs were fed three times a week, in the morning (Monday, Wednesday, Friday), with floating food pellets (121).

Figure 20. *Xenopus* facility aquarium system.

3.2 Obtaining embryos

3.2.1 Inducing ovulation

Ovulation was induced by administering an injection of 600-750 IU of human Chorionic Gonadotropin (hCG; Sigma) into the dorsal lymph sac of the female frog. Using a fine needle (26 gauge, Fisher) attached to a 1-ml syringe, the injection was performed posteriorly, at the level of the hind limb near the lateral line "stitch" (Figure 21). After the injection, we waited

few seconds and then slowly pulled out the needle. The "primed" frogs were kept at 18-20 °C and started laying eggs approximately 12 hours after injection (the hours required for laying eggs is temperature dependant) (23). Primed females were kept separately from the aquarium so each one could be observed independently.

Figure 21. Priming of *Xenopus laevis* female.

3.2.2 Isolating the testes

The male was euthanized by submersion into a 0.05% benzocaine (Sigma) solution for 30 minutes at room temperature (RT). The male frog was then placed belly up and using scissors and forceps the testes were removed from the body. The testes are about 1cm long and lie at the base of the fat bodies. Isolated testes were placed in sterile petri dish, in a solution containing 10% serum (Fetal calf serum, Gibco), 90% Leibovitz (L-15 Medium Leibovitz, Sigma) and 50μg/mL Gentamycin and stored at 4ºC. Under these conditions, testes can be stored for about 5 to 7 days, after which sperm viability drops (23). Testis viability was assessed by adding a small amount of macerated testis in 0.3X MMR (Marc's Modified Ringers solution; Annex6.2) on a microscope slide (MMR activates the sperm to begin swimming), covered with coverslip and viewed under the microscope. The sperm were easy to identify by their fine helical shape and the characteristic movement.

3.2.3 Collecting eggs

The primed female frog was held using the proper method (23) and simultaneous lateral and vertical pressure was applied by massaging the belly, in order to release the eggs which collect in the sac near the cloaca. One thumb was kept over a clean glass petri dish (90cm) containing 0.33X MMR (122) (Figure 22). Egg collection was carried out every hour for the first 2-3 hours of laying and then more often as the day progressed. Females usually laid eggs for about 8 hours. A maximum of 6-8 collections are expected from a frog in 1 day. Each batch of oocytes obtained from the female frog was kept in a separate glass petri dish.

Figure 22. Manual collection of eggs.

3.2.4 In vitro fertilization

Fertilization was performed immediately after laying and time of fertilization was noted. Before *in vitro* fertilization, excess 0.3xMMR buffer was removed from the petri dish containing eggs using a plastic Pasteur pipette (3ml). A small piece of testis was cut and macerated using forceps (cleaned with 70% ethanol before use) and mixed with the eggs in order to evenly distribute the sperm throughout the eggs. The eggs were left for roughly 20 minutes in order for fertilization to occur. The eggs should rotate within the vitelline membrane so the animal hemisphere (pigmented half) faces upward (122) (Figure 23). These batches of embryos were used in all the experimental procedures.

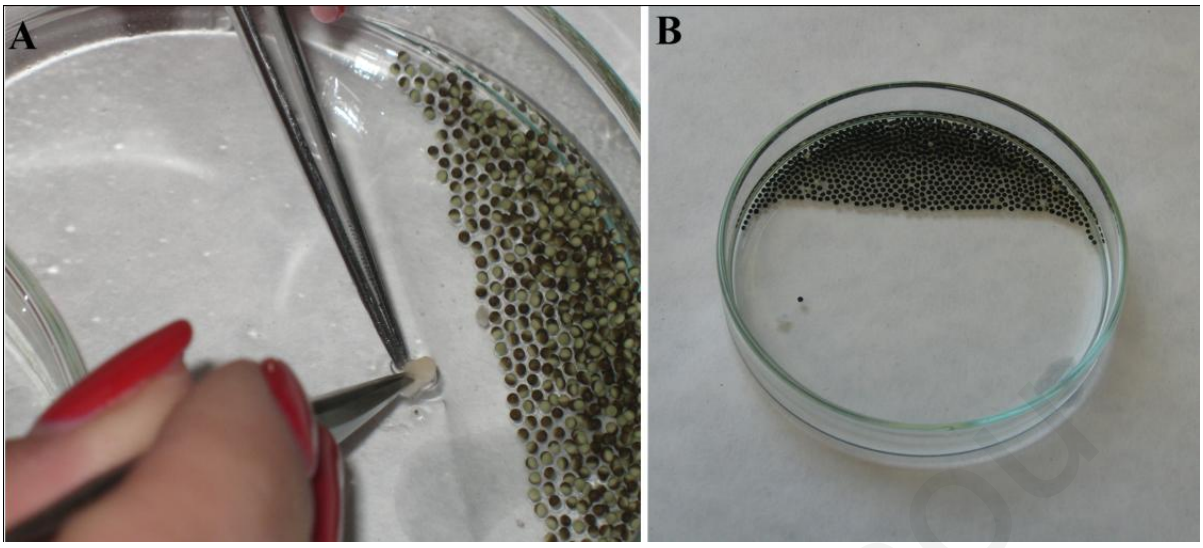

Figure 23. *In vitro* fertilization.

(A) Maceration of testes using forceps. (B) 20 minutes after fertilization, 100% fertilization efficiency is observed.

3.2.5 Dejellying embryos

In order to manipulate *Xenopus* embryos, the thick jelly membranes surrounding the embryos must first be removed. In order to achieve this, embryos were gently swirled in a solution of 2% cysteine (Annex 6.2) in 0.3X MMR at pH 8 for 2-3 min (23). When the embryos began packing closely together and the jelly coats could be seen floating in the buffer, the cysteine was promptly removed and the fertilized eggs were rinsed at least 10 times in an excess of 0.33X MMR. After dejellying, the embryos were placed in a clean dish either in 0.1X MMR or 4% Ficoll in 0.33X MMR (if the embryos were going to used for microinjection procedures) and the dead embryos removed (122).

3.2.6 Microinjections

For microinjections, dejellied embryos were placed in a solution of 4% Ficoll in 0.33x MMR. Ficoll collapses the vitelline space, reduces the pressure on the embryo and therefore prevents leakage due to the microinjection procedure. The embryos were injected using a glass

capillary pulled needle, forceps, a Singer Instruments MK1 micromanipulator and Harvard Apparatus pressure injector (Figure 24). Embryos were microinjected with capped mRNA which was *in vitro* transcribed using mMessage machine kits (Ambion), antisense Morpholino oligonucleotides (MOs; see Table 5) and DNA constructs. Injection volumes were kept below 10nl per blastomere (for 2 -8 cells stage embryos) (123). For most experiments, injections were made at the 4-cell stage, into either the ventral blastomeres (lighter) to target the epidermis, or the dorsal blastomeres (darker) to target neural or mesodermal tissue (Figure 25). Embryos were staged according to Neiuwkoop and Faber (124). After injections, embryos were reared for 2 hours or until stage 8 in 4% Ficoll in 0.33x MMR and then washed and maintained in 0.1x MMR alone. For all experiments, we injected morpholinos at 4 to 46ng per blastomere and mRNAs at various amounts. Embryos were allowed to develop to the appropriate stage and then imaged live, dissected, or fixed in 1x MEMFA (Annex6.2) (23) for 1-2 hours at room temperature (RT). Fixed embryos were either used immediately or serially dehydrated in methanol and stored at -20°C. For Live imaging, embryos were anesthetized in 0.01% benzocaine in 0.1x MMR.

Figure 24. Pressure injector and micromanipulator setup.

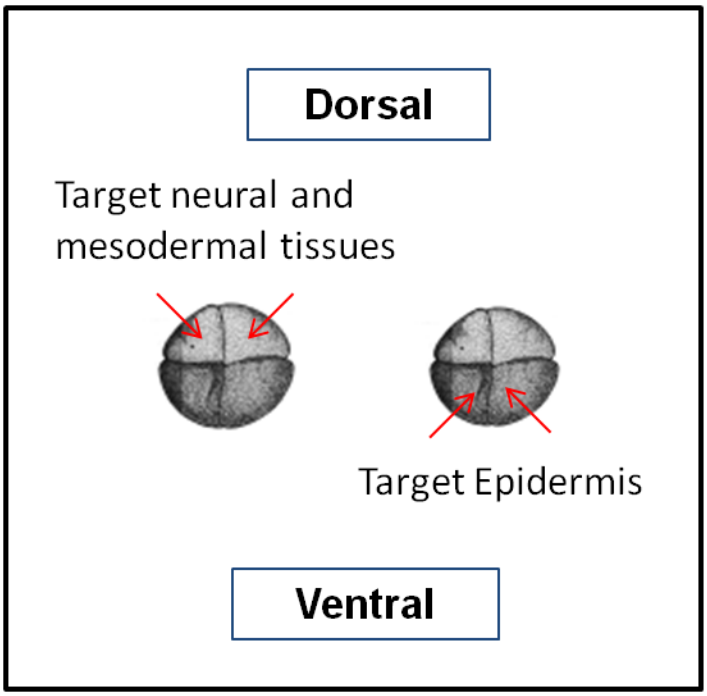

Figure 25. Blastomeres targeted during injections.

Schematic of four cell stage embryos. The lighter pigmented dorsal blastomeres give rise to mesodermal and neural tissues when targeted. The darker pigmented ventral blastomeres give rise to the epidermis when targeted.

3.2.7 Removing the vitelline membrane

Once the embryos reached the desired stage for micro-dissection or further processing, the vitelline membrane was manually removed with the forceps. The procedure was facilitated by coating the bottom of the dish with 1% agarose (electrophoresis grade) in 0.1x MMR. With two forceps, one to hold the embryo steady and the other (sharper pair) make a tear in the vitelline membrane. If the tear was large enough, the embryo could pop out. The naked embryos were stored in 0.1x MMR or fixed in 1x MEMFA and used for the future experiments.

3.3 RNA isolation and cDNA synthesis for RT-PCR

Embryos were placed in an autoclaved 1.5 ml capped centrifuge tube (~5 per tube). 500 µl TRIzol reagent (Invitrogen) was added, and embryos were homogenized by pipetting up and down until the sample was uniform. The sample was allowed to incubate for 10min at RT. Tubes were then centrifuged at 14k rpm for 10min at 4°C. The supernatant (RNA) was removed and placed into a new autoclaved 1.5ml tube. An equal volume (as supernatant) of chloroform was added, the tubes were vortexed for 15sec and allowed to incubate at RT for 3min. Tubes were then spun in a 4°C microfuge at 12k rpm for 15min. The top phase (RNA; clear layer - not the pink layer) was placed into a new autoclaved tube. 500 µl of isopropanol was added and the tubes were allowed to stand for 10min at RT, spun at 12K for 10min at 4°C, the supernatant was decanted and the pellet was washed with 500 µl RNAase-free 70% ethanol and RNA was recovered by centrifugation at 9K rpm for 5min at 4°C. The supernatant was removed and the pellet was allowed to dry before being resuspended in 30 µl of sterile water. cDNA was then synthesized from RNA using the SuperScriptIII First strand synthesis kit from Invitrogen.

3.4 Cloning and RT-PCR

Using cDNA prepared as described above (section 2.3), xNubp1 was amplified by standard PCR (list of primers found in Table 2). The xNubp PCR fragments were then cloned into the SalI – XbaI sites of the pCS108 vector. The clones were then verified by sequencing and then using the verified pCS108-xNubp1and 2 vectors, we constructed the various tagged and untagged versions of the xNubp1 and xNubp2 constructs (refer to Table 3 for list of constructs used). For RT-PCR, cDNA was synthesised using the same method mentioned above (section 2.3) for different developmental stages and different tissues. The PCR was carried out using specific primer pairs. The PCR products were run on a 1-1.5% agarose gel and images were captured using UVP iBox imaging system.

Isolation of stage 31 tailbud skin for RT-PCR was carried out as follows: tailbuds were dissected into three regions in order to separate the regions of the embryos which were shown by ISH to express high amounts of xNubp1. The anterior region which contained the head,

branchial arches and pronephros was removed and the dorsal region containing the neural tube, notochord, somites and tailbud were then removed. The skin surrounding the remaining ventral/belly region was then carefully peeled from the endoderm. RNA isolation, cDNA synthesis and RT-PCR was carried out on all three regions separately.

3.5 Mutagenesis

Mutagenic primer design: Both primers were designed such that they both contained the desired mutation and annealed to the same sequence on opposite strands of the plasmid. The primers were between 25-45 bases, the melting temperatures (T_m) were ≥ 78°C, the GC content over 40% and the mutated sequence was located in the middle of the primers. xNubp1$_{K72Q}$ primers were 30 base pairs long (Table 2), had a T_m of 86.6°C and a 60% GC content and xNubp1$_{G68V}$ primers were 29 bases pairs long (Table 2), had a T_m of 82.5°C and a 52% GC content.

Procedure: In a PCR tube we added: 125ng of each primer 22.5µl Accuprime (Invitrogen) polymerase mix and 100ng HA-xNubp1 plasmid DNA. The cycling conditions were: 95°C for 1 min, 18 cycles of 95°C for 50 sec, 60°C for 50 sec and 68°C for 7.5min (1.5min per Kb of plasmid), 1 cycle at 68°C for 10 min. The PCR was immediately cooled to 37°C, 1µl of Dpn1 (10U/µl) restriction enzyme was added and the reaction incubated for 1 hour. 2µl of the PCR reaction was then used for transformation.

Primer Name	Primer Sequence 5' to 3'
F/SalI-xNubp1a	CTGTCGACATGGCTGATATACCAGATAATGCACC
F/SalI-xNubp1b	CTGTCGACATGGCTGATATACCAGAAAATGCACC
R/XbaI-xNubp1a	CTTCTAGATCACTTCTTTTTTTCACAATAGTCTTGAA
F/SalI-Flag-xNubp1a	CTGTCGACATGGACTACAAGGATGACGATGACAAAGCTG ATATACCAGATAATGCACC
F/SalI-HA-xNubp1a	CTGTCGACATGTACCCATACGATGTTCCAGATTACGCTGC TGATATACCAGATAATGCACC
F/SalI-5'UTR-xNubp1a	CTGTCGAC CCAATTCAAGATGCAATTATTG
R/XbaI-3'UTR-xNubp1a	CTTCTAGA GTCCTTTAATATGAGCTTTATTGCAAT
R/ XbaI-3'UTR-	CTTCTAGAGCAGGTTTGGCATAGTCTAGGCGG

xNubp1b	
F/SalI-xNubp1a (surrogate)	CTGTCGACGAAGTGTTTTTCGCAGGCATGGCTGATATACC
R/xNubp1-up to 429bp	ATCGGGACTGCTAAGCAAGA
F/SalI-xN1 (exon-1 end)	AAGTCGACCTGATATACCAGATAATGCA
R/XbaI-xN1 (exon- 2start)	AATCTAGACTCAGTACTGTCTGTACCTGG
R/Xba-xNubp1-Exon 5 (Start)	AATCTAGAATCCTGATCCACTCTGGT
F/SalI-Nubp2	CTGTCGACATGGAGCAGACTCAGGATGG
R/XbaI-Nubp2	CTTCTAGATCAGGATTGTGGAGAGGCC
F/xNub1 $_{K72Q}$	GGTGGTGTGGGCCAGAGTACATTCAGTGCC
R/xNub1 $_{K72Q}$	GGCACTGAATGTACTCTGGCCCACACCACC
F/xNub1 $_{G68V}$	CTCTCTGGAAAGGTTGTGGGCAAGAGTAC
R/xNub1 $_{G68V}$	GTACTCTTGCCCACAACCTTTCCAGAGAG

Table 2. Sequences of all primer sets used.

Name	
Generated	**Gifted/Bought**
pCS108-xNubp1	pCS-Centrin2-YFP (Dr. Reinhard Köster)
pCS108-Flag-xNubp1	pmKate2-Actin (Evrogen)
pCS108-HA-xNubp1	pCS-H2B-RFP (Dr. Reinhard Köster)
pCS108-GFP-xNubp1	pCS-EMTB-3XGFP (Dr. Brian Mitchell)
pCS108-xNubp1-(-)NTerminus	pCS-Histone-GFP (Dr. Chenbei Chang)
pCS108-xNubp1-NTerminus-only	pCS-Utr-RFP (Dr. John Wallingford)
pCS108-GFP-xNubp1-(-)NTerminus	pCS-H2B-CFP (Dr. Reinhard Köster)
pCS108-GFP-xNubp1-NTerminus-only	pCS-Sox2 (Dr. Chenbei Chang)
pCS108-Flag-xNubp1-(-)NTerminus	pCS-Chordin (Dr. Chenbei Chang)
pCS108-Flag-xNubp1-NTerminus-only	pCS-Centrin2-RFP (Dr. Brian Mitchell)
pCS108-HA-xNubp1-(-)NTerminus	pBSSK-Pax3 (Dr. John Wallingford)
pCS108-Flag-xNubp1-NTerminus-only	pCS-MyoD (Dr. Ali Brivanlou)
pCS108-HA-xNubp1-(-)NTerminus	pCS N-Tubulin (Dr. Richard Harland)

pCS108-HA-xNubp1-NTerminus-only	pCS-RhoA-GFP (Dr. John Wallingford)
pCS108-xNubp2	pCS-rGBD-GFP (Dr. John Wallingford)
pCS108-Flag-xNubp2	pCS-Dvl-GFP (Dr. John Wallingford)
pCS108-HA-xNubp2	pCS2+-GFP-Clamp (Dr. John Wallingford)
pCS108-GFP-xNubp2	pCS-Pitx2c (Dr. Martin Blum)
pCS108-HA-xNubp1$_{K72Q}$	pCS- Xnr1 (Dr. Chenbei Chang)
pCS108-HA-xNubp1$_{G68V}$	pCS-xTwist (Dr. Chenbei Chang)

Table 3. List of constructs used.

3.6 Cloning of introns and design of splice blocking morpholinos

Introns in xNubp1 were identified first by comparing cDNA sequence to the *Xenopus tropicalis genome* sequence and then the analogous primers were designed (Table 2). *Xenopus laevis* Nubp1 genomic DNA, including the intronic regions, was then amplified by PCR, cloned into the CS108 vector and sequenced. Splice-blocking antisense morpholino oligonucleotides (MO's) were designed (Table 5) and ordered from Gene Tools, LLC. To determine the effectiveness of the splice disruption by the MO, RNA was extracted from MO-injected and control embryos and cDNA was prepared using the Superscript^{TM} kit (Invitrogen). PCR was then performed using the same primers used for amplifying the intronic regions.

3.7 Convergent extension assay

For CE elongation assays; animal caps were dissected at stage 8 and cultured on agarose-coated petri dishes in 0.5x MMR containing gentamycin and activin protein (10ng/ml) (125) until sibling embryos completed neurulation. The caps were then fixed in 1xMEMFA and images were captured using a Zeiss LumarV12 fluorescent stereomicroscope (Figure 26).

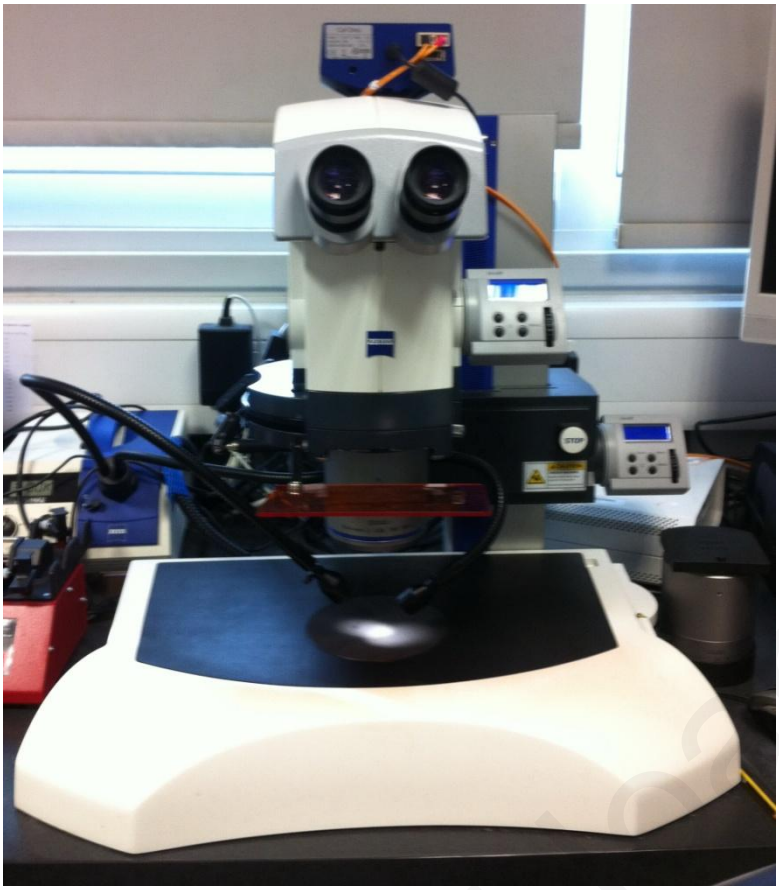

Figure 26. Zeiss LumarV12 fluorescent stereomicroscope.

3.8 Whole-mount i*n situ* hybridization (WISH)

Whole-mount in situ hybridization of *Xenopus* embryos was performed according to Harland (1991) (126). The basic ISH steps are as follows:

1. **Digoxigenin labelled probe preparation.** Antisense (3' to 5') Digoxigenin –labeled RNA probes were synthesized by *in vitro* transcription (IVT) from linearized plasmid templates using bacteriophage RNA polymerases (T3, T7 or SP6) and a ribonucleotide mixture in which the UTPs were labeled with Digoxigenin (DIG-11-UTP). To test the success of the IVT 3-5 µl of the probe was run on a1% TAE agarose gel (RNase free). The probe was then stored at -80° until use.
2. **Day1 of ISH:** The embryos were first transferred to 4ml glass vials and rehydrated through a methanol series (100% methanol, 75%methanol in PBTw (Annex 6.2),

50%methanol in PBTw, 25%methanol in PBTw and 100%PBTw). Next, the embryos were permeabilized by incubation at room temperature for 5 min in 10μg/ml Proteinase K, washed 2X5min in 0.1 M Triethanolamine pH7-8 (TEO), 2X5 min in TEO with acetic anhydride and then post fixed in 4%PFA (paraformaldehyde) for 20 min at RT. Embryos were then incubated for 5-6 hours in Prehybridization solution (Annex 6.2) at 60-65°C and then incubated overnight at 60-65°C in hybridization solution containing the probe. Probes used: xNubp1, Sox2, Chrd, MyoD, Pax3, N-Tub, Twist, Pitx2c, Xnr1

3. **Day2 of ISH:** Post-hybridization washes in SSC, RNase step at 37°C, block (in order to prevent unspecific binding), and antibody (Ab) incubation (Anti-DIG- AP fab fragments. 1:2000) at 4°C overnight or 4hour at RT followed by a brief wash in 1xMAB (Maleic acid buffer) (Annex 6.2) and then overnight wash in 1xMAB at 4°C .
4. **Day3-4 of ISH:** Post-antibody washes with MAB solution (5x1 hour washes for overnight Ab incubation and3-4 10min washes for 4hr RT Ab incubations) and washed in Alkaline phosphatase (AP) buffer (Annex 6.2) which contained levamisole to inhibit endogenous phosphatases (2x10min washes). Visualization of the probe using BM purple. Color development varied depending on the probe used. To stop the color reaction, the embryos were washed in MAB and fixed overnight in 1xMEMFA at RT. Embryos were then bleached (Annex 6.2). Bright field images were captured on a Zeiss LumarV12 fluorescent stereomicroscope.

3.9 Cell culture/lines

Xenopus XL-177 (epithelial) and A6 (kidney epithelial) cell lines were cultured in L-15 (leibowitz) supplemented with 10% FBS and 1% Antibiotics/antimycotics in 30cm flasks at RT. Mouse embryonic fibroblast (NIH3T3) were cultured in DMEM supplemented with 10% FBS, 1% antibiotics/antimycotics, 1% sodium pyruvate in a 37°C 5% CO_2 incubator.

Electroporation

Electroporation of *Xenopus* cell lines was carried out using the Neon Electroporation system from Invitrogen. Cells were electroporated with 1.5μg plasmid DNA and seeded in 12 well

culture flasks. The parameters used for XL-177 and A6 cell lines were 1300V, 20ms pulse width, 2 pulses at roughly 2-4x10^5 cell density. When cells were ready for imaging, they were seeded onto fibronectin (50µg/ml) coated, HCl charged coverslips.

Nocodazole treatment

A 4-5µg/ml dilution of nocodazole (Sigma Aldrich) made in culture media for cells or MMR for embryos, was added to the cells or embryos and they were imaged immediately on the Zeiss LSM710 confocal microscope (Figure 27). For nocodazole washout, the solution was removed and the cells/embryos were washed several times to ensure complete removal of nocodazole. The cells/embryos were then imaged again.

Figure 27. Zeiss 710 Laser Scanning Confocal Microscope.

3.10 Immunofluorescence

Stored embryos were rehydrated by serial washes. Embryos were then permeabilized in PBDT (Annex 6.2) for several hours at RT. The permeabilization step can be omitted for epidermal staining. Embryos were then blocked in PBDT + 1% normal goat serum for 1 hour at RT. Primary antibodies diluted in block solution were then added (Table 4), and embryos were incubated for 4 hours at RT or overnight at 4°C. The next day, embryos were washed 4x10min in PBDT. Embryos were then incubated in secondary antibodies (Table 4) at RT for 2 hours and then washed 4x10 minutes in PBDT again. Embryos were then post-fixed in MEMFA for 15-30 minutes at RT, washed in 1xPBS, imaged immediately or dehydrated in methanol and cleared in a 2:1 mixture of BB:BA (Benzyl benzoate: Benzyl alcohol). The embryos were imaged on a Zeiss LSM 710 laser scanning confocal microscope and Zen 2010 software or a Zeiss Axio Imager Z1 using a Zeiss Axiocam MR3, the Axiovision software 4.7.

For cell lines the IF procedure was modified slightly. Cells were seeded on charged coverslips and fixed in 4%PFA in 1xPBS or in methanol for 10min. Coverslips were then washed in 50mM Glycine for 10min and cells were permeabilized in 0.2% triton-100 in PBS for 10 min. Cells were washed several times with 1xPBS and blocked in 10% Goat serum in 1xPBS. Primary antibodies were then added (in block solution) and cells were incubated for 1 hour at RT. Primary antibodies were then washed off with 1xPBS and cells were incubated with secondary antibody solution for 1 hour at RT and then washed several times in 1xPBS. A drop of Prolong (Invitrogen) was added to a microscope slide and the coverslip was inverted onto the drop and allowed to dry before viewing under the microscope.

For Pre-extraction, 0.2% triton was added to the cells before fixation for 20 seconds and then they were fixed. No further permeabilization is necessary.

Antibodies	Dilutions (in block solution)
GFP (Invitrogen)	1:500
Acetylated α-tubulin (sc-23950, Santa Cruz)	1:500
Zo-1 (Invitrogen)	1:500
Nubp-r (gifted by Dr. Niovi Santama)	1:500
Nubp-g (K-14) (sc-160613, Santa Cruz)	1:500
Actin (sc-1616R , Santa cruz)	1:500
Tubulin (E7, Hybridoma)	1:500
Alexa 488 anti-mouse (Invitrogen)	1:500
Alexa 488 anti-rabbit (Invitrogen)	1:500
Cy3 anti-mouse (Jackson Immunoresearch)	1:500
Cy3 anti-rabbit (Jackson Immunoresearch)	1:500
Cy3 anti-rat (Jackson Immunoresearch)	1:500
HA (Y-11) rabbit (sc-805, Santa Cruz)	1:500
HA (F-7) mouse (sc-7392 Santa Cruz)	1:500
Flag rat (Novus)	1:500
Phalloidin 488 (Invitrogen)	1:500

Table 4. List of antibodies used.

3.11 Western blots and Immunoprecipitation

Protein lysates were prepared by homogenizing embryos in ice cold MK's modified lysis buffer (Annex 6.2) supplemented with protease inhibitors. Embryos were homogenised by pipetting up and down. Homogenates were then cleared by centrifugation at 15000g for 15-30min at 4°C. Protein lysates (usually ½-1 embryo equivalents) were run on an SDS-page gel and then blotted onto a PVDF membrane. Membranes were then blocked in 5% milk in TBSTw (1xTBS buffer + 0.1%Tween-20). Blots were incubated with primary antibodies (Table 4) in 5% milk overnight at 4°C. Visualization was performed using HRP-conjugated antibodies (Santa Cruz Biotechnology anti-rabbit, mouse and goat) and detected using the Lumisensor chemiluminescent reagent kit (Genscript).

For Co-immunoprecipitation (IP), protein lysates were prepared by homogenizing embryos in ice cold MK's modified lysis buffer (Annex 6.2). Homogenates were cleared by centrifugation at 15000g for 30min at 4°C (127). The lysates were incubated with 0.5-1 µL of antibody and rotated for 1-4 hours at 4°C. 40µL protein-A-agarose beads (Santa Cruz) were added to the lysates and incubated for 1-2 hours at 4°C. The beads were recovered by centrifugation at 4°C for 2 minutes at 2000 rpm. The samples were washed four times using MK's buffer. After the last centrifugation, loading dye (Laemmli + ßmercaptoethanol) was added to the beads (heat at 80°C for 5 minutes) and beads were spun to the bottom of the tube. The samples were separated on SDS-polyacrylamide gels and the rest of the procedure was the same as above (western blot procedure).

3.12 Whole-mount TUNEL

Stored embryos were rehydrated and washed in 1xPBS. They were then incubated for 1hour at RT in TdT buffer (Invitrogen). Then, 150U/ml TdT enzyme (Invitrogen) and 0.1 µl of DdUTP (Roche) per 100 µl buffer were added to the buffer solution and the embryos were incubated overnight at RT. The next day, embryos were first washed 2x1hour at 65°C in 1 mM EDTA/PBS. Next, embryos were washed in 1xPBS 4x1hour at RT followed by 2-10min washes in 1xMAB. Embryos were then blocked in 2%BMB blocking solution for 1 hour at RT and incubated in a 1/3000 dilution of anti-digoxigenin AP antibody in BMB block for 4hours RT or overnight at 4°C. Antibody was washed away by 5x1hour washes in MAB. Endogenous phosphatases were blocked by 2x10min washes in alkaline phosphatase buffer and then NBT/BCIP (Roche) was added to the embryos (embryos were kept in the dark). Chromogenic reaction was stopped by a quick wash in 1XMAB and then the embryos were fixed overnight in 1xMEMFA at RT. The next day embryos were imaged before and after clearing in 2:1 BB: BA.

3.13 Touch response assay

The touch response assay was carried out as previously described (76). Briefly, in order to test for sensory rather than motor function, we limited our test of touch intensity to embryos that could swim away with a normal pattern. The dorsal trunk of stage 33 embryos was gently poked with a hair knife. After a period of approximately 3 seconds, the embryo was poked again for a total of 10 trials. Responses were scored as following: 0, no response; 0.5, non-swimming response (restricted trunk bend); 1, normal swimming response. The scores of each 10 trials were summed to yield a final touch response score between 0 and 10.

3.14 Fluid flow

For the assessment of fluid flow, 31/32 stage embryos were anaesthetized in 0.01% benzocaine and placed in silicone grease (High Vacuum Grease, Dow Corning) wells on glass slides with a clover glass on top. 655nm Quantum dots (QTracker non-target QDs, Invitrogen) were then added to the media. We carried out time-lapse microscopy using the Zeiss Axio Imager Z1 using a Zeiss Axiocam MR3, the Axiovision software 4.7.

3.15 Transmission electron microscopy (TEM)

Electron microscopy was done essentially as described by Steinmen 1968 (90). Briefly, embryos were fixed in 2.5% phosphate- buffered gluteraldehyde over-night at 4°C and then post-fixed in 1% phosphate-buffered osmium tetroxide for 1hr at room temperature. The embryos were then dehydrated in a graded series of ethanol. Embryos were then washed in propylene oxide and embedded in epoxy resin. Embedded embryos were sectioned (60-70 nm). Sections were mounted on copper grids, counter stained with uranyl acetate and lead citrate and imaged in the TEM (Jeol, JEM 1010). TEM was carried out in Dr. Kyriakos Kyriakou's lab at the Cyprus Institute of Neurology and Genetics with the help of Marianna Nearchou.

3.16 Gastrocoel roof plate assay

Embryos were fixed in 1X MEMFA at stage 17. The GRP was then manually dissected and post fixed for a further 15min. GRP tissue was then used for immunofluorescence as described above (section 2.10).

3.17 Fluorescence recovery after photobleaching (FRAP)

The FRAP experiments were conducted using a laser scanning confocal microscope (Zeiss LSM 710). Stage 27-29 mKate2-actin expressing embryos were anaesthetized in 0.01 % Benzocaine in MMR and immobilized in silicone grease wells on glass slides. A small area of an mKAte2-actin positive epidermal cell was imaged (11.5μm x 11.5μm) using a Plan-Apochromat 63x/1.40 Oil DIC M27 objective lens (Zeiss) and a 543nm laser was used both during acquisition (2.8%) and bleaching (100%). Emission of mkate2 was detected between 572-754 nm. A total of 30 of frames were acquired at 5 second intervals. Two frames were acquired as a pre-bleaching control, the region of interest (rectangular region roughly 4x5 μ m) was bleached within one frame, and the fluorescence recovery was measured in frames 4-30. In order to obtain full recovery rates for control ciliated cells the interval between acquired frames was changed to 20 seconds for the 11-30th frames. The Zeiss Zen 2010 software was used for FRAP analysis. The fluorescence recovery curve was fitted by single exponential function, given by: $F(t) = A(1-e^{-R}) + B$; where F(t) is the intensity as time t; A and B are the amplitudes of the time-dependent and time-independent terms, respectively; τ is the lifetime of the exponential term (time constant), and the recovery rate is given by $R = 1/\tau$.

4 Results

4.1 Cloning of *Xenopus* Nucleotide Binding Protein 1 (xNubp1)

Xenopus laevis is alloteraploid due to a whole genome duplication event that occurred roughly 40 million years ago(128), which means it has four copies of each gene. The online database revealed that *Xenopus laevis* Nubp1 has two paralogs; Nubp1a and Nubp1b. Primers were designed based on the provisional sequences of *Xenopus laevis* Nubp1a and Nubp1b from www.xenbase.org (XB-GENE-992731 and XB-GENE-6252195) (129) and the NCBI database (GenBank: 494723 and 496286). First strand cDNA was reverse transcribed from gastrula stage *Xenopus laevis* mRNA, and the xNubp1 specific primers were used to amplify the coding and untranslated regions of xNubp1-a and xNubp1-b paralogs respectively, and clone them into the pCS108 vector. Sequenced clones were identical to the provisional sequences from Xenbase and NCBI. The xNubp1 paralogs had very few minor amino acid differences (96% sequence identity) (Figures 28, 29), therefore, only xNubp1a was used to generate most of the constructs.

```
xNubp1a         CCAATTCAAGATGCAATTATTGAAACGAGGCTTGGAACGCAAAGAGCATATCGGAAGCAG 60
xNubp1b         -------------------------------------------------------GAAGTAG 7
                                                                       **** **

xNubp1a         GAAGTGTTTTTCGCAGGCATGGCTGATATACCAGATAATGCACCCCAGCATTGCCCAGGT 120
xNubp1b         GAAGTGGTTTTCGCAGGCATGGCTGATATACCAGAAAATGCACCCCAGCATTGCCCAGGT 67
                ****** *************************** ************************

xNubp1a         ACAGACAGTACTGAGGCTGGCAAGAGTTCTGCGTGCCAGGGATGCCCCAATCAATCAATA 180
xNubp1b         ACAGGCAGCACTGAGGCTGGCAAGAGTTCTGCGTGCCAGGGATGCCCAAATCAATCAATA 127
                **** *** ************************************ ************

xNubp1a         TGCGCATCAGGAGCTGCGGCAGGACCAGACCCAGCTATAGAAGAAATAAAAGAAAAAATG 240
xNubp1b         TGCGCATCAGCAGCAACATCAGCTCCAGACCCAGCTATAGAAGAAATAAAAGAAAAGATG 187
                ********** ***  *  ***  ******************************** ***

xNubp1a         TCATTGGTTAAACACAAGATATTGGTTCTCTCTGGAAAGGGTGGTGTGGGCAAGAGTACA 300
xNubp1b         TCATTGGTTAAACACAAGATTTTGGTTCTCTCTGGAAAGGGTGGTGTGGGCAAGAGTACA 247
                ******************* ****************************************

xNubp1a         TTCAGTGCCCACCTGGCACATGGTTTAGCCCAAGATGAGGGCAAAGAGGTGGCTCTGCTT 360
xNubp1b         TTTAGTGCCCACCTGGCACATGGTTTGGCACAAGATGAGGGCAAAGAGGTAGCTTTGCTT 307
                ** ********************** ** ******************* *** *****

xNubp1a         GATGTGGACATCTGTGGACCATCGATTCCAAAAATGATGGGCTTGGAAGGAGAACAGGTT 420
xNubp1b         GATGTGGACATCTGTGGACCATCGATTCCAAGAATGATGGGCTTGGAAGGAGAACAGGTT 367
                ****************************** ****************************
```

```
xNubp1a         CACCAGAGTGGATCAGGATGGTCACCAGTGTATGTAGAAGATAACCTGGCTGTAATGTCT 480
xNubp1b         CACCAGAGTGGCTCAGGATGGTCACCGGTGTATGTAGAAGACAACCTGGCTGTAATGTCT 427
                ********** ************** ************** ******************

xNubp1a         GTTGGATTCTTGCTTAGCAGTCCCGATGATGCGGTCATATGGAGAGGGCCTAAAAAAAAT 540
xNubp1b         GTTGGATTCTTGCTTAGCAGTCCTGATGATGCTGTTATATGGAGAGGTCCTAAAAAAAAT 487
                ********************** ******** ** ********** ************

xNubp1a         GGGATGATCAAACAGTTTTTGCGAGATGTGGACTGGGGTGATGTGGATTATCTGATAGTA 600
xNubp1b         GGAATGATCAAACAGTTTTTGCGAGATGTAGACTGGGGTGAAGTGGATTATTTGATAGTA 547
                ** ************************** ********** ********* ********

xNubp1a         GATACCCCTCCTGGTACATCAGACGAGCATCTTTCTGTAGTACAGTATCTCAGTGCAGCA 660
xNubp1b         GACACCCCTCCTGGTACATCAGACGAGCACCTCTCTGTGGTACAGTATCTCAGTGCGGCA 607
                ** ************************** ** ***** ***************** ***

xNubp1a         GGAATCGATGGAGCAGTAATCATTACAACTCCGCAAGAGGTCTCACTTCAGGATGTCCGA 720
xNubp1b         GGAATTGATGGTGCAGTAATCGTTACAACTCCTCAAGAGGTGTCACTACAGGATGTCCGA 667
                ***** ***** ********* ********** ******** ***** ************

xNubp1a         AAAGAAATCAACTTCTGCCGCAAAGTAAAACTTCCCATTATAGGTGTAGTGGAAAATATG 780
xNubp1b         AAAGAAATCAACTTCTGTCGCAAAGTGAAACTTCCCATTATAGGTGTAGTGGAAAATATG 727
                ***************** ******** ***********************************

xNubp1a         AGTGGGTTTATTTGTCCTAAATGTAAGAATGAATCACAGATATTTCCTCCAACTACTGGG 840
xNubp1b         AGTGGATTTATTTGTCCTAAGTGTGAGAATGAATCACAGATATTTCCTCCAACTACTGGA 787
                ***** ************** *** ***********************************

xNubp1a         GGAGCAGAGAAGATGTGCACTGATCTCAGTGTTTCTCTACTGGGCAAAGTTCCCTTAGAT 900
xNubp1b         GGAGCAGAGAAGATGTGCACTGATCTCAATGTTTCTCTACTGGGCAAAGTTCCCTTAGAT 847
                **************************** ******************************

xNubp1a         CCAAATATAGGAAAGAGCTGTGACACAGGGAAATCATTTTTTACTGAAATTCCAGATTCC 960
xNubp1b         CCAAACATAGGAAAGAGCTGCGACACAGGGAAATCATTTTTTACTGAAATTCCAGATTCG 907
                ***** ************** ***************************************

xNubp1a         CCAGCAACATTATCCTACAGAAAAATAATCCAGAGAATTCAAGACTATTGTGAAAAAAAG 1020
xNubp1b         CCAGCAACATTATCCTACAGAATAATAATCCAGAGAATTCAAGACTATTGTGAGAAAAAG 967
                ********************** ****************************** ******

xNubp1a         AAGTGACTTCCTTTTCCCAATGGTACAGAGAAGTTCTGATAAGCAGTTTTGCATTATGCC 1080
xNubp1b         AAGTGACTTGCTTTTCCAAATGGAACAGAGGCGTTCAGCTCCGCAGTTTTGCACTTTGCC 1027
                ********* ******* ***** ******  **** * *  *********** * ****

xNubp1a         ACAGATTACGGATTTTTTGCATTTCACTGTTACCTTAAGAGAAAAATCAGCGTTAAAAAA 1140
xNubp1b         ACAGATTACGGATTTTCCACATTTCACCATCACCTTAAGAGGAACATCCGCATTCCAAAA 1087
                ***************   ********  * ********** ** *** ** **  ****

xNubp1a         TAATTTCAATGTGGAAATAATGC--------ACTAGGCCA-------TGTATCACTTAAG 1185
xNubp1b         AAATGTAAATGTGGAAATAATGCCCGCCTAGACTATGCCAAACCTGCTGTAGCACTTAAG 1147
                 *** * ****************        **** ****       **** ********

xNubp1a         TGGTATCCTAGCCAGTAAATCAAAGTATTTGTTACCAGCTGTTTACCTTCTCTTTCATTT 1245
xNubp1b         TAGTATCACAGCCGGTAAATCAAAATATTTGTCCCCAGCTGCTTA------CATTCATTT 1201
                * *****  **** ********** *******  ******* ***      * *******

xNubp1a         TGCTGGCCAGAGCATGAACGGGAATGTTGTTACAGCCATGGGGTTGCAGGGCACAAGCAG 1305
xNubp1b         TGTTGGCCAGAGC----------------TTTCAAC--TGAATTTGC------TAA---- 1233
                ** **********                ** ** *  **   ****       **

xNubp1a         CATCGTTTAGAAACAAAATATGTATTTAGAACCTCTAATTTAATAATAATAGTAATAATA 1365
xNubp1b         ------TTGGGAACA-----TG---------------------------------AATG 1248
                      ** * ****     **                                  ***

xNubp1a         TTTTCTTTATAAAAATAACTCTAAACATATCTGTTTTATAGCACTATTTAGGAGAATGAT 1425
```

Figure 28. xNubp1 paralog nucleotide alignment (ClustalW2).

Non-coding regions are red and start and stop codons are in blue. Asterisks indicate identical sequences.

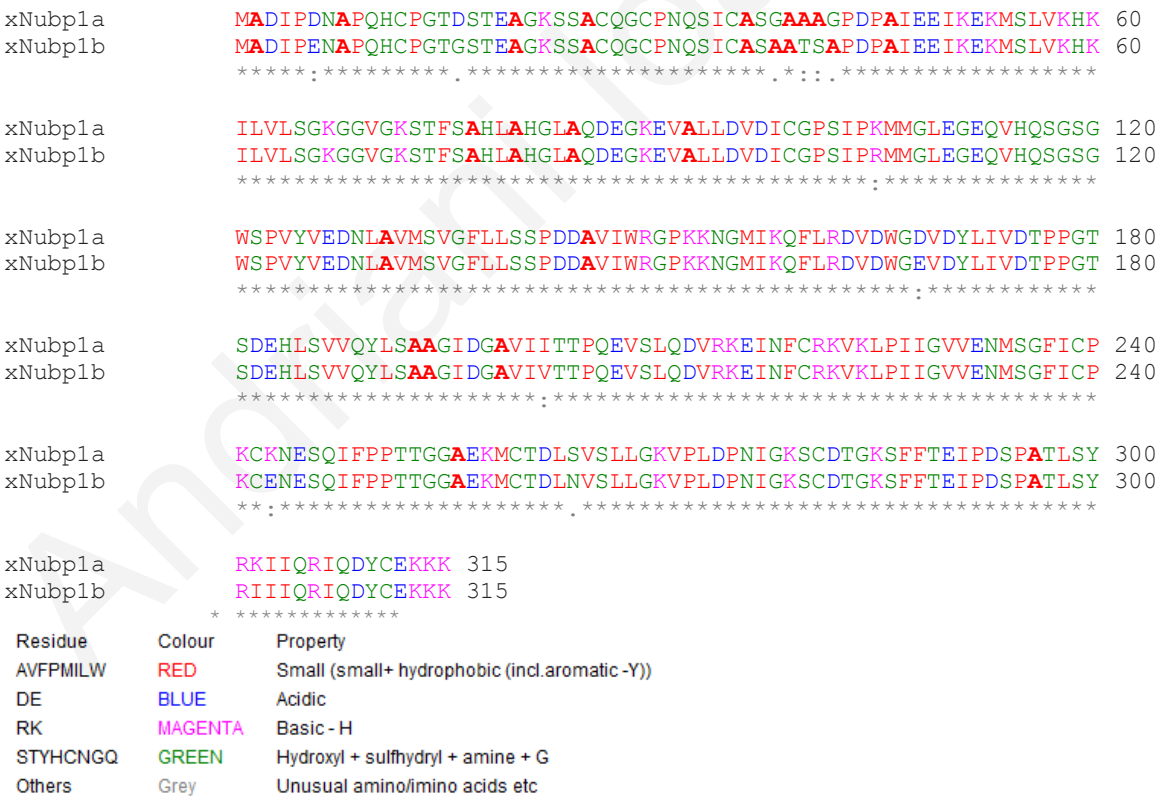

Figure 29. xNubp1 paralog amino acid alignment (ClustalW2).

xNubp1a and xNubp1b share 96% sequence identity. Amino acids are color coded according to their physicochemical properties. Asterisks indicate identical sequences.

4.2 Expression pattern of xNubp1

The temporal expression pattern of xNubp1 was examined by RT-PCR from oocytes and stage 8 to 34 embryos. xNubp1 expression was present at all stages (Figure 30A), indicating that xNubp1 is a maternal gene and is expressed throughout early development. This data is in agreement with the previously published data showing that Nubp1 is ubiquitously expressed throughout embryogenesis (6). We next used WISH to determine where in the embryo xNubp1 was expressed. During gastrulation, xNubp1 showed elevated expression in the animal hemisphere (Figure 30Bi). During neurulation, elevated xNubp1 expression was observed in the neural plate (stage 19) (Figure 30Bii) and at stage 22 expression expanded to the streaming cranial neural crest cells, the neural fold, the developing eye and to a small extent in the epidermis (Figure 30Biii). By stage 29/30, xNubp1 expression was observed in the otic placodes, developing eye, branchial arches, neural tube, heart anlage, pronephros and also weakly in the epidermis and somites (Figure 30Biv). These data show that xNubp1 is expressed in various tissues throughout development and its expression is elevated in neural tissues, which suggest a possible involvement of xNubp1 in neural development.

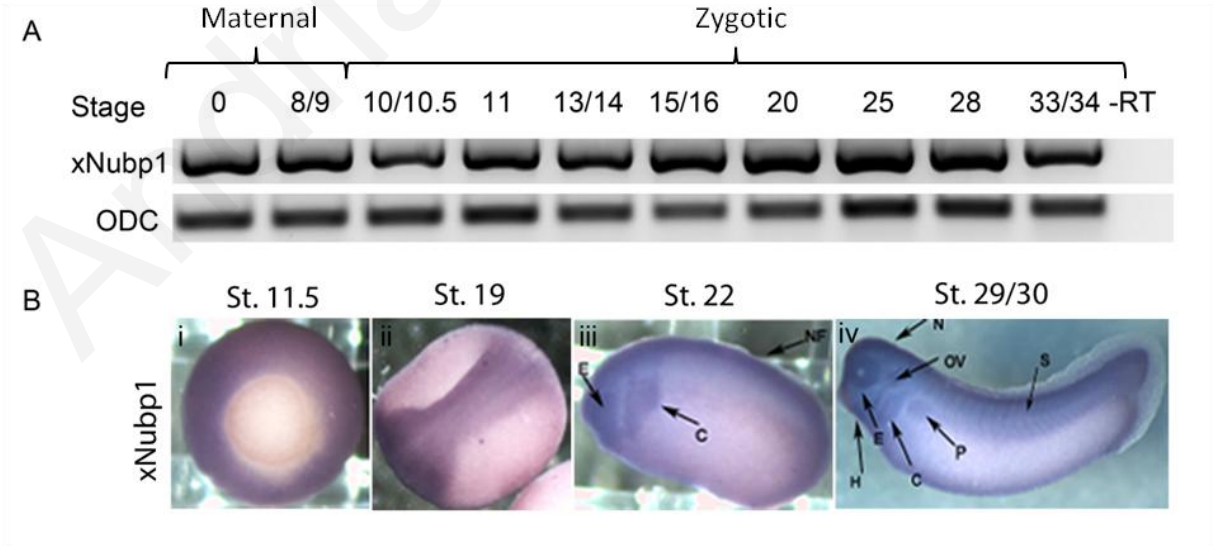

Figure 30. xNubp1 is a maternal gene expressed throughout development.

(A) RT-PCR of different stages of *Xenopus laevis* embryonic development. xNubp1 is expressed at all stages of embryonic development tested. (B) Whole-mount in situ hybridization to detect xNubp1 expression. (Bi) xNubp1 is expressed in the animal hemisphere. (Bii) xNubp1 expression is elevated in the neural plate. (Biii) Stage 22 embryos show expression in the neural folds [NF], presumptive eye [E] and neural crest cells [C]. (Biv) In stage 29/30 tailbuds, xNubp1 is expressed in the otic vesicle [OV], the eye, the branchial arches [B], neural tube [N], heart anlage [H] the pronephros [P] and also weak epidermal and somitic [S] expression is visible.

4.3 Nubp1 localization

4.3.1 Cell lines

Immunofluorescence (IF) experiments on paraformaldehyde (PFA) fixed mammalian and *Xenopus* cell lines using an antibody against a recombinant Nubp1 protein have shown that during interphase, Nubp1 localized to the nucleus and to a golgi apparatus-like structure just under the microtubule organizing center (MTOC) (Figure 31A,C,E). During mitosis, Nubp1 staining was observed on the spindle (Figure 26B, D, F). Both *Xenopus* cell lines tested also showed Nubp1 localization on certain actin fibers; specifically, stress fibers (Figure 32). In addition to the cross-linking fixative PFA, we also fixed cells using methanol, which precipitates out diffused proteins and is commonly used for viewing cytoskeletal components. Most of these cells lost the strong nuclear staining during interphase, but retained strong perinuclear staining as well as the golgi-like staining and during mitosis Nubp1 was still clearly visible on the spindle (Figure 33).

Nubp1 has been shown to localize at the centrosomes (7). However, using PFA and methanol fixation on *Xenopus* cell lines, we could not detect Nubp1 on the centrosomes. Therefore, in order to deplete cytosolic proteins which may be masking the Nubp1 signal on the centrosomes, we pre-extracted the cells using triton before fixation and IF. In addition to nuclear localization of Nubp1, antibody staining against Nubp1 and acetylated α-tubulin also showed localization of Nubp1 at what appeared to be the centrosome/basal body and along the axoneme of primary cilia (Figure 34). IF on pre-extracted cells also confirmed the Nubp1 spindle localization (Figure 35). These data are in agreement with previously published data

regarding Nubp1 localization in vitro, and also reveal that Nubp1 also localizes to the mitotic spindle.

To reinforce the IF data, we also examined the localization of xNubp1 in live cells by means of electroporation and confocal microscopy using a GFP fusion construct we generated (GFP-xNubp1). GFP-xNubp1 plasmid DNA was electroporated alone or with either RFP-Utrophin (an actin marker) or RFP-H2B (histone marker). Images and stills from timelapse movies showed that GFP-xNubp1 was mainly perinuclear during interphase (Figure 36A); however, some cells did exhibit staining within the nucleus. When mitosis began and the nuclear envelope broke down, we observed an abrupt translocation of xNubp1 to the nuclear space, and as mitosis proceeded, xNubp1 became concentrated on the mitotic spindle. Then, during roughly mid-anaphase, xNubp1 became concentrated to the central spindle (Figure 36B-D; Movies 1,2), which has been implicated in cytokinesis (130). Finally, during late-anaphase and telophase, in addition to being present on the central spindle, we also observed a transient burst of strong localization on the membrane, in the area where the contractile ring forms during cytokinesis (Figure 36E). These data indicate, as predicted due to homology, that xNubp1, like its mammalian counterpart, may be involved in cell division and cytokinesis.

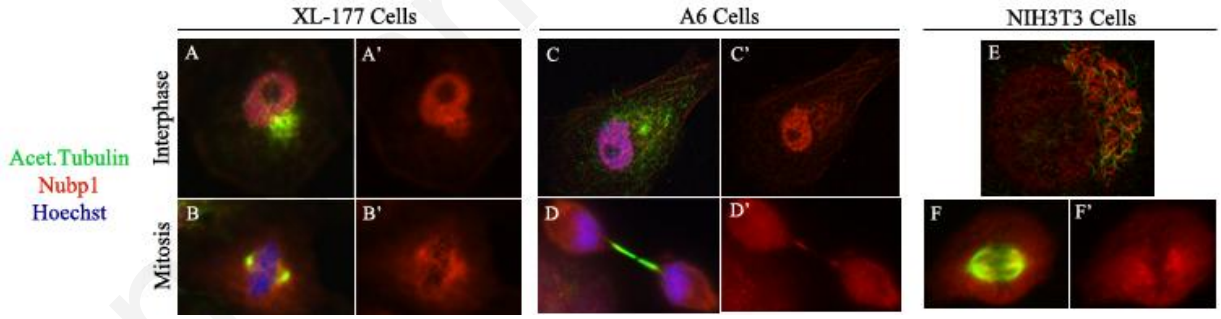

Figure 31. Localization of endogenous Nubp1 in vitro.

Immunofluorescence using rabbit anti-Nubp1 and anti-acetylated α-tubulin and Hoechst. In XL-177 *Xenopus* cell lines, Nubp1 is localized to the nucleus and golgi-like structures just under the MTOC during interphase (A) and the mitotic spindle during mitosis (B). In A6 *Xenopus* cells, Nubp1 localizes to the nucleus and golgi-like structures just under the MTOC during interphase (C) and to the mid-body during mitosis. In NIH3T3 mammalian cell lines Nubp1 is also detected in the nucleus and golgi-like structures just under the MTOC during interphase (E) and the mitotic spindle during mitosis (F).

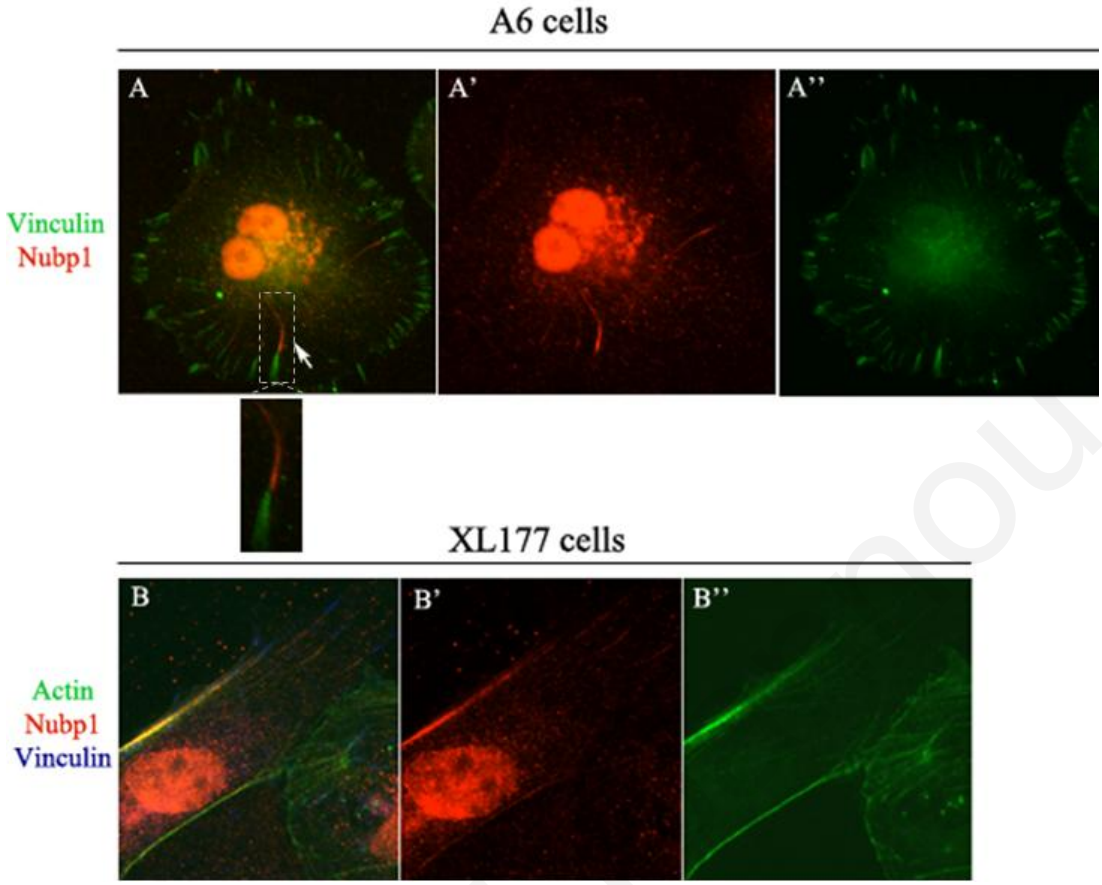

Figure 32. xNubp1 colocalizes with actin in *Xenopus* cell lines.

(A) IF on A6 cells shows distinct actin like structures (arrow and inset) which terminate where focal adhesions (indicated by Vinculin) begin. (B) IF on XL-177 cells shows co-localization between xNubp1 and actin *in vitro.*

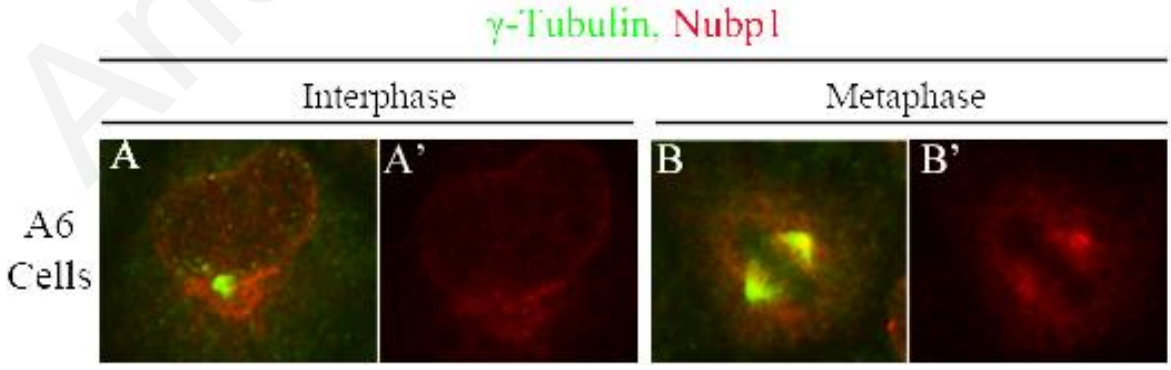

Figure 33. Methanol fixation of Xenopus cell lines.

IF on methanol fixed A6 cells shows (A) perinuclear localization of xNubp1 and in MTOC area at interphase and (B) on the spindle during mitosis.

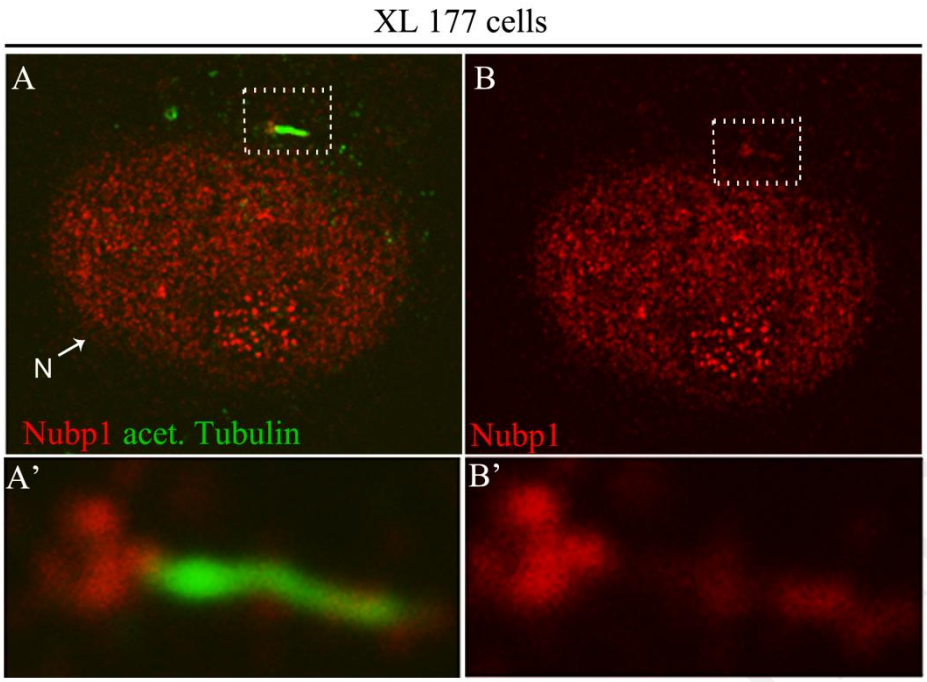

Figure 34. Pre-extraction of XL-177 *Xenopus* cell line.

IF on triton pre-extracted XL-177 cells shows (A-B) localization of xNubp1 in the nucleus (N) and at the basal body and along primary cilia axoneme. (A', B') Enlarged inlay of (A, B) showing Nubp1 colocalizing with primary cilium marked by acetylated tubulin and what appears to be the basal body.

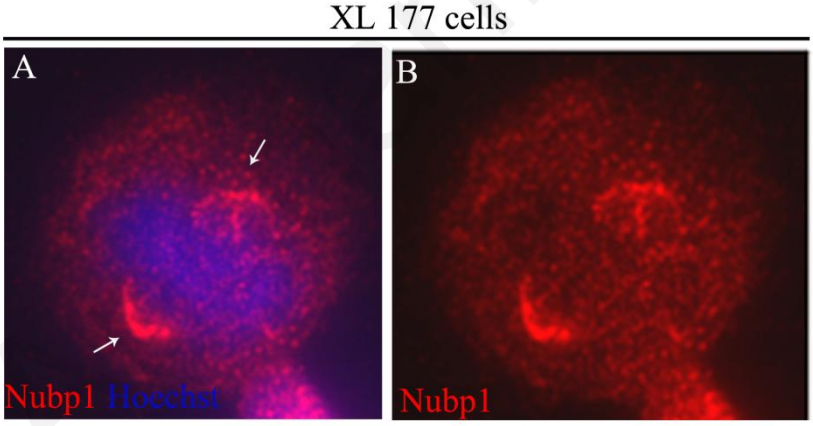

Figure 35. Spindle localization of Nubp1 in pre-extracted of XL-177 *Xenopus* cell line.

(A-B) IF on triton pre-extracted XL-177 cells shows localization of xNubp1 at the mitotic spindle (white arrows).

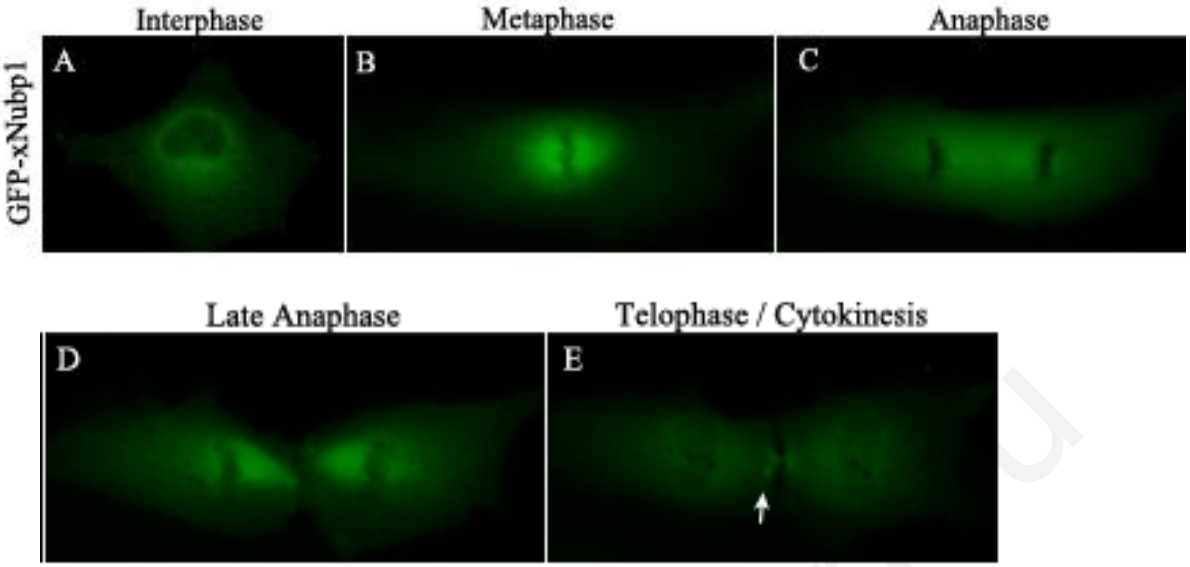

Figure 36. GFP-xNubp1 localizes to the spindle during mitosis.

Still images from a timelapse movie of GFP-xNubp1 electroporated A6 cells showing (A) perinuclear GFP-xNubp1 localization at interphase, spindle localization during; (B) metaphase, (C) Anaphase and on the (D) central spindle during late anaphase. (E) GFP-xNubp1 is observed on the membrane of the cleavage site during cytokinesis (arrow).

4.3.2 Xenopus embryos

After initial testing of the Nubp1 antibody by whole mount IF, we concluded that the antibody gave non- specific staining in *Xenopus* embryos. We therefore conducted all further experiments using exogenously expressed xNubp1. Exogenously expressed GFP-xNubp1 localized within the cytoplasm and was concentrated at the perinuclear area (Figure 37A). During mitosis however, when the nuclear envelope broke down, we observed an intense concentration of GFP-xNubp1 in the nuclear space (Figure 37A, C) and subsequently on the spindle in a similar fashion to what was observed *in vitro* (Figure 37B).

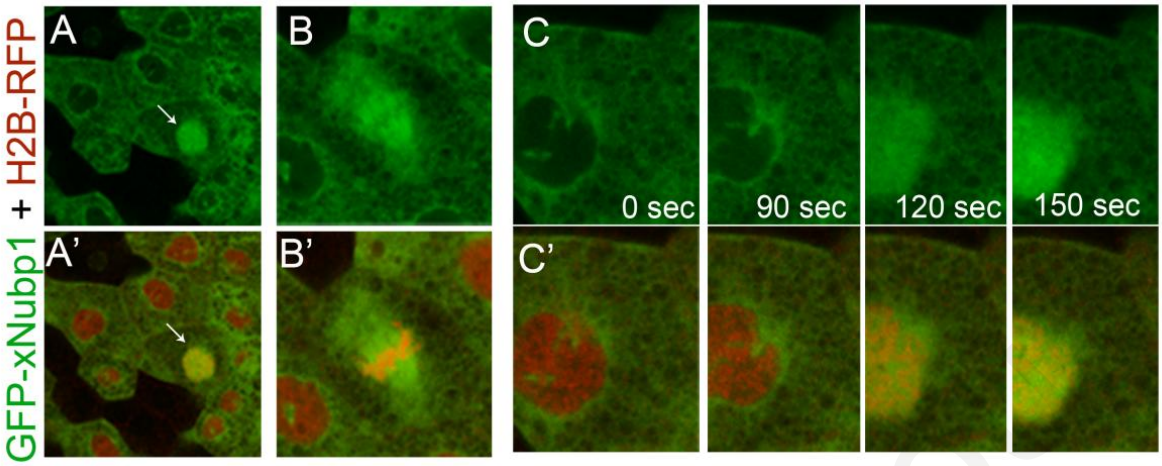

Figure 37. xNubp1 dynamics during mitosis in the embryo.

(A-C) Live fluorescent imaging during interphase and mitosis. (A) During Interphase, GFP-xNubp1 is localized within the cytoplasm and in the perinuclear region. Once the Nuclear envelope breaks down during prophase GFP-xNubp1 concentrates in the nuclear space (arrow). (B) During metaphase, GFP-xNubp1 is localized on the spindle. (C) Stills from a time-lapse video showing influx of GFP-xNubp1 in the nuclear space once the nuclear envelope breaks down.

4.3.2.1 xNubp1 localizes to apical actin network and ciliary axonemes

Using the GFP tagged variant of Nubp1, we saw that xNubp1 co-localized with the apical actin cytoskeleton in multiciliated epidermal cells (Figure 38 A-C) and at distinct puncta along the ciliary axonemes. To validate these findings, both FLAG and HA tagged versions of Nubp1 were also generated, and both gave similar results (Figures 38 D-F and 39).We went on to examine the possibility of direct binding of Nubp1 on actin and carried out co-immunoprecipitation using tagged versions of xNubp1. However, no association between actin and xNubp1 was detected, suggesting that xNubp1 may be interacting with actin indirectly or interacting specifically with F-actin.

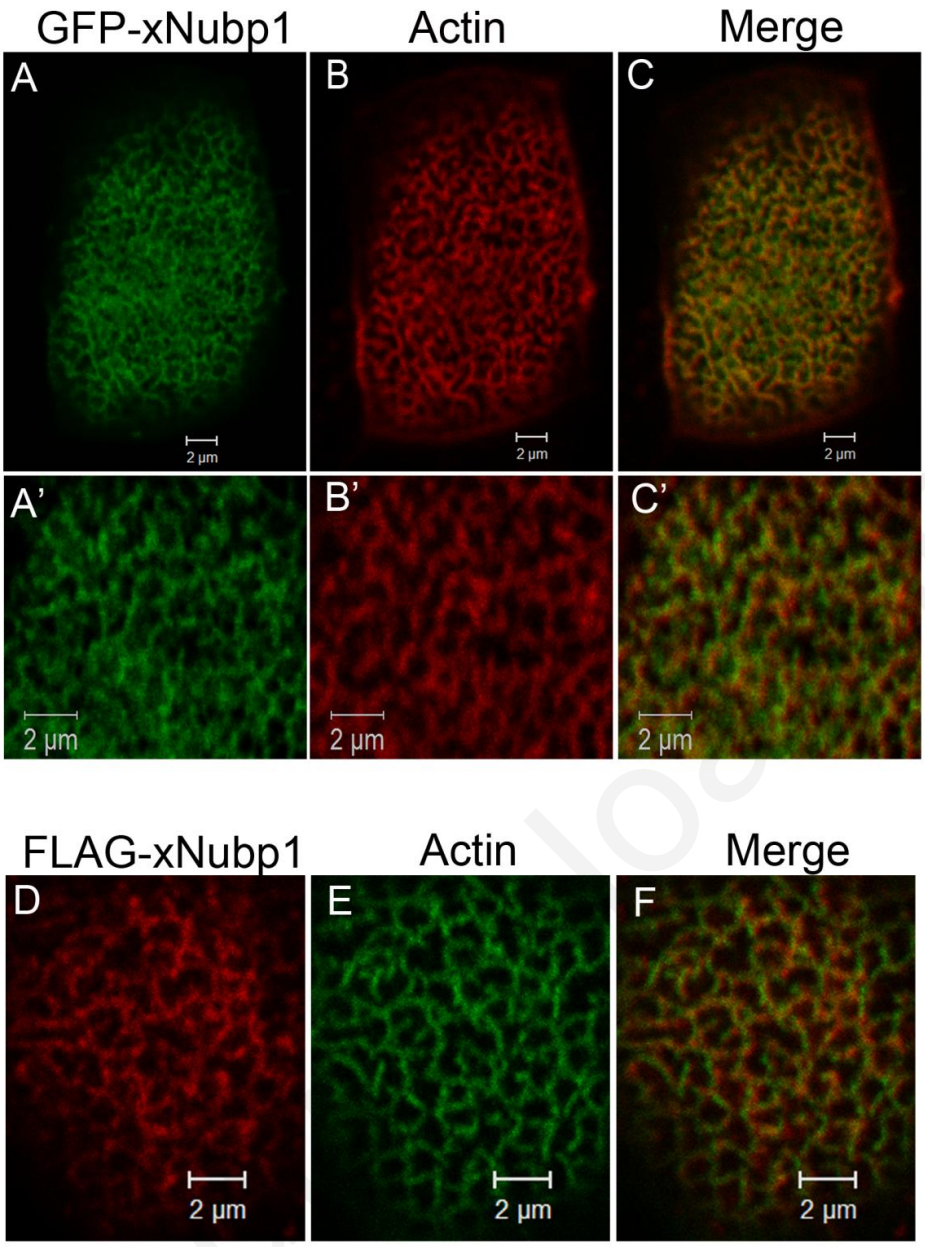

Figure 38. xNubp1 colocalizes with apical actin in multiciliated cells.

Immunofluorescence on stage 31 embryos expressing GFP-xNubp1 (A-C) or FLAG-xNubp1. (D-F) using phalloidin (binds F-actin) shows co-localization of xNubp1 and actin at the apical surface of ciliated cells.

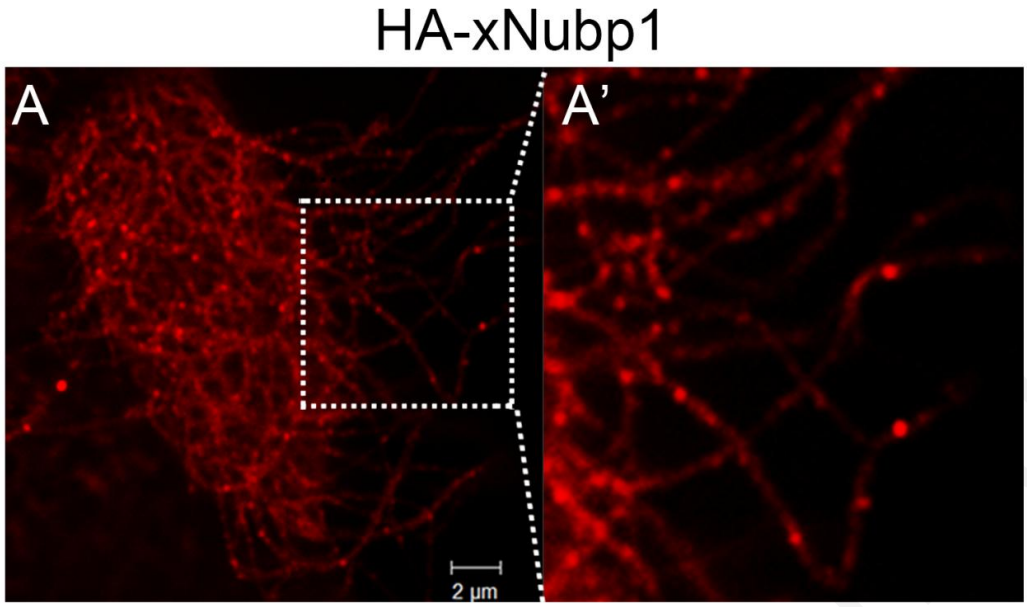

Figure 39. xNubp1 localizes to puncta on ciliary axonemes.
Immunofluorescence of stage 31 embryo expressing HA-xNubp1. (A) xNubp1 can be seen at distinct puncta along the ciliary axonemes. (A') Enlarged inlay of (A) showing a individual xNubp1 puncta along the cilia.

4.3.3 Nocodazole treatment of GFP-xNubp1 expression cells in vitro and in embryos

In order to determine if the localization of xNubp1 to the perinuclear area, the MTOC and the spindle was related to a direct or indirect association with microtubules we treated tailbud stage GFP-xNubp1 injected embryos and electroporated *Xenopus* cell lines with nocodazole; a microtubule destabilizing agent, and imaged the embryo and cells in real-time. In interphase cells *in vitro*, we observed that the strong perinuclear and MTOC localization of GFP-xNubp1 became less intense and GFP-xNubp1 diffused after nocodazole treatment (Figure 40A) and slowly began returning after nocodazole washout (Figure 40B). *In vivo*, we also observed a diffusion of the spindle localization of GFP-xNubp1 during mitosis (Figure 41). These data show that the localization pattern of xNubp1 is indeed determined by an association Nubp1 either directly or indirectly with the microtubule network. This is consistent with previously published work showing that mammalian Nubp1 binds KifC5A, a kinesin superfamily protein (7). KIFs have been shown to transport membranous organelles and protein complexes in a microtubule- and ATP-dependent manner.

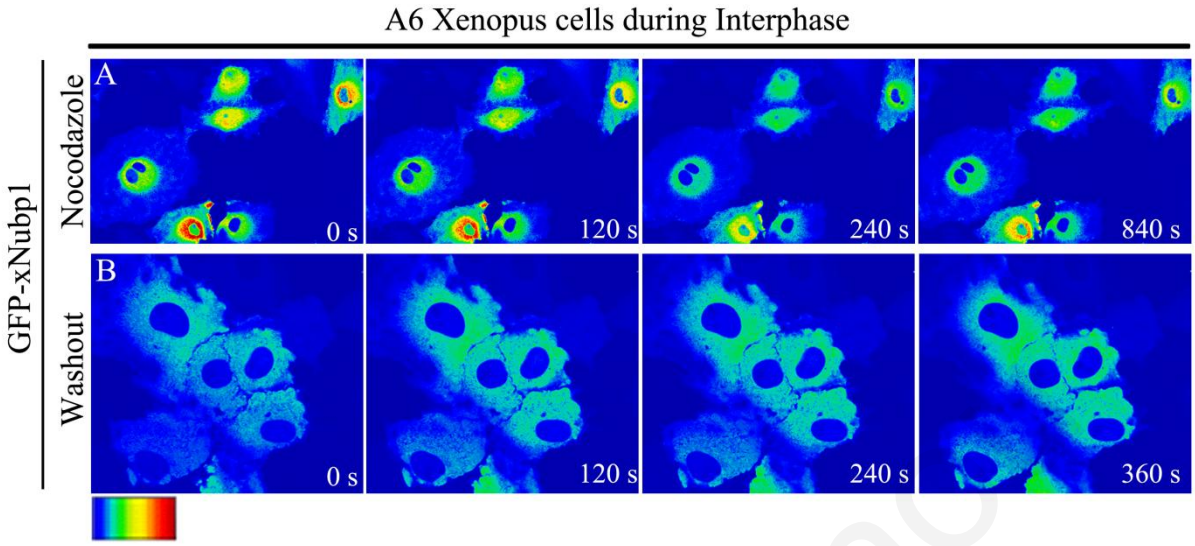

Figure 40. Nocodazole treatment causes a diffusion of xNubp1 signal during interphase in vitro. Color-coded still images taken from time-lapse movies. Colors indicate increasing levels of intensity (from blue to red) of GFP-xNubp1. (A) Nocodazole treated GFP-xNubp1 electroporated A6 cells. As time progresses, you can see the concentrated perinuclear localization becoming less intense (from red to yellow or even to green). (B) Images after nocodazole washout show the diffuse signal slowly intensifying (from blue to green) and becoming more concentrated perinuclear.

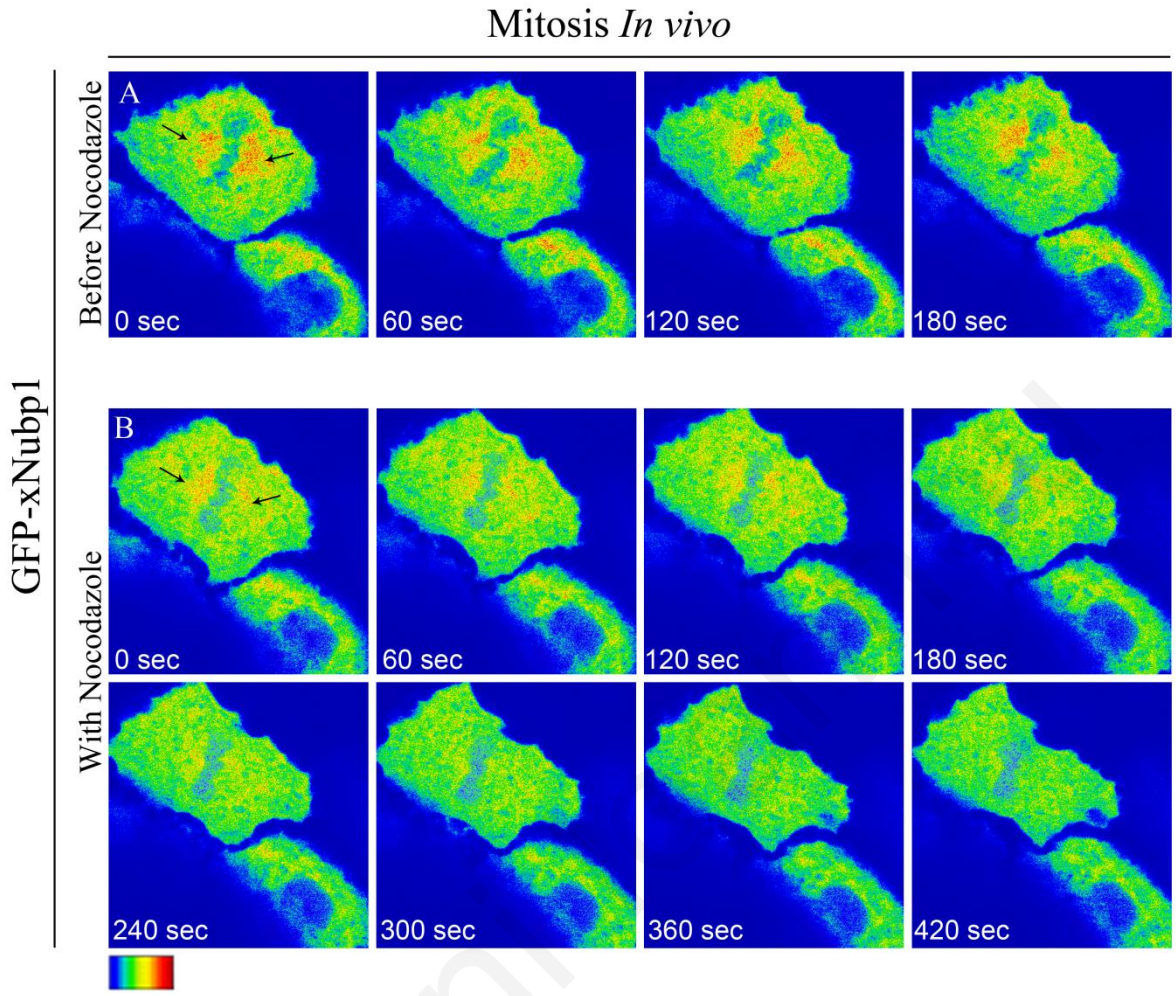

Figure 41. Nocodazole treatment causes a diffusion of xNubp1 signal from mitotic spindle *in vivo*. Color-coded still images taken from time-lapse movies. Colors indicate increasing levels of intensity (from blue to red) of GFP-xNubp1. (A) Time-lapse images showing GFP-xNubp1 spindle localization (black arrows). (B) With the addition of nocodazole the strong spindle localization (green area) becomes more diffuse with time as indicated by the color shift from green to blue.

4.4 Gain and loss of function of xNubp1

Overexpression of xNubp1 did not lead to any developmental phenotypes. In order to explore the role of Nubp1 in *Xenopus* development further, we carried out loss of function experiments using antisense morpholino oligonucleotides (MOs). To deplete xNubp1 at the protein level, we designed three distinct morpholinos (MO1, MO2 and SpMO) (Table 5). Two of the three xNubp1 MOs were translation blocking MOs targeting separate areas of the xNubp1 mRNA. xNubp1-MO1 targeted a sequence identical to both xNubp1 paralogs (xNubp1a and xNubp1b) and xNubp1-MO2 targeted a sequence which was not identical to both paralogs and was more effective against xNubp1a mRNA. We also obtained a general control MO (CoMO) and designed an xNubp1 specific 5-base pair mismatch control MO (mmMO) (Table 5). We tested the efficiency of the translation blocking MOs by co-injection of the MOs with an xNubp1 surrogate containing the sequence recognized by the MOs (Figure 42A, B). The third MO (SpMO) was a splice blocking MO which targeted the exon1- intron1 splice junction of xNubp1 pre-mRNA. This led to an intron inclusion of intron1 (94 base pairs) which in turn led to a premature stop codon (Figure 42C). The efficiency of this morpholino was examined using RT-PCR. Morphant embryos retained xNubp1 intron 1 (Figure 42D). At high amounts of SpMO (68ng) the correctly spliced xNubp1 transcript is entirely absent (Figure 42D). Embryos injected with more than 60ng of any of the three MOs but not the CoMO or mmMO died before completing neurulation which is in agreement with previous studies showing that Nubp1 is required for cell survival (2, 4, 21).

MO Name & Sequence	Target Sequence
xNubp1 MO #1 5'-GTATATCAGCCATGCCTGCGAAAAA-3'	CCAATTCAAGATGCAATTATTGAAACGA GGCTTGGAACGCAAAGAGCATATCGGAA GCAGGAAGTG[TTTTTCGCAGGC(ATG)GC TGATATAC]CAGATAATGCAC
xNubp1 MO #2 5'-CACTTCCTGCTTCCGATATGCTCTT-3'	CCAATTCAAGATGCAATTATTGAAACGA GGCTTGGAACGCA[AAGAGCATATCGGAA GCAGGAAGTG]TTTTTCGCAGGC(ATG)GC TGATATACCAGATAATGCAC
xNubp1 SpMO (Exon1-Intron1boundary) 5'-ACTTTTCCTTTTTTACTCACGCTGG-3'	(ATG)GCTGATATACCAGATAATGCACC[C CAGCGTGAGTAAAAAAGGAAAAGT]AAT GCTTTCAGTTAGTTTTGAAGGTGGTCTTC ATTTCTTTTACATTGTGTTAATCAAAGTTA CTTTCAATACAGATTGCCCAGGTACAGAC AGTACTGAGGCTGGCAAGAGTTCT
xNubp1 5bp mismatch MO 5'- GTATATGAGCGATCCCTCCCAAAAA-3'	CCAATTCAAGATGCAATTATTGAAACGA GGCTTGGAACGCAAAGAGCATATCGGAA GCAGGAAGTG[TTTTTCGCAGGC(ATG)GC TGATATAC]CAGATAATGCAC
xNubp2 MO 5'-TTTCCCCCATCCTGAGTCTGCTCAT-3'	CCGCCTCCTAGAAGTCCTGAATGGGAGCC TAATGTAGCCTTCTGTTCGCTGATTGGTG GGTGGATGTATCCATCTTTTTACATGCGG AAGTAGGTCTGAAGC[(ATG)GAGCAGACT CAGGATGGGGGAAA]TCTTTCCGGGGTGC

Table 5. Sequences and target sequences of MOs used.

Blue = MO target Red = Start codon Green = mismatched base pairs

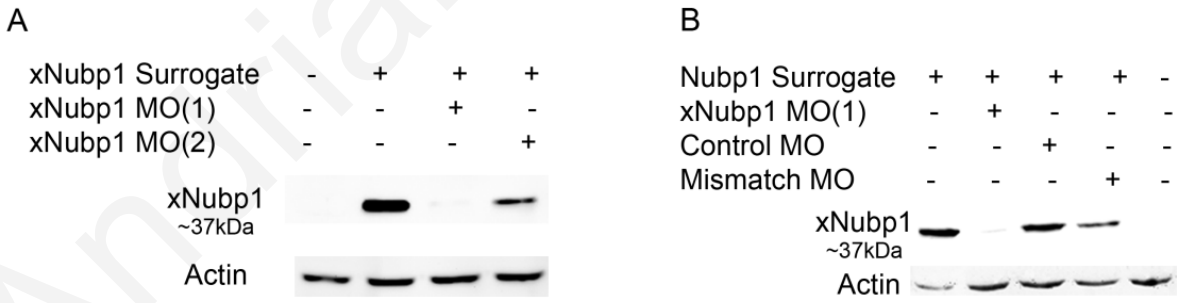

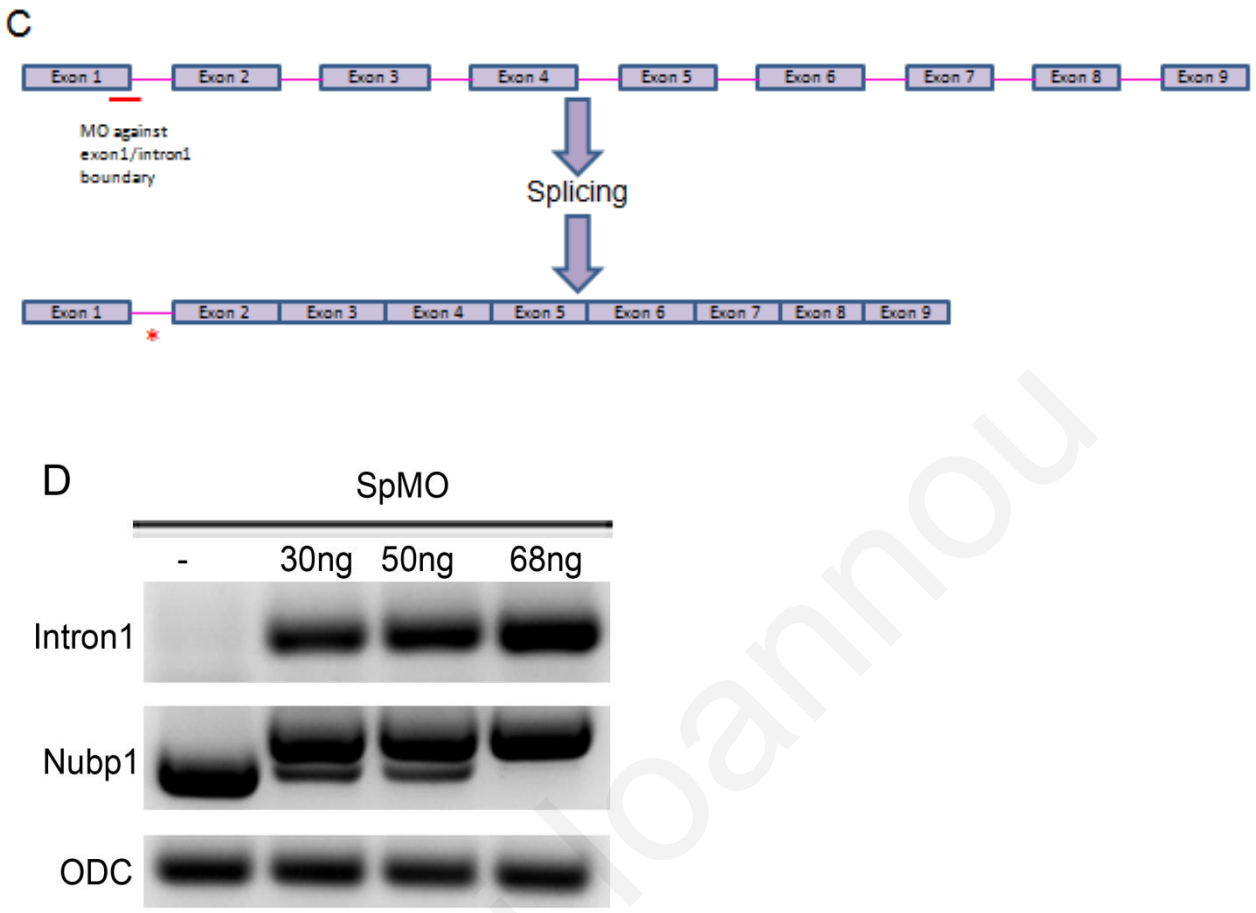

Figure 42. xNubp1 MO specificity.

(A-B) Western blots using Xenopus embryo lysates. xNubp1 surrogate mRNA (240pg total) and Morpholinos (25ng total) were injected at the one cell stage. xNubp1 MO1 and MO2 block translation of xNubp1 surrogate mRNA. Control Mo (CoMO) does not knock down xNubp1 protein expression. xNubp1 mismatch MO does not significantly block xNubp1 translation, however it does have some underlying activity at this amount. (C) Schematic showing target of SpMO. Red asterisk depicts a premature stop codon (D) RT-PCR across the splice junction targeted by xNubp1 SpMO. Intron 1 is absent from the normally spliced product, but is retained in morphant embryos. PCR using primers for exon one and exons 4/5 shows that the morphants have transcripts which are slightly larger than the control transcript. Embryos injected with a total of either 30 or 50ng of SpMO also have a small amount of the original functional transcript. However, with 68ng of SpMO there is a complete loss of the original xNubp1 transcript.

4.5 Role of xNubp1 during neurulation

4.5.1 xNubp1 is involved in convergent extension and neural tube closure

Due to the elevated expression levels of xNubp1 in neural tissues, we initially targeted the MOs into the 2 dorsal blastomeres at the 4 cell stage. xNubp1 morpholino injected embryos (morphants) began showing dose dependent developmental defects from the onset of neurulation. Morphants from all three MOs (10-25ng) exhibited delays and defects in neural tube closure (95%; n=60) (Figure 43A) and had shortened trunks (shorter along the anterior-posterior axis) (100%; n=73) (Figure 43B, C). Although the neural tube did eventually close in most xNubp1 morphants, roughly 8% (n=60) of morphant embryos displayed a failure of posterior neural tube closure (Spina bifida) leading to an open-back phenotype (Figure 43B). The frequency of this phenotype increased (15-20%; n=50) at higher amounts of MO (25-35ng). At these amounts, we also observed embryos which lacked some anterior structures (20%; n=50) (Figure 43C). The neural tube closure and axis elongation phenotypes were suggestive of a defect in convergent extension (CE). These defects could be partially rescued by co-injection of xNubp1 mRNA with MOs (Figure 43A, C-E), suggesting that the phenotypes were specific and induced due to loss of xNubp1. Embryos injected on one side curved towards the side of injection (75.5%, n=80) (Figure 43E middle panel), which also pointed to a problem with CE. Co-injection of xNubp1 mRNA with MOs also rescued the curved embryo phenotype (Figure 43E, last panel). 80% of the embryos were no longer curved, roughly 16% had a slight curve and only about 4% of the embryos were not rescued (n=122). As mentioned above, all three MOs induced very similar phenotypes, while the two control MOs did not elicit any phenotype (Figure 43C, D, F; Figure 44), providing further evidence that the phenotype was specific. In order to determine whether CE was in fact affected by the depletion of xNubp1, we conducted an *in vitro* elongation assay. We observed that morphant caps did not undergo convergent extension to the same degree as control caps (Figure 43F). Overall, these data suggest that the loss of xNubp1 leads to convergent extension related defects.

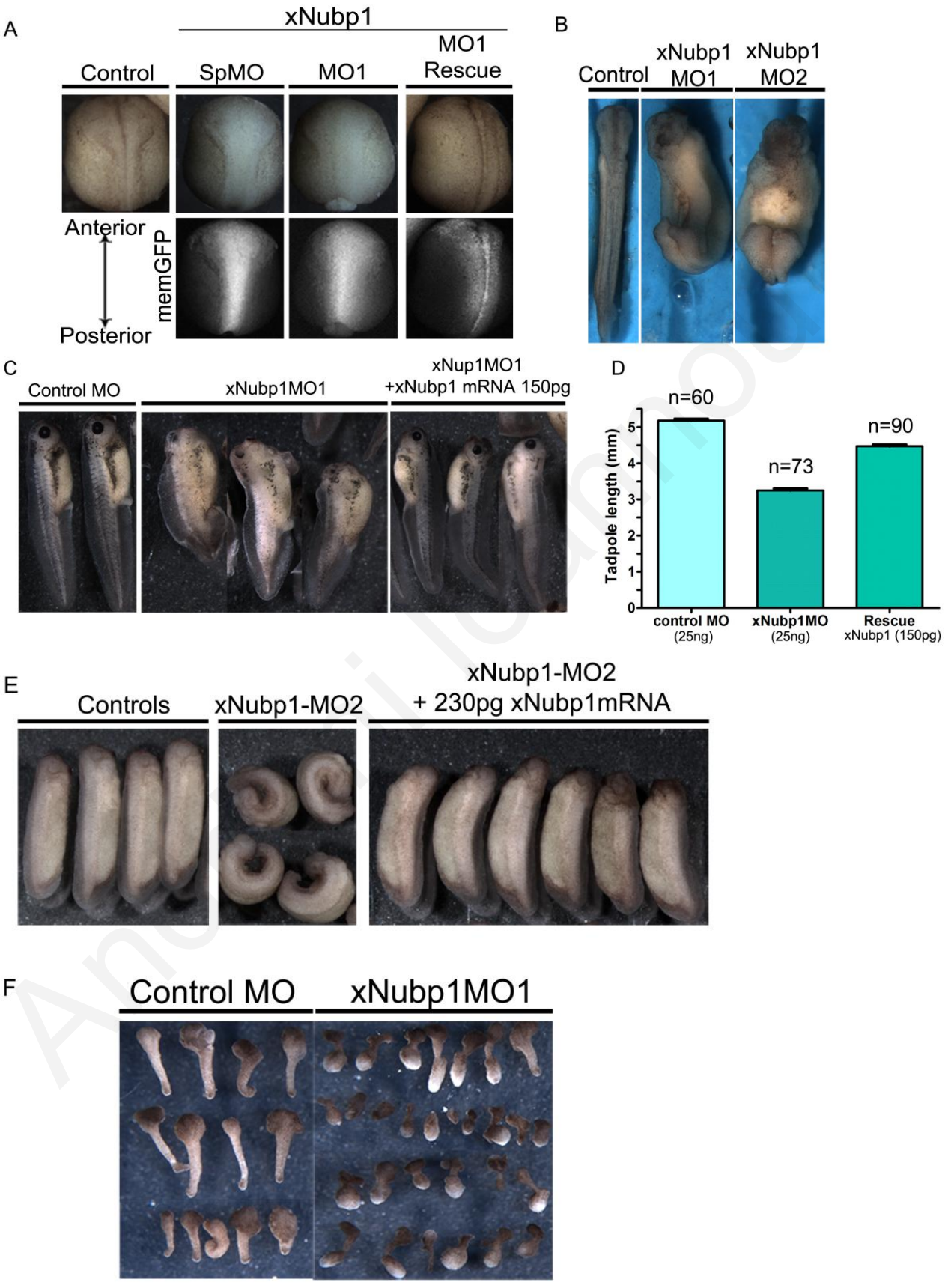
A
xNubp1
Control
SpMO
MO1
MO1 Rescue
Anterior
memGFP
Posterior
B
Control
xNubp1 MO1
xNubp1 MO2
C
Control MO
xNubp1MO1
xNup1MO1 +xNubp1 mRNA 150pg
D
n=60
n=73
n=90
Tadpole length (mm)
0
1
2
3
4
5
control MO (25ng)
xNubp1MO (25ng)
Rescue xNubp1 (150pg)
E
Controls
xNubp1-MO2
xNubp1-MO2 + 230pg xNubp1mRNA
F
Control MO
xNubp1MO1

Figure 43. xNubp1 knock-down causes failure of neural tube closure and other CE related phenotypes.

(A) Dorsal view of stage 19/20 embryos injected in the dorsal blastomeres at the four cell stage. xNubp1 SpMO (17ng) and MO1 (25ng) injected embryos show a delay in neural tube closure and an open neural plate. Co-injection of MO1 (25ng) with 200pg xNubp1 mRNA rescued neural tube closure delay. (B) Dorsal view of a stage 28 uninjected control embryo, xNubp1- MO1 and MO2 injected embryos (~35ng). Morphants have an open back due to posterior neural tube closure failure. (C) xNubp1-MO1 (~25ng) tadpoles have a shortened axis. Co-injection of xNubp1 mRNA partially rescues the shortened axis. (D) Bar chart showing the average length of Stage 37/38embryos from three separate experiments. Error bars indicate standard error of the mean (SEM). Control embryos had mean length of 5.18 ± 0.046 mm, morphants displayed a mean length of 3.24 ± 0.05mm and rescues showed a mean length of 4.47 ± 0.046 mm. (E) Injection of xNubp1 MO2 (15ng) in 1 of 4 dorsal blastomeres leads to curved embryos. This can be rescued by co-injection with xNubp1 mRNA. (F) xNubp1 MO1 and CoMO (25ng) injected caps induced with activin. xNubp1 MO injected caps do not elongate as well as controls.

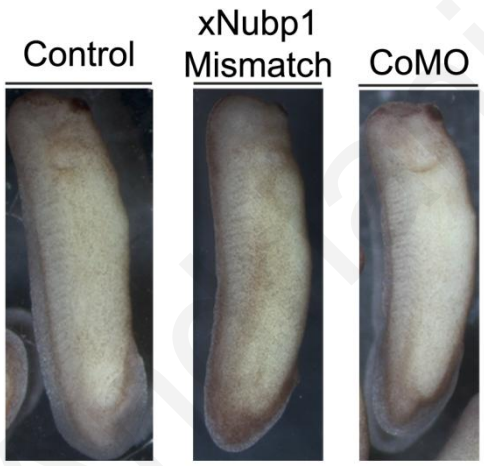

Figure 44. Control MOs do not cause developmental phenotypes.

General control MO (CoMO) and xNubp1 specific five base-pair mismatch MO (mmMO) do not elicit a phenotype.

4.5.2 xNubp1 knockdown affects apical constriction during anterior neural tube closure

In addition to posterior NTC defects (Section 3.5.1), xNubp1 morphant embryos also displayed defects in anterior NTC. In some xNubp1 MO injected embryos, the anterior most section of the neural tube failed to close (Figure 45). This defect could not solely be explained by a problem with CE due to the fact that the morphogenetic movement which is essential for anterior NTC is apical constriction (58) and not CE. Actin is highly concentrated at the apical surface of neuroepithelial cells during apical constriction and neural plate bending, and plays an important role in generating the physical forces required for bending the neural plate and elevating the neural folds (67). Since xNubp1acts by regulating the actin cytoskeleton in ciliated cells (Section 3.6.6), we hypothesized that xNubp1 knockdown may lead to neural tube closure defects by affecting actin organization.

xNubp1 morphants were fixed at stage 17 and stained with fluorescently labeled Phalloidin, which binds to F-actin. The embryos were then cross-sectioned and the neural plate was imaged using a laser scanning confocal microscope. Neuroepithelial cells in control embryos were elongated and their apical surface was highly constricted and actin was concentrated apically, thus making the medial hinge point clearly visible (Figure 46A). Unilateral injection of xNubp1MOs blocked elevation of the neural tube only on the injected side and cells showed little or no apical constriction or apical accumulation of actin (Figure 46B, C). Apical constriction did however occur on the uninjected side, which led to the formation of a laterally displaced "medial" hinge point which was not at the midline, but towards the uninjected side (Figure 46B, C arrows). These data suggest that xNubp1 may be facilitating the accumulation or organization of apical actin in neural plate cells and demonstrate that the loss of xNubp1 blocks hinge point formation and apical constriction, leading to defects in the shaping of the neural plate and elevation of the neural folds.

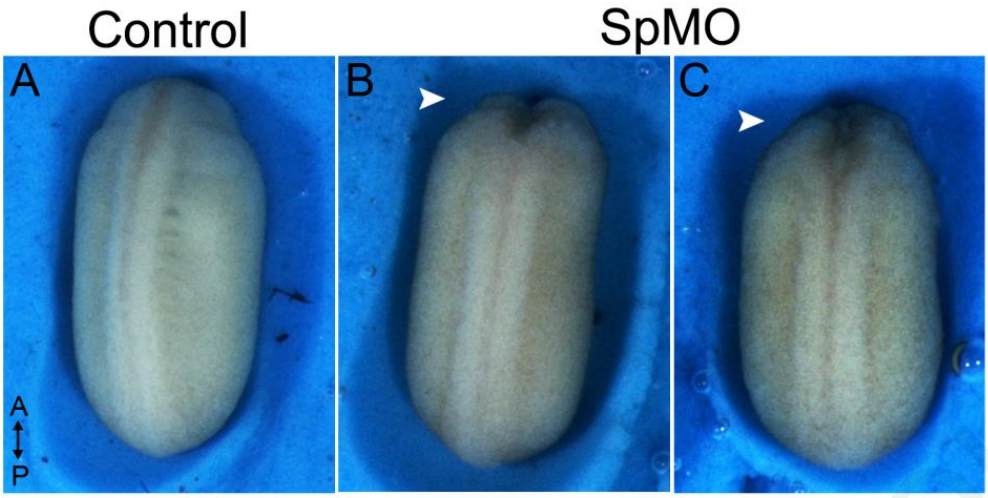

Figure 45. xNubp1 morphants have anterior neural tube closure defects.

(A) Dorsal view of a stage 20/21 control embryo. (B, C) Stage 20/21 xNubp1 morphant embryos injected with 15 ng SpMO per dorsal blastomere at the four cell stage. White arrowheads indicate open anterior neural plate.

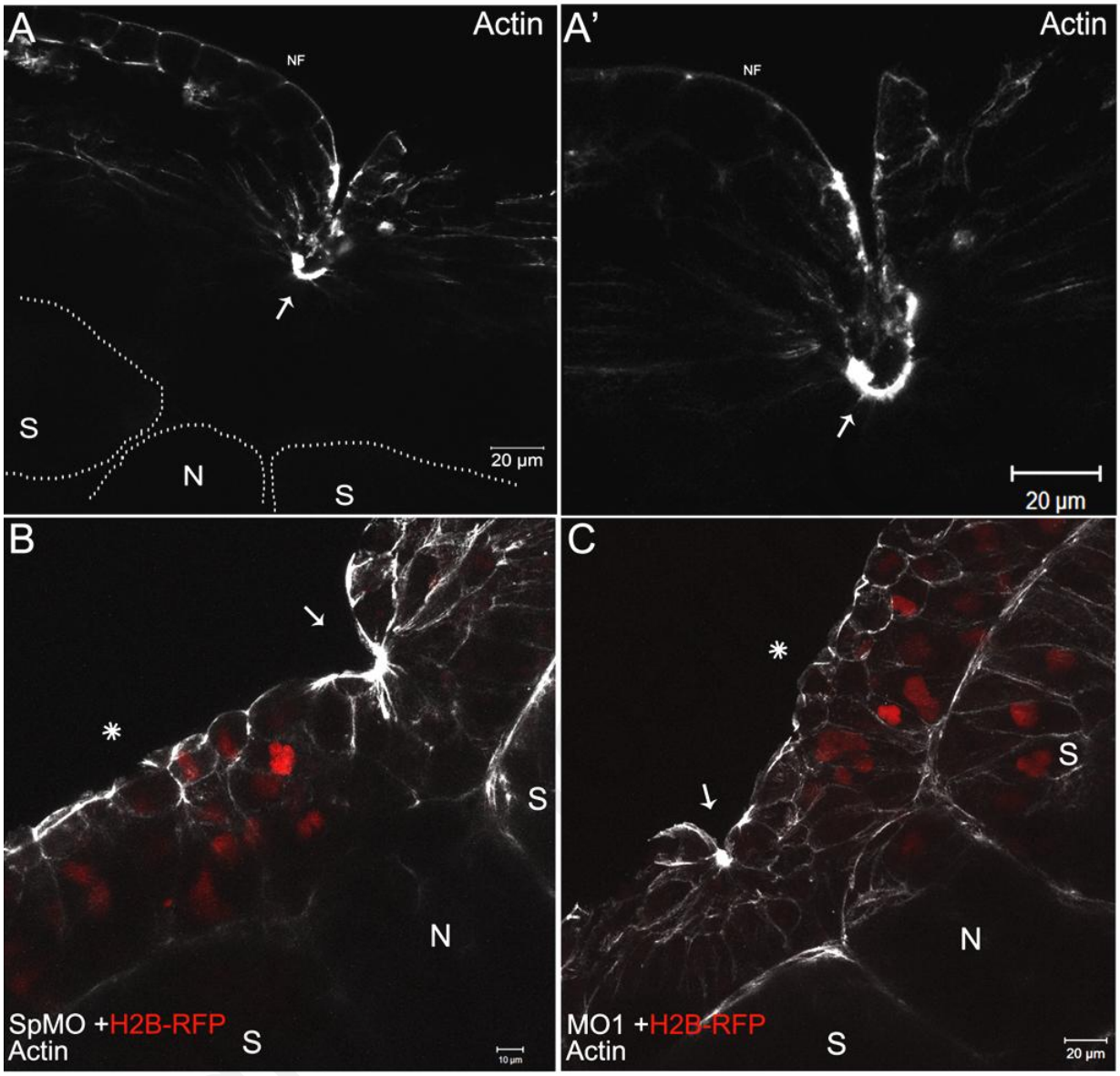

Figure 46. Loss of xNubp1 leads to defects in apical constriction and hinge point formation.

(A-C) Cross-section of the anterior neural plates of stage 17 embryos stained with phalloidin to mark actin. (A) In control embryos, actin accumulates apically in cells undergoing apical constriction (arrow; hinge point). This allows the neural folds (NF) to elevate. The medial hinge point forms at the midline, generally right above the notochord (N), which is flanked by the somites (S). (A') Enlarged view of (A). (B, C) SpMO (B; 13ng) and MO1(C; 15ng) unilaterally injected xNubp1 morphants co-injected with a histone maker (H2B-RFP) as a lineage tracer. No apical accumulation of actin is observed in xNubp1 MO positive cells. These cells fail to undergo apical constriction and the neural plate does not elevate in the injected side (asterisks). However, the cells on the uninjected side accumulate apical actin and undergo apical constriction to form a hinge point (arrows). The hinge

points do not form at the midline but are displaced laterally and now form above somites (S) or at the notochord (N)-somite boundary.

4.5.3 xNubp1 knockdown does not affect germ layer specification

In order to examine if the developmental defects elicited by the morpholinos were due to problems with cell fate specification, we carried out whole mount *in situ* hybridization (WISH) on MO injected and control embryos. We used probes against the neural markers Sox2, Pax3 and N-tubulin, the neural crest marker Twist (Figure 47) and the mesodermal markers; chordin, and MyoD (Figure 48). These experiments showed that both neural and mesodermal specification were unaffected in morphant embryos, and suggested that the observed morphogenetic defects were not due to changes in either mesodermal or neural specification. In addition, from the *in situ* experiments it also became clear that the neural plate in morphant embryos was indeed wider than that of control embryos, confirming the effects of xNubp1 down regulation on neural tube closure (Figure 47AII).

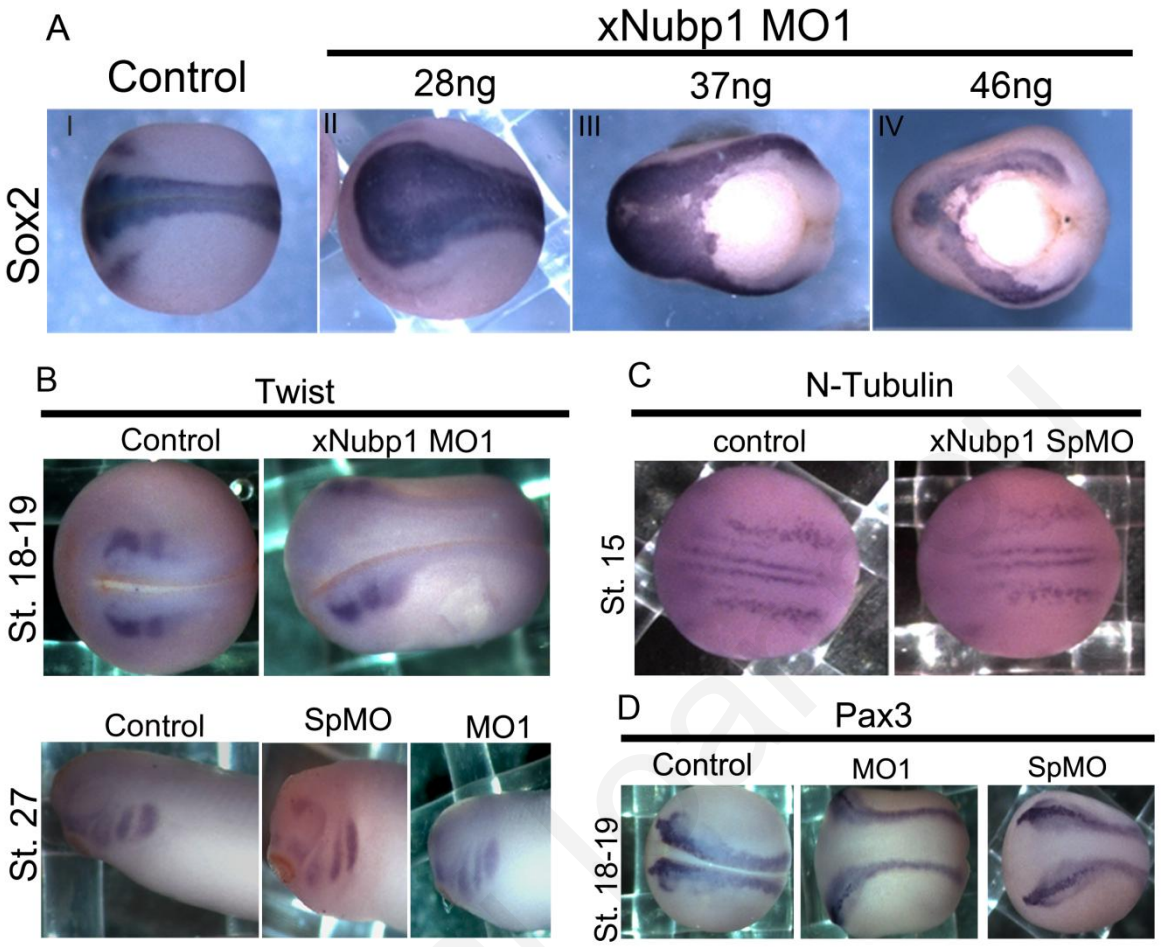

Figure 47. xNubp1 knock-down does not affect neural specification.

Control and morphant embryos processed by whole mount in situ hybridization to visualize expression of neural markers. (AII-IV) *Sox2* is expressed in morphants with varying concentrations of MO. Neural plates are significantly wider than in controls. (B) Expression of the neural crest marker *xTwist* is not affected in xNubp1 morphants. Neural crest cells migrate normally in xNubp1 morphants. 30 ng of SpMO was injected at the 1 cell stage. 25ng of MO1 was injected into both blastomeres at the 2 cell stage. (C) The early neural specification marker *N-tubulin* is expressed in xNubp1 embryos injected with SpMO (13ng; 2of2). (D) Expression of the dorsal neural marker *Pax3* was also unaffected in xNubp1 morphants injected with either MO1 (24ng 20f2) or SpMO (15ng 2of2). The delay in neural tube closure is also apparent in these embryos.

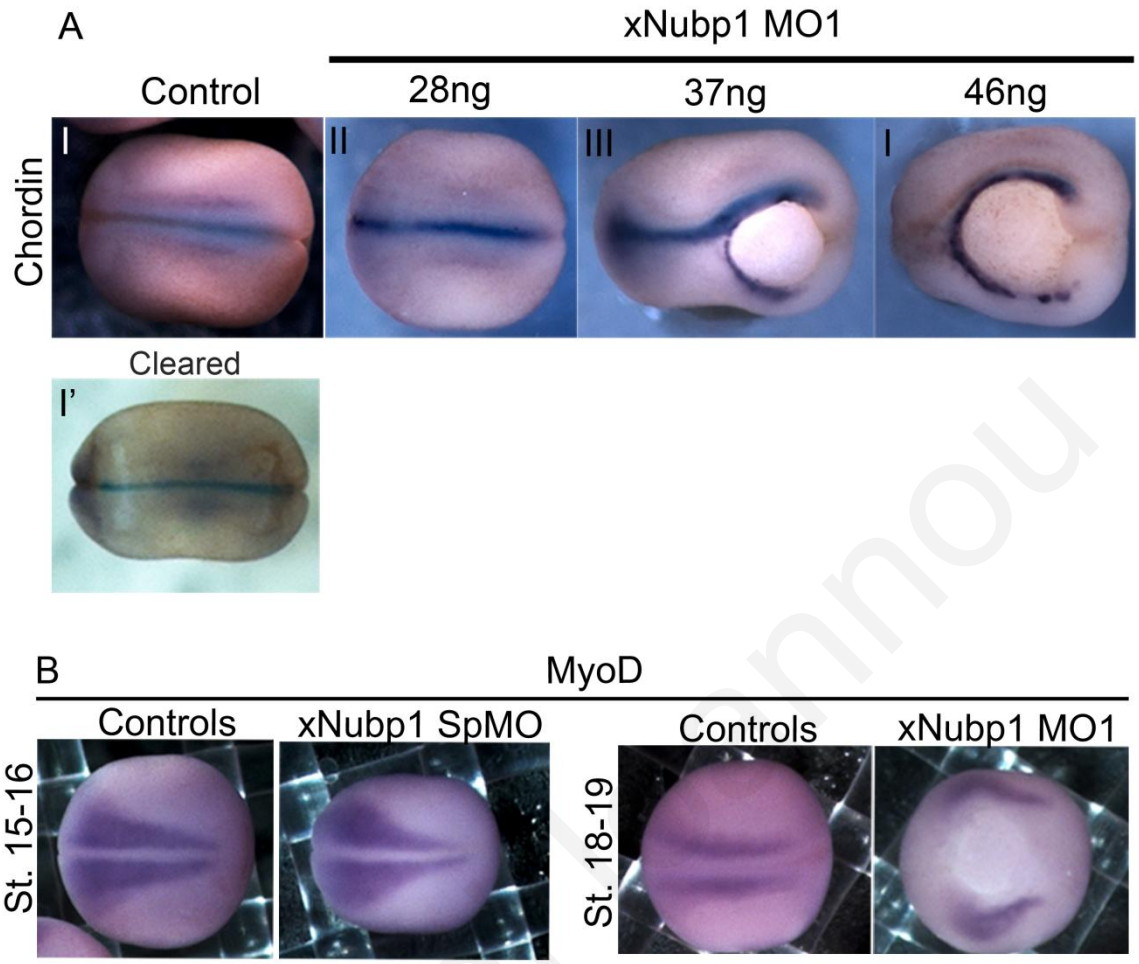

Figure 48. xNubp1 knock-down does not affect mesodermal patterning.

Control and morphant embryos processed by whole mount *in situ* hybridization to visualize expression of mesodermal markers. (AI-IV) Chordin is expressed in all morphant embryos; however the staining appears more intense due to fact that chordal mesoderm is exposed due to the open neural tube. (B) Expression of the mesodermal marker *MyoD* is not effected in xNubp1 MO1 (25ng per blastomere at the 2 cell stage) and SpMO (15ng per blastomere at the 2 cell stage) morphants.

4.5.4 Apoptosis in xNubp1 morphants

Although xNubp1 was observed at the mitotic spindle, when injecting the amounts of MO needed to elicit a phenotype without causing embryonic lethality (10-45ng), we could not detect any defects in mitosis similar to those observed when Nubp1 was depleted *in vitro* (7, 21). However, whole mount TUNEL assay on morphant embryos did show a considerable

amount of apoptosis from tailbud stages onwards, particularly in neural tissues (Figure 49). Therefore, even though mitotic defects such as multiple spindles could not be detected *in vivo*, the observed increase in apoptosis indicates that xNubp1depletion may indeed be affecting mitosis, which is in agreement with previous studies regarding Nubp1 function in cell survival (2, 4, 21) and during mitosis (7).

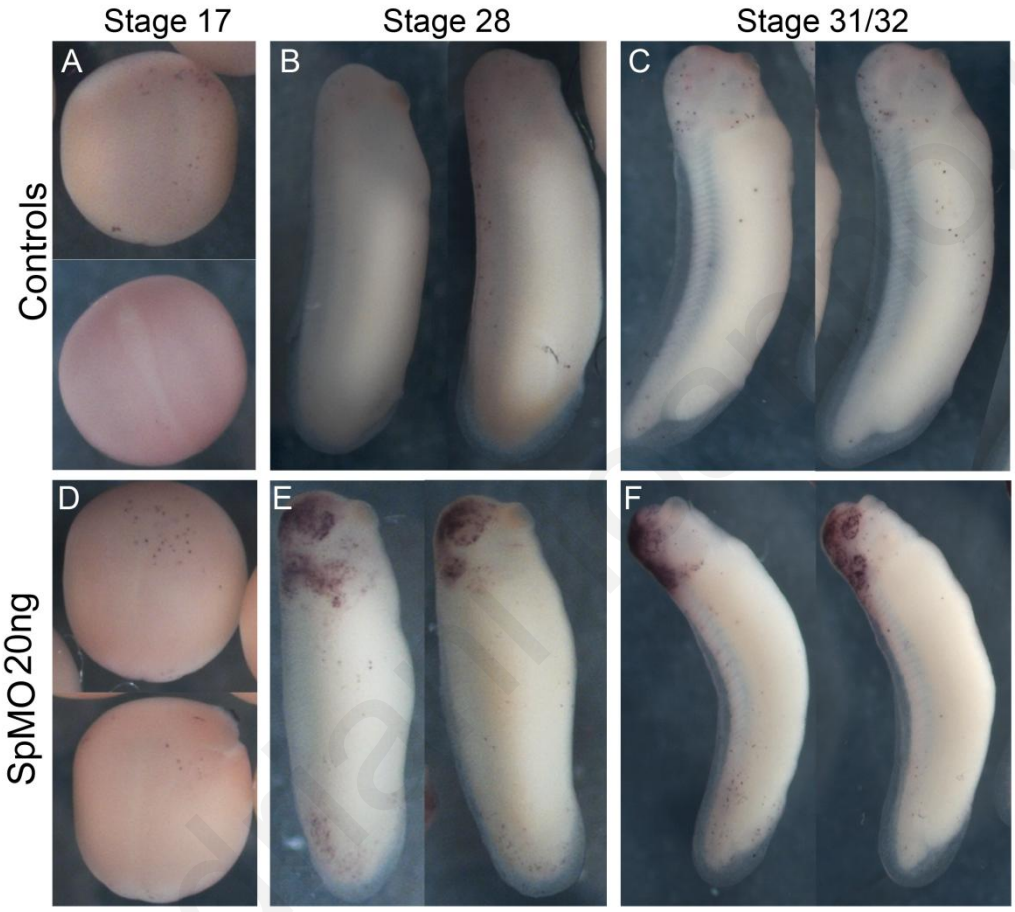

Figure 49. Loss of xNubp1 induces apoptosis in neural tissues.

(A-C) uninjected control embryos at various developmental stages show few apoptotic cells (dark purple spots). (D-F) Embryos injected bilaterally at the animal pole at the two cell stage with 20ng (per blastomere) xNubp1 SpMO. (D) At neurula stages, the number of apoptotic cells is comparable to control embryos. (E, F) During later tailbud stages there is an increase in apoptosis occurring mainly in the eye other neural tissues.

4.5.5 Rohon-Beard neurons fail to project axons which innervate the skin in xNubp1 morphant embryos, leading to loss of touch response.

Upon phenotypic examination of xNubp1 morphant (13ng SpMO) tailbuds (Stages 29-33) in which neural tissue was targeted, we observed that unlike control embryos which had a normal mechanosensory response (Figure 50; Movie 3), xNubp1 SpMO (13ng) morphants displayed a significant reduction in touch sensitivity (Figure 50; Movie 4). These embryos however, were not completely paralyzed and when allowed to develop, were able to swim. This indicated that the motor neurons which are responsible for tadpole swimming were not affected. In addition, WISH using the terminally differentiated neuronal marker N-Tubulin and the neural plate specifier Pax3 (Figure 50C, D) indicated that there was not a general problem with neural specification or neuronal differentiation. During embryogenesis, *Xenopus* embryos develop a light-touch sensory response which is largely mediated by Rohon-Beard sensory neurons (79). These neurons extend naked neurites from the dorsal neural tube and form a loose network just below the skin (131). These neurons serve as the primary mechanosensory neurons and help create an escape response when the embryo is lightly touched. We therefore wanted to examine these neurons in xNubp1 morphants. We conducted whole mount IF against acetylated α-tubulin to observe the mature RB neurons. In uninjected embryos, we observed the RB peripheral axons just below the skin extending dorso-ventrally (Figure 51A; red arrowheads). In xNubp1 morphants, the neurites were shorter and did not project ventrally (Figure 51B; red arrowheads). Cross-sections of unilaterally injected embryos clearly showed that the RB neurons did project peripheral axons from the dorsal spinal cord on both the injected and uninjected sides (Figure 51C; white arrows). However, the axons on the SpMO injected side failed to elongate and innervate the skin (Figure 51C; left side, white arrowheads), whereas the axons on the uninjected side, could be seen just below the skin along the length of the DV axis of the embryo (Figure 51C, right side, white arrowheads). Due to the fact that we could observe the presence of RB neurons by IF and that neural specific tubulin (N-Tubulin), which expressed in RB progenitors (76) was not affected in xNubp1 morphants (Figure 47C), we were able to conclude that RB neurons were specified. Taken together, these data reveal that RB neurons do form in xNubp1 morphants, however their peripheral axons fail to elongate and innervate the skin.

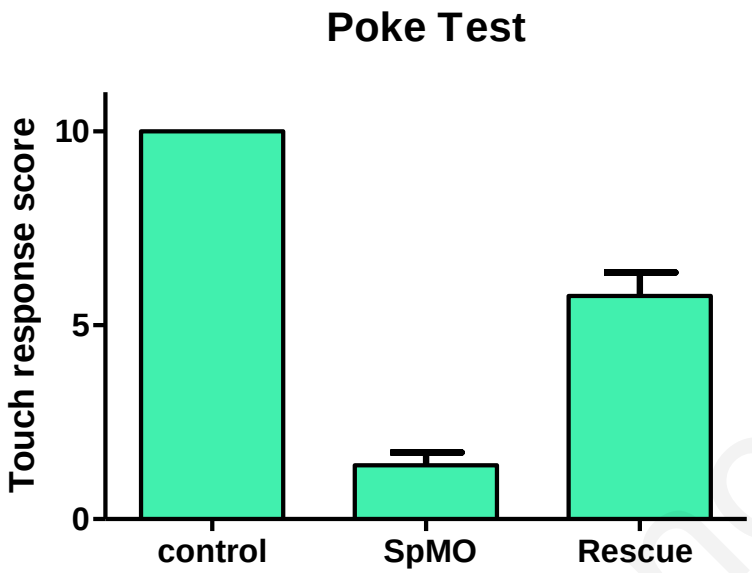

Figure 50. xNubp1 deficient tadpoles lose response to touch.

At stage 33 xNubp1 MO injected embryos show a severely reduced mechanosensory response compared to control embryos. Quantification: Controls, 10±0 (n=21); SpMO (13ng). 1.39±0.33 (n=13); Rescue (SpMO13ng + xNubp1-GFP 240pg). 5.75±0.61 (n=18). Statistical significance was determined using one-way ANOVA. SEM, p<000.1.

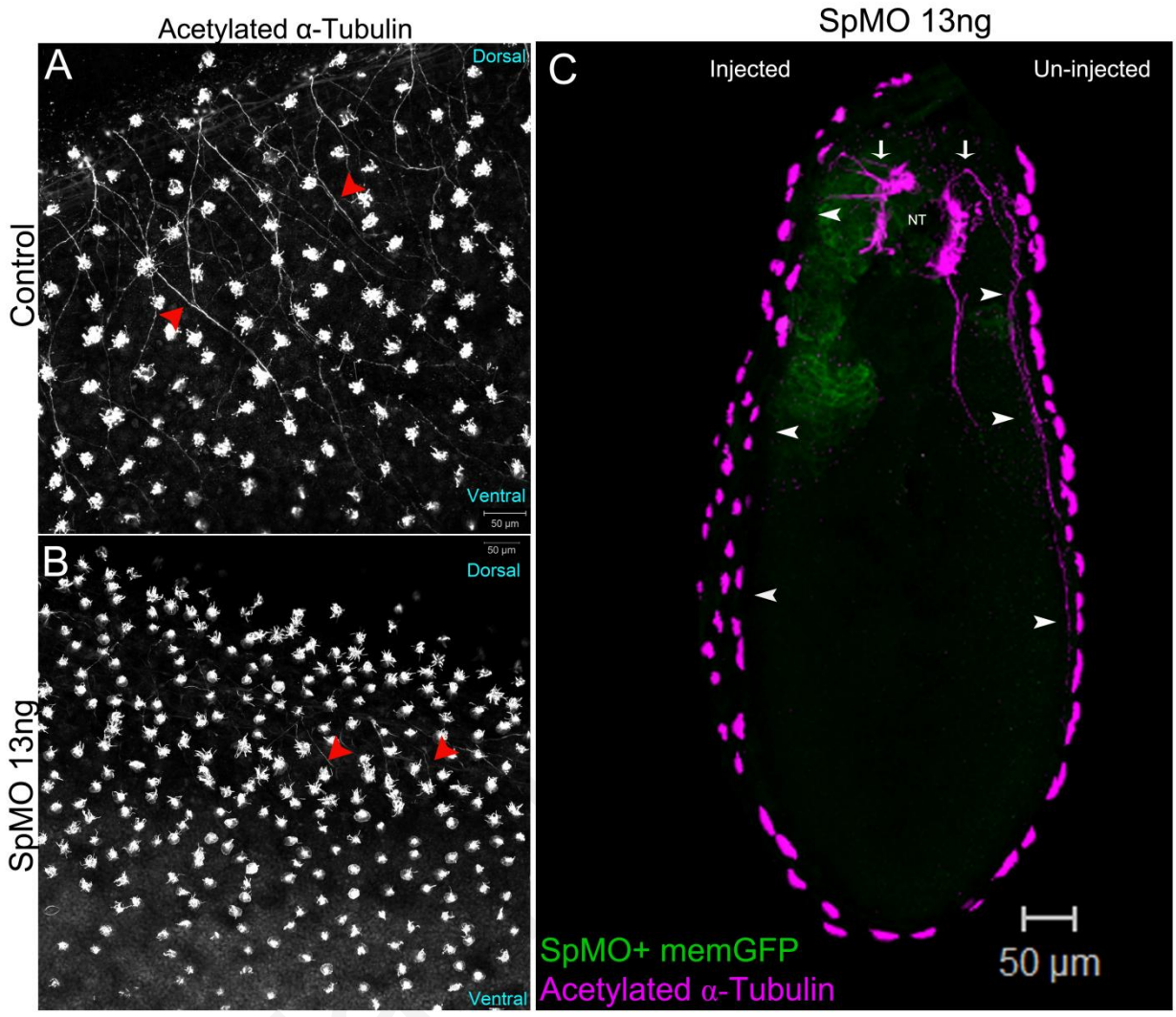

Figure 51. Failure of RB neurons to innervate the skin of xNubp1 morphants.

Whole mount Immunofluorescence staining using Anti-acetylated α-tubulin on stage 32 embryos. (A-B) Maximum intensity projection (MIP) of serial confocal z-plane sections, from a portion of the surface of an embryo. The bright spots of staining are the multi-ciliated epidermal cells. (A) Control embryo has long RB neurites originating from the dorsal spinal cord which extend ventrally and form a network just below the skin (red arrowheads). (B) xNubp1 morphant embryo injected bilaterally. The RB neurites are short, remain dorsally located and do not successfully innervate the skin. (C) Cross-section of an embryo injected unilaterally with xNubp1 SpMO together with membrane-injected morphants the GFP as a lineage tracer. RB neurons extend peripheral axons from the dorsal neural tube (NT) on both the injected and uninjected side (white arrows). Long peripheral axons can be seen in the uninjected site extending ventrally just below the surface of the skin (right side, white arrowheads). The skin surface can be distinguished by the bright staining of the cilia. However, the axons do not elongate and innervate the skin on the injected side (left side, white arrowheads).

4.6 Role of xNubp1 during ciliogenesis

4.6.1 xNubp1 is involved in ciliogenesis in the Xenopus laevis epidermis

When we used MOs to block xNubp1 translation or splicing in ventral tissues, we observed that xNubp1morphants failed to undergo the characteristic drifting motion caused by beating of the cilia on multiciliated epidermal cells. We therefore went on to investigate whether xNubp1 was required for ciliogenesis in multiciliated epidermal cells. Immunostaining of morphant embryos at stage 29-31 with acetylated α-tubulin revealed a dose dependent effect on ciliogenesis. With low amounts of MO (5-8ng), most of the "low-dose" morphant epidermal ciliated cells did project cilia from the apical surface; however the embryos still failed to undergo the drifting motion. At slightly higher amounts (8-15ng), the ciliated epidermal cells in xNubp1 "high-dose" morphants projected fewer and shorter cilia from the apical surface and showed an enrichment of polymerized cytoplasmic acetylated α-tubulin (Figure 52B, D). This phenotype was observed with all three xNubp1-MOs, but not with control or mismatch MOs (Figure 53), and could be partially rescued by co-injection with xNubp1 mRNA (Figure 52C, E). Transmission electron microscopy (TEM) revealed the presence of internal ciliary axonemes (Figure 52F). Interestingly, preliminary data showed that down regulation of xNubp2, using a xNubp2 specific MO (Table 5) also led to a similar phenotype (Figure 54). These data show that the down regulation of xNubp1 leads to defective ciliogenesis in the *X.laevis* epidermis; however, the problem is not due to a failure of axonemal microtubule polymerization.

Due to the fact that WISH did not reveal a high expression of xNubp1 in ciliated cells and our data indicated that xNubp1 is involved in ciliogenesis, we carried out reverse transcription PCR on isolated tailbud skin in order to verify the expression of xNubp1 in the epidermis. RT-PCR verified that xNubp1 was also expressed in the skin (Figure 55).

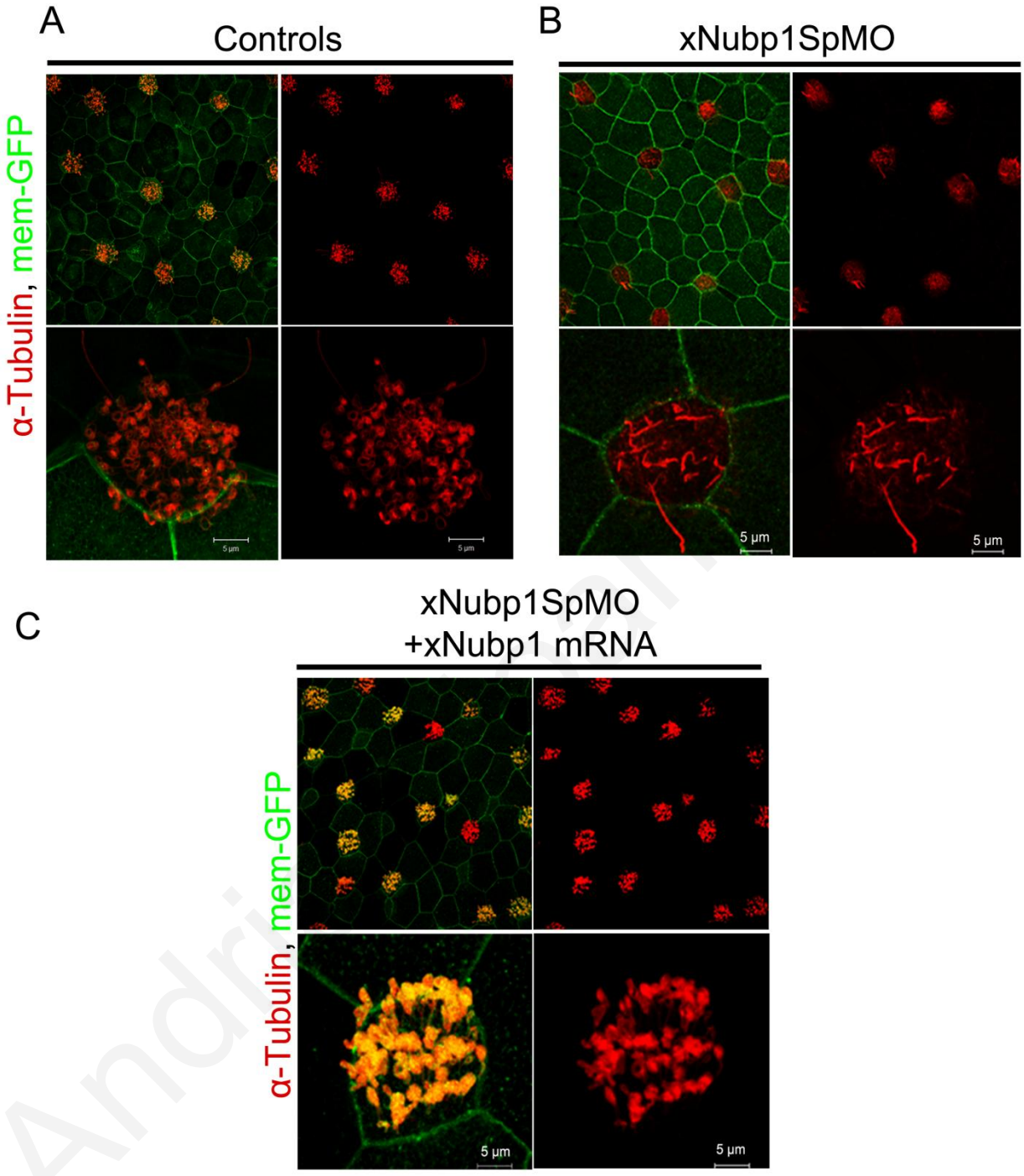
A
Controls
B
xNubp1SpMO
α-Tubulin, mem-GFP
5 µm
5 µm
5 µm
5 µm
C
xNubp1SpMO
+xNubp1 mRNA
α-Tubulin, mem-GFP
5 µm
5 µm

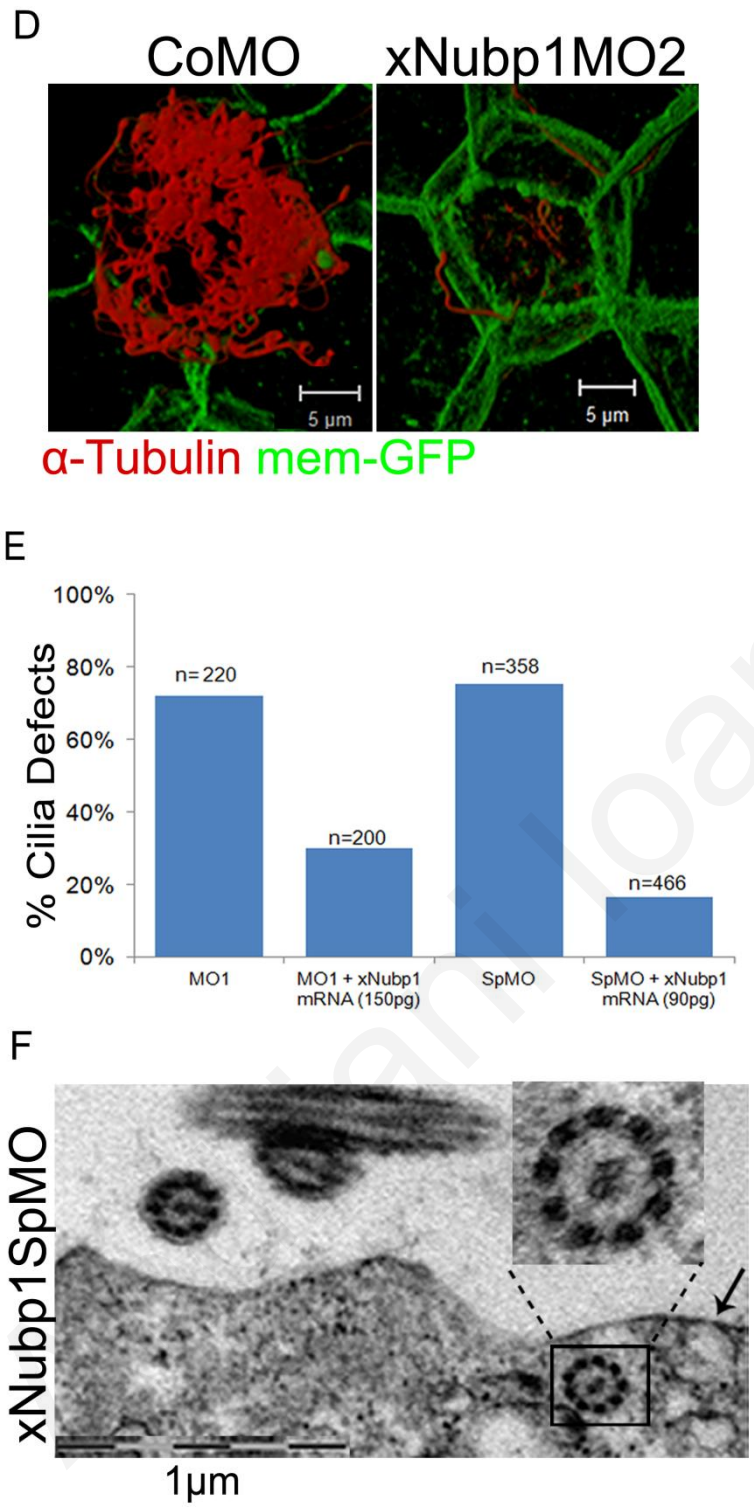

Figure 52. Knockdown of xNubp1 leads Ciliogenesis defects.

(A-C) Immunofluorescence data showing surface views of ciliated epidermis from intact embryos. (A) Control epidermis showing normal ciliated cells. (B) xNubp1 SpMO (13ng) morphant embryo, showing mainly internal acetylated α-tubulin positive structures. Very few cilia project outward from the apical surface. (C) Co-injection of xNubp1 SpMO with xNubp1 mRNA (90pg) rescues the

phenotype and confirms the specificity of the MO. (D) 3D reconstruction of optical sections from immunostaining showing cilia projecting out from the apical surface of a CoMO injected cell and polymerized cytoplasmic acetylated α-tubulin in embryos injected with xNubp1 MO2 (20ng). (E) Quantification of ciliated cells which lack cilia and have internal acetylated tubulin positive structures. Co-Injection of xNubp1 mRNA with either xNubp1MO1 or SpMO partially rescues cilia phenotype (F) TEM of cross section from stage 31 tailbud injected with xNubp1-SpMO, showing an internal ciliary axoneme right below the apical surface (black arrow).

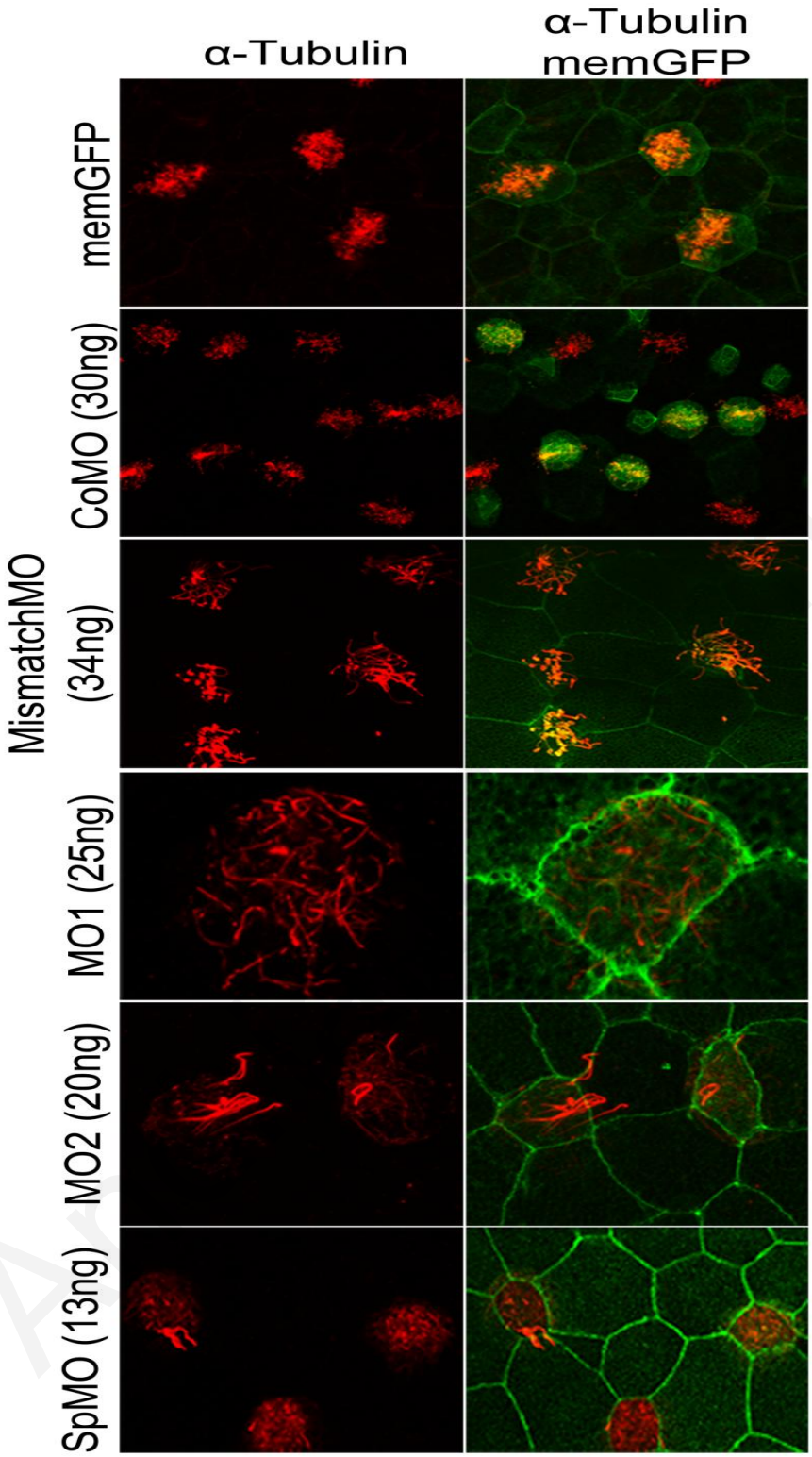

Figure 53. xNubp1 Cilia phenotype is specific.

Both the general control MO and the xNubp1 specific 5 base pair mismatch control MO do not lead to defects in multiciliated epidermal cells. However, all three xNubp1 MOs (MO1, MO2, SpMO) elicit similar effects.

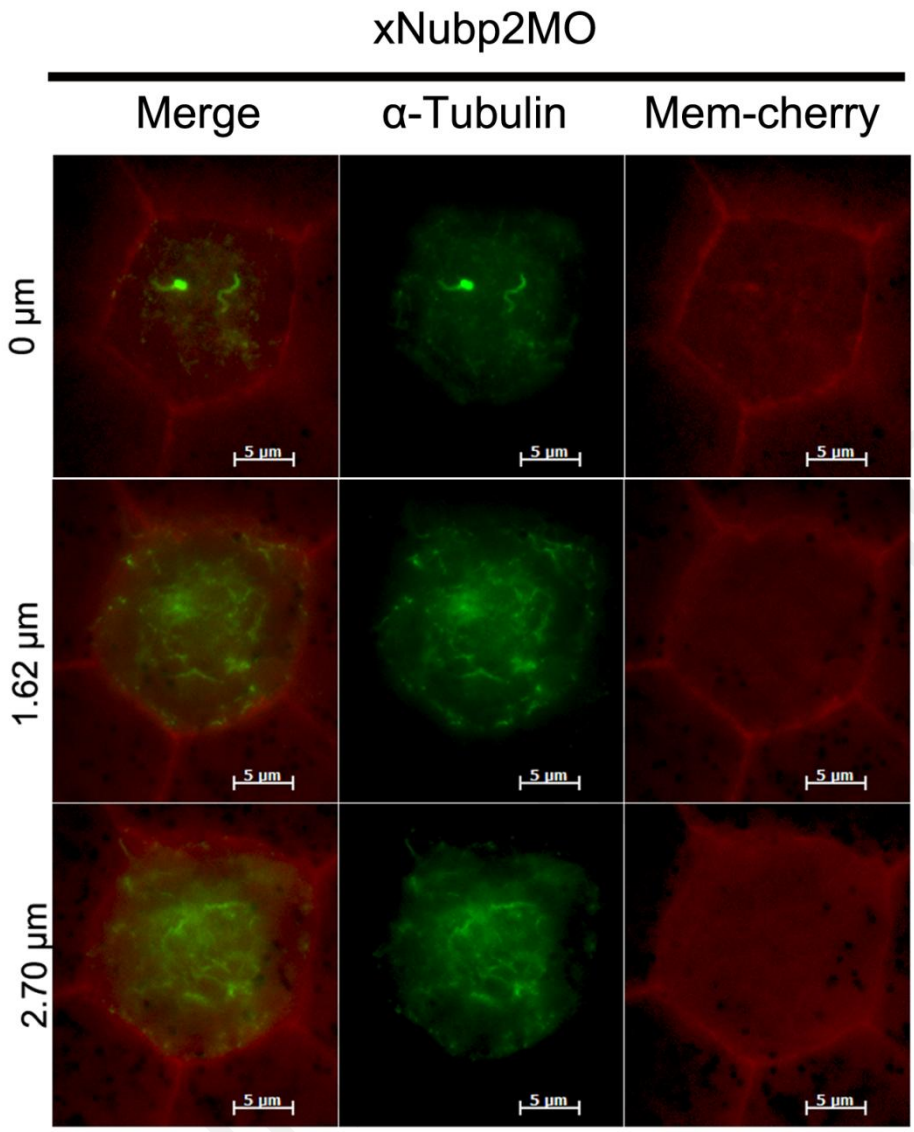

Figure 54. xNubp2 MO causes cilia defects.

Multi-ciliated X.laevis epidermal cells have very few and short cilia projecting from the apical surface when xNubp2 is knocked down using xNubp2 specific MO. Optical sectioning reveals acetylated tubulin positive internalized structures.

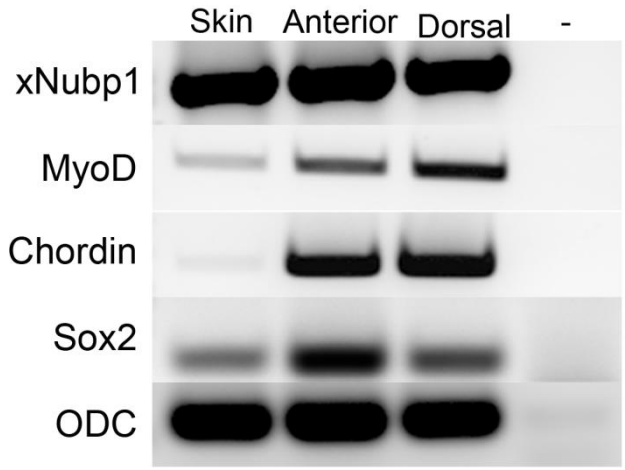

Figure 55. xNubp1 is expressed in the skin.

RT-PCR of various regions of *Xenopus* tailbuds. The anterior region of the embryo contained the head up to and including the branchial arches and pronephros. The dorsal region included the neural tube somites and tailbud. The remaining skin was peeled from the belly region. xNubp1 is present in the epidermis which was removed of all xNubp1 high expressing regions.

4.6.2 xNubp1 is required for gastrocoel roof plate ciliogenesis and left-Right asymmetry

The *Xenopus* gastrocoel roof plate (GRP) is a planar polarized monociliated epithelium derived from the superficial mesoderm. It is homologous to the mouse Posterior notochord (PNC, Node) and Kuppfer's vesicle (KV) in teleost fish and contains posterior localized motile cilia which beat in a circular clockwise fashion to create a leftward flow of extracellular material which is required for left-right asymmetry (87, 132, 133).

xNubp1 morphants displayed gut development defects when dorsal tissues were targeted. The gut either failed to loop or displayed heterotaxia (Figure 56A) in morphant embryos (100%, n= 60). Situs inversus of the gut was difficult to determine due to the fact that in many cases, the positioning/orientation of the gut was affected. Since the correct looping of the gut is linked to cilia-driven leftward flow (87, 132, 133), we decided to examine the GRP cilia in xNubp1 morphant embryos in order to determine whether or not xNubp1 had a generalized role in ciliogenesis. We targeted GRP cells by injecting xNubp1MOs into the dorsal marginal zone (DMZ) of two cell stage *X.laevis* embryos, dissected the GRP tissue at stage 17 and conducted immunostaining against acetylated α-tubulin. We observed that xNubp1 morphant GRP cells had shorter cilia (Mean= 2.4 μm) than control cells (Mean 6.7μm) (Figure 56B, C). It was also apparent that many of the cilia of morphant cells were located more centrally (Figure 56 B") compared to the posterior positioning of cilia of wild-type cells (Figure 56 B'). In order to determine whether left-right asymmetry was disrupted in xNubp1 morphants, we examined the expression of left-right lateralization markers by WISH. In control embryos, *Pitx2c* was expressed in the left lateral plate mesoderm (LPM), however, was absent from the right side (100%, n= 30) (Figure 56D; top panels). When xNubp1 was knocked down, left LPM expression of *pitx2c* was absent (100%, n=59) (Figure 56D; bottom panels). Similar results were obtained for *xnr1*. Control embryos displayed expression of xnr1 in the left LPM (100%, n= 30) (Figure 56E; top panels), whereas xNubp1 MO injected embryos lacked xnr1 transcripts in the LPM (100%, n= 33) (Figure 56E; bottom panels). Together, these results indicate that xNubp1 is also important for regulating GRP ciliogenesis and cilia polarity, which in turn are essential for the establishment of left-right asymmetry.

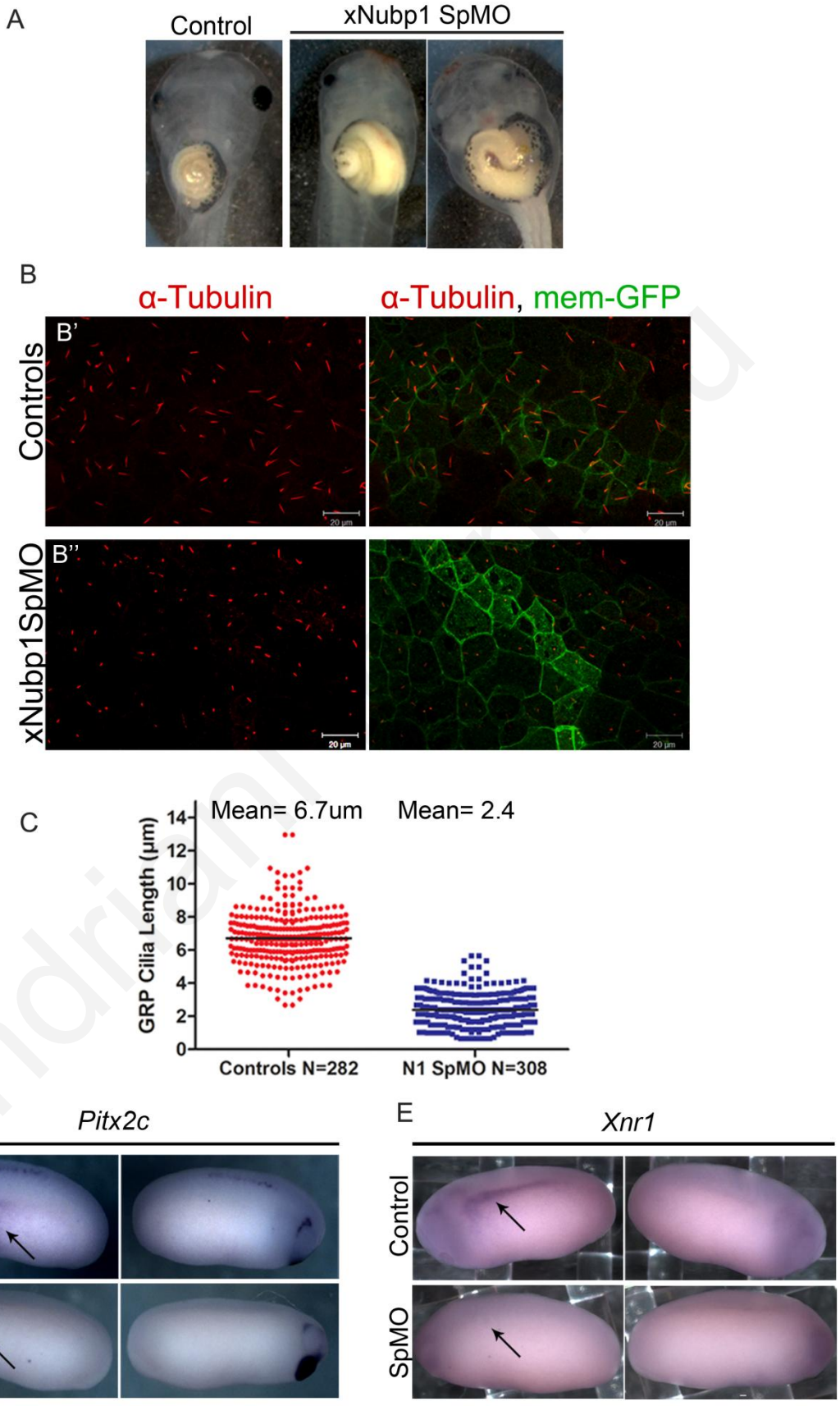
A
Control
xNubp1 SpMO
B
α-Tubulin
α-Tubulin, mem-GFP
Controls
B'
xNubp1SpMO
B''
20 µm
C
Mean= 6.7um
Mean= 2.4
GRP Cilia Length (µm)
0
2
4
6
8
10
12
14
Controls N=282
N1 SpMO N=308
D
Pitx2c
Control
SpMO
E
Xnr1
Control
SpMO

Figure 56. xNubp1 knockdown affect GRP ciliogenesis and left/right asymmetry.

(A) Ventral view of *X.laevis* tadpoles. Unlike control embryos, xNubp1 morphants have various gut looping defects. (B) Maximum intensity projection (MIP) of optical sections from immunostaining showing cilia projecting out from posterior apical surface of a normal GRP (B') and shorter cilia projecting for the apical surface of a SpMO morphant GRP (B''). In some morphant cells the cilia remain centrally localized and have not migrated to the posterior side of the cell. (C) Average length of GRP cilia is significantly reduced in xNubp1 morphants (2.4± 0.06 μm) compared to controls (6.7± 0.1 μm). Horizontal lines indicate the mean, Vertical line SEM, $p<0.0001$ Mann-Whitney test. (D, E) *Pitx2c* and *Xnr1*expression at stage 24. (D) In wild type embryos Pitx2c is expressed in left lateral plate mesoderm (LPM) (black arrow). In xNubp1 morphants *Pitx2c* is absent. (E) *Xnr1* expression is also lost from in xNubp1 morphants (black arrow, bottom panel).

4.6.3 xNubp1 is required for the apical migration/docking of basal bodies in multiciliated epidermal cells

The presence of internal ciliary axonemes and polymerized acetylated α-tubulin structures in xNubp1 high-dose morphants suggested that basal body transport may be compromised. We went on to examine the position of basal bodies in xNubp1 morphants. In controls, Centrin-YFP (basal body marker) was tightly localized at distinct foci on the apical surface of ciliated cells and absent from deeper areas of the cell as expected (Figure 57A). xNubp1 morphants showed a clear dose dependent phenotype in terms of basal body migration and docking. At high MO amounts (15-20ng; high-dose morphants), basal bodies were almost exclusively found deep within the cell body in close association with acetylated α-tubulin positive structures (Figure 57B, D); while at lower amounts (5-8ng; low-dose morphants) the majority reached the apical surface. At intermediate amounts of MO (8-13ng), basal bodies were seen both at the apical surface in addition to deep within the cell, with considerable variation from cell to cell within each tadpole (Figure 57C). Even morphant cells, in which the basal bodies migrated to the apical surface, had polymerized acetylated α-tubulin structures just below the apical surface and displayed incorrect basal body spacing (Figure 57E). To confirm these results, we examined ciliated cells using TEM. Basal bodies in xNubp1 morphants failed to localize and dock to the apical surface of ciliated cells (Figure 57G), which is consistent with

live fluorescent imaging and immunostaining data. Immunostaining with Zo-1 (Figure 58) confirmed that apico-basal polarity was not affected in morphant embryos. Taken together, these data suggest that the defect in ciliogenesis observed in xNubp1 high-dose morphants is due to a failure of basal body migration and docking at the apical surface.

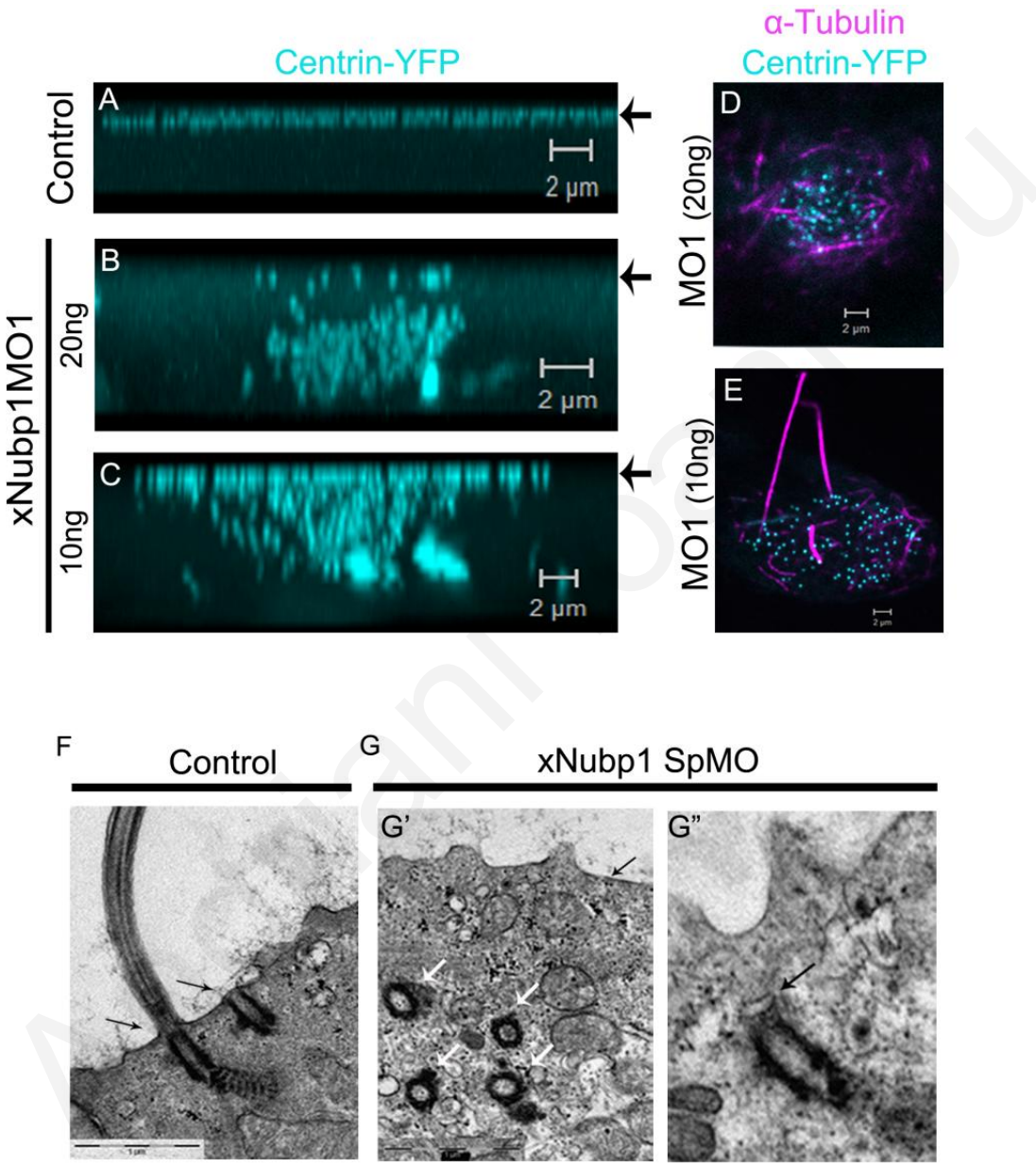

Figure 57. xNubp1 is required for basal body migration and docking at the apical surface of ciliated epidermal cells.

(A-C) 3D reconstructions from confocal optical sections projected in the x-z plane with the position of the apical surface indicated by black arrows (A) Centrin2-YFP in control cells is localized at the apical surface of ciliated cells. (B-E) A dose dependent range of effects on basal body migration is seen

in Nubp1 morphants. (B) In high-dose morphant cells, most of the basal bodies fail to reach the apical surface remaining deep within the cell. (C) In cells with an intermediate amount of MO, some me basal bodies do reach the apical surface with most still remaining in the cytosol. (D) Optical section from a xNubp1 morphant ciliated epidermal cell showing internal acetylated tubulin in close association with the basal bodies deep within the cell body. (E) Cells with apically localized basal bodies have polymerized cytoplasmic acetylated α-tubulin just below the apical surface. (F, G) TEM on cross-sections from stage 31 tailbuds. (F) In control cells, basal bodies in have migrated and docked to the apical surface (black arrows). (G') In xNubp1 morphants, basal bodies (white arrows) fail to migrate to the apical surface (black arrow). (G") Basal body in a xNubp1 morphant cell has migrated to the apical surface but has not docked properly (black arrow).

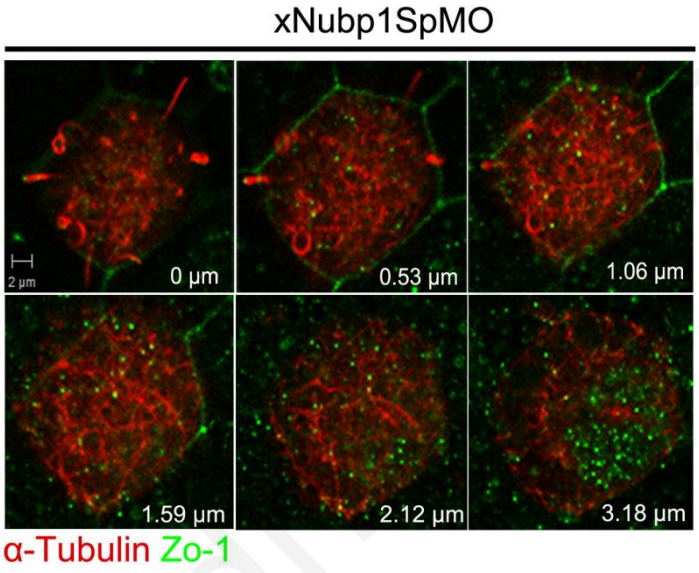

Figure 58. xNubp1 knockdown does not affect apico-basal polarity.

Optical sections from a xNubp1 morphant ciliated cell labeled with acetylated tubulin and Zo-1. Apical surface has very few short cilia projecting outward

4.6.4 xNubp1 is required for polarized ciliary beating and basal body polarization

In order for ciliated cells across ciliated epithelia to undergo polarized beating, the basal bodies must first be polarized correctly (88, 115). In low-dose xNubp1 morphants, the majority of the ciliated cells projected cilia which appeared normal. However, as mentioned above, even those embryos failed to undergo the characteristic drifting motion caused by the polarized beating of the epidermal ciliated cells, suggesting that polarized ciliary beating and directional flow was disrupted. In order to examine the directional fluid flow we used Quantum Dot (QD) nanocrystals in combination with live imaging. We observed distinct directional (anterior to posterior) fluid flow across the epidermis of control embryos (Figure 59A; Movie 5), however, xNubp1 low-dose morphants showed impaired directional fluid flow across the epithelium (Figure 59B; Movie 6). The presence of cilia on the epidermis of these embryos was subsequently confirmed by immunostaining with acetylated α- tubulin (data not shown). Co-injection of xNubp1 mRNAwith the MO partially rescued this phenotype (Figure 59C). In order to assess whether the motility of cilia was affected in morphant embryos, we used live bright field imaging. Ciliary beating in xNubp1 morphants was disorganized and unlike controls (Movie 7) cilia did not beat in a synchronized whip-like manner (Movies 8). Instead, their beating was asynchronous and individual cilia moved slowly and appeared to be more rigid than in controls (Movie 9).

Following basal body docking during ciliogenesis, basal bodies must be polarized along the long axis (A-P) of the embryo in order to create directional fluid flow (88, 110, 112, 115). Since xNubp1 knockdown led to decreased fluid flow and disorganized ciliary beating, we sought to determine whether xNubp1 was also necessary for the polarization of basal bodies. To assess the planar polarization of basal bodies, embryos were co-injected with Centrin-RFP to mark the basal body and Clamp-GFP to mark the striated rootlet (88, 110, 112, 115). From these experiments, it became clear that in xNubp1 low-dose morphants with apically localized basal bodies, spacing and polarity were both compromised. Confocal imaging and quantification of the polarity using circular plots of the angular orientation and the circular standard deviation (CSD) showed that knockdown of xNubp1 led to a great deal of variation with regards to angular orientation of basal bodies (Figure 59E, G), compared to that of control embryos (Figure 59D ,F). In addition, as noted above, the spacing between the basal

bodies on these cells was also compromised (Figure 59E). The CSD of xNubp1 morphants (Figure 59G) was considerably higher (39.4°) than that of controls (13.5°) (Figure 59F). In many of the morphant ciliated cells, the angle of the rootlet seemed to be perpendicular to that of the basal body, making it difficult to quantify the polarity of those particular basal bodies (Figure 59E'; white box). These data indicate that at low amounts of Nubp1 MOs, although basal bodies reach the apical surface, they fail to space and polarize correctly.

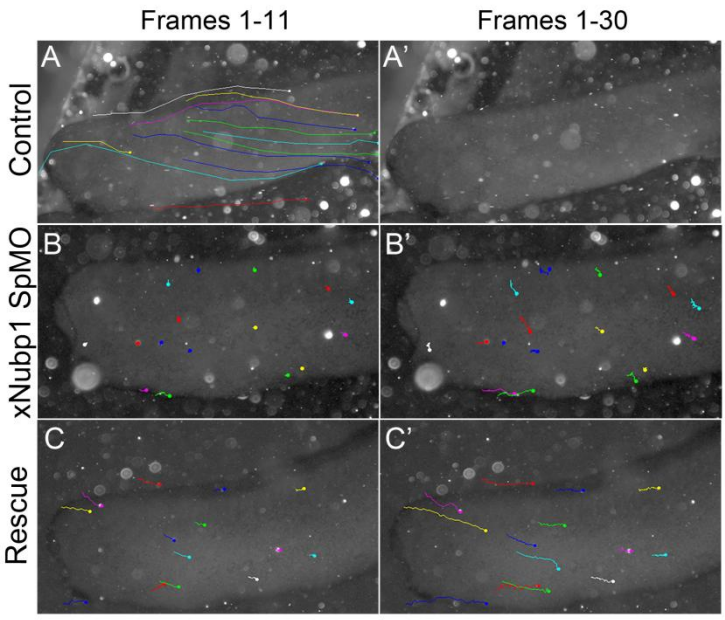
Frames 1-11
Frames 1-30
A
A'
Control
B
B'
xNubp1 SpMO
C
C'
Rescue

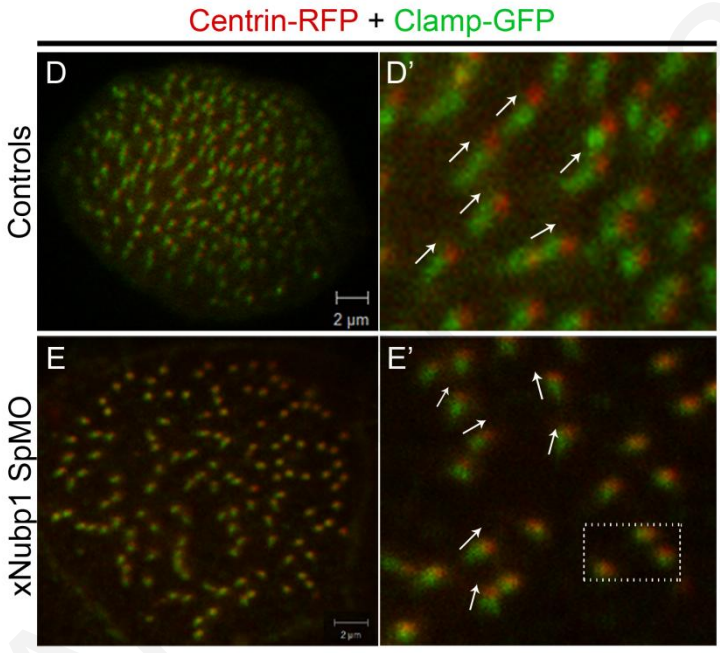
Centrin-RFP + Clamp-GFP
D
D'
Controls
2 µm
E
E'
xNubp1 SpMO

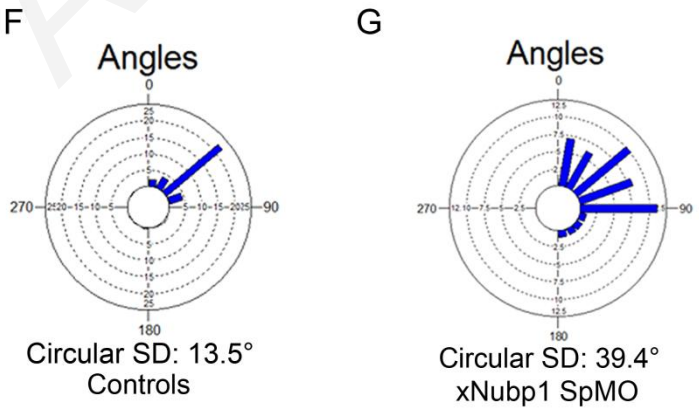
F
Angles
0
90
180
270
Circular SD: 13.5°
Controls
G
Angles
0
90
180
270
Circular SD: 39.4°
xNubp1 SpMO

Figure 59. xNubp1 knockdown disrupts directional fluid flow and basal body polarization.

(A-C) The flow of QDs was tracked along the surface of the embryos from anterior to posterior. (A) In control embryos, QDs flow rapidly from dorso-anterior to ventral-posterior. (B) xNubp1 morphants (7ng) show severely disrupted fluid flow. (C) Co-injection of xNubp1 MO with xNubp1 mRNA (114pg) partially rescues ciliary flow. (D-E) Confocal images of Centrin2-RFP and Clamp-GFP. (D) Basal bodies in controls are polarized along the anterior-posterior axis in the direction of the effective stroke (Direction of polarity is depicted by white arrows). (E) Knockdown of xNubp1 (6ng) leads to a great deal of variation with regards to angular orientation of basal bodies. Many of the morphant ciliated cells the angle of the rootlet is perpendicular to that of the basal body (white box), making it difficult to quantify the polarity of the basal bodies. (F-G) Quantification of the polarity using circular plots of the angular orientation and the Circular Standard Deviation (CSD). The blue bars depict the mean direction of the cilia and the bar length depicts the variance around the mean. CSD of controls (F) is considerably lower than that of xNubp1 low-dose morphants (G).

4.6.5 Loss of xNubp1 leads to apical microtubule disorganization

The apical microtubule network in multi-ciliated cells has been shown to be essential for the correct polarization of basal bodies (110). Cytoplasmic microtubules form an organized network at the apical surface of multiciliated cells (110). These microtubules interact with basal bodies specifically at the basal foot (134, 135), and although they do not appear to be involved in the migration of basal bodies to the apical surface (136), they are required for local coordination of basal body polarization (110). In order to visualize the apical network of microtubules, a GFP-tagged enconosin binding domain (EMTB-3XGFP) construct was used. Embryos injected with EMTB-3XGFP and Centrin-RFP displayed an organized interconnected apical network of microtubules and basal bodies (Figure 60A, C). In xNubp1 morphants, this apical network was disorganized (Figure 60B, D) and in cells with internal basal bodies the microtubule network formed around the internal basal bodies (Figure 60B, last panel). However, the apical microtubule network appeared much more organized in low-dose morphant ciliated cells (data not shown). These data show that the apical microtubule network in xNubp1 morphant ciliated cells is compromised, and may partly cause the basal body rotational polarity defects seen in xNubp1 morphants. However, the microtubules were still able to organize around basal bodies and therefore the unorganized microtubule network at the apical surface may be a consequence of the basal body spacing problems and the reduced number of basal bodies properly docked at the apical surface in xNubp1 intermediate-dose morphants.

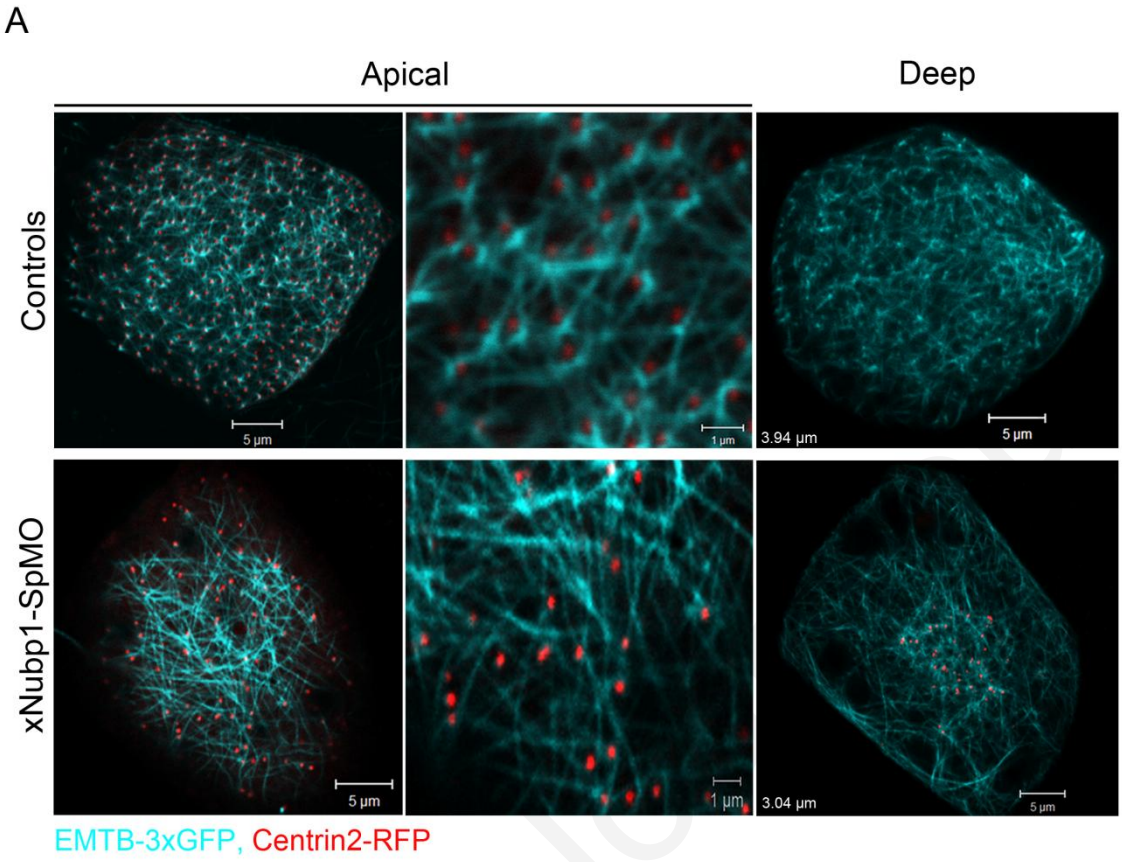
A
Apical
Deep
Controls
xNubp1-SpMO
5 µm
1 µm
3.94 µm
3.04 µm
EMTB-3xGFP, Centrin2-RFP
B
EMTB-3xGFP
Controls
2 µm
Centrin2-RFP
C
EMTB-3xGFP
xNubp1-SpMO
Centrin2-RFP

Figure 60. xNubp1 knockdown leads to apical microtubule disorganization in multiciliated epidermal cells.

(A-C) Stage 31 embryo injected with EMTB-3xGFP to and Centrin2-RFP. (A) Cytoplasmic microtubules in control ciliated cells form an organized interconnected network around the basal bodies at the apical surface of multiciliated epidermal cells. Microtubules are evenly distributed throughout the cytoplasm deep within the cell. Apical network of cytoplasmic microtubules in xNubp1 morphant multi-ciliated cells is disorganized. Microtubules deep within the cell nucleate around internalized basal bodies. (C-D) Three dimensional reconstruction of serial confocal images projected in the x-z plane. (C) Microtubules together with basal bodies are enriched at the apical surface (indicated by black arrows) in control multiciliated epidermal cells. (D) Microtubules in xNubp1 morphant ciliated cells are enriched apically and in regions within the cell which contain internalized basal bodies.

4.6.6 Loss of xNubp1 leads to apical actin disorganization but does not act through the PCP pathway

The apical surface of *X.laevis* ciliated epidermal cells have a dense meshwork of actin (106, 137) comprised of two distinct but interconnected pools; the apical and sub-apical pools of actin (110). Loss of apical and sub-apical actin localization leads to problems with basal body localization and polarity respectively (88, 103, 106, 110). Collectively, the phenotypes observed in xNubp1 morphant embryos are quite similar to those seen when members of the PCP pathway, such as Dishevelled (Dvl), RhoA, Inturned (Int) and others are disrupted (88, 106, 138), raising the possibility that xNubp1 may somehow be involved in the planar cell polarity pathway.

4.6.6.1 High-dose xNubp1 morphants

Given that Dvl is a core PCP protein required for basal body docking and planar polarization of basal bodies (88); we decided to assess whether or not Dvl localization was affected in xNubp1 morphants in which the basal bodies failed to migrate to the apical surface (high-dose morphants). In *Xenopus* multiciliated epidermal cells, Dvl localizes to distinct puncta at the apical cell surface (Figure 61A, G; (88). In xNubp1 morphant ciliated epidermal cells, we observed a significant loss of Dvl puncta from the apical surface (Figure 61B). Optical sectioning revealed Dvl-GFP foci within the cytoplasm (Figure 61H); in close association with internal acetylated tubulin positive structures (Figure 61L). We could not however detect a physical interaction between xNubp1 and Dvl biochemically nor did xNubp1 regulate the activation of Dvl in animal cap explants (data not shown).

The PCP effector RhoA associates with and is activated by Dvl (88, 139), and regulates actin organization (111). Recent work has shown that RhoA is enriched at the apical surface of ciliated cells (88, 107), and is essential for the apical docking of basal bodies by mediating apical actin enrichment (107). Taking these data into account, we decided to examine the localization of RhoA in xNubp1 morphant ciliated epidermis. In control ciliated cells, we observed enrichment of RhoA-GFP at the apical surface, as previously reported (Figure 61C). However, in xNubp1 morphant cells with internal basal bodies, RhoA-GFP was greatly decreased at the apical surface and mainly concentrated within the cytoplasm (Figure 61D, I), together with internalized basal bodies (Figure 61J). The RhoA-GFP signal at the cell-cell boundaries however was not affected (Figure 61D, I, J). We next wanted to determine whether

the RhoA pool, which was found surrounding the internalized basal bodies, was active. Using the active RhoA sensor rGBD-GFP, we noted that in controls, active RhoA was localized at distinct foci on the apical surface associated with basal bodies (Figure 61E; data not shown) while in morphants it remained associated with the internalized basal bodies (Figure 61K). These data reveal that the down regulation of xNubp1 leads to the mislocalization of PCP pathway members in ciliated cells with internal basal bodies.

Since RhoA has a critical role in the formation of the apical actin network, we therefore wanted to examine if apical actin was affected in xNubp1 high-dose morphants with internalized basal bodies. Fluorescent immunostaining revealed that xNubp1 high-dose morphant embryos failed to accumulate the dense actin meshwork (Figure 62C) found in control (Figure 62A) and CoMO (data not shown) injected ciliated cells, but retained the cortical actin at cell borders (Figure 62B, D). Together, these data indicate that the failure of basal body apical migration in high-dose morphants leads to a mislocalization of PCP pathway members and as a result, apical actin fails to accumulate.

4.6.6.2 Low-dose xNubp1 morphants

We next wanted to examine the apical and sub-apical actin networks in xNubp1 low-dose morphants. As shown in Figure 63 B and D, apical actin, although enriched, appeared reduced and less organized in xNubp1 low-dose morphants which had apically localized basal bodies and extended cilia outward. Specifically, the apical actin in morphants failed to organize into an interconnected network but rather appeared as disconnected puncta. Co-injection of xNubp1 mRNA partially rescued the apical actin disorganization (Figure 64), thus verifying the specificity of this phenotype. The sub-apical actin pool has been shown to be important for both the spacing of basal bodies as well as overall rotational polarity at a distance. Use of Cytochalasin D to disrupt the sub-apical actin connections between basal bodies, leads to both loss of spacing as well as loss of cell-wide rotational polarity and metachronal synchrony (110), raising the possibility that loss of xNubp1 may also disrupt this network. We observed that the sub-apical actin network in xNubp1 low-dose morphants was nearly absent (Figure 63B"). We therefore went on to examine RhoA localization in low-dose morphant embryos and saw that despite the loss of sub-apical actin and disorganized apical actin; RhoA was in fact apically enriched in these cells (Figure 63E). Using an active RhoA sensor (rGBD-GFP)

we examined whether RhoA was active in xNubp1 low-dose morphant ciliated cells. As shown in Figure 63F, we saw that this was in fact the case. These data suggest that loss of Nubp1 may be affecting the formation/stabilization of the apical and sub-apical actin networks through a Rho/PCP independent mechanism. Taken together, the data lead to the conclusion that the mislocalization of PCP proteins in high-dose mutants is a secondary affect due to failure of basal bodies to successfully migrate to the apical surface.

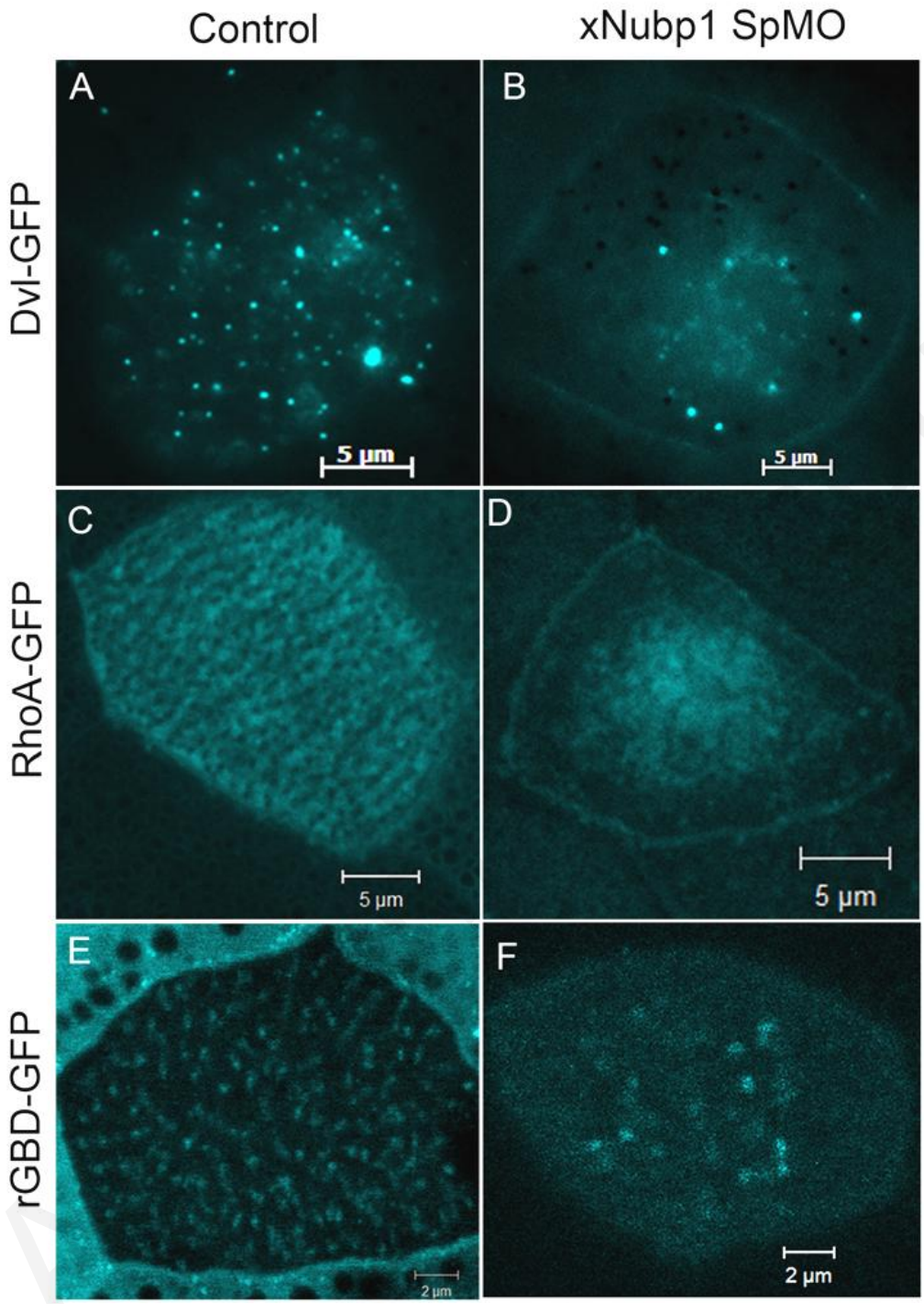
Control
xNubp1 SpMO
Dvl-GFP
RhoA-GFP
rGBD-GFP
A
B
C
D
E
F
5 µm
5 µm
5 µm
5 µm
2 µm
2 µm

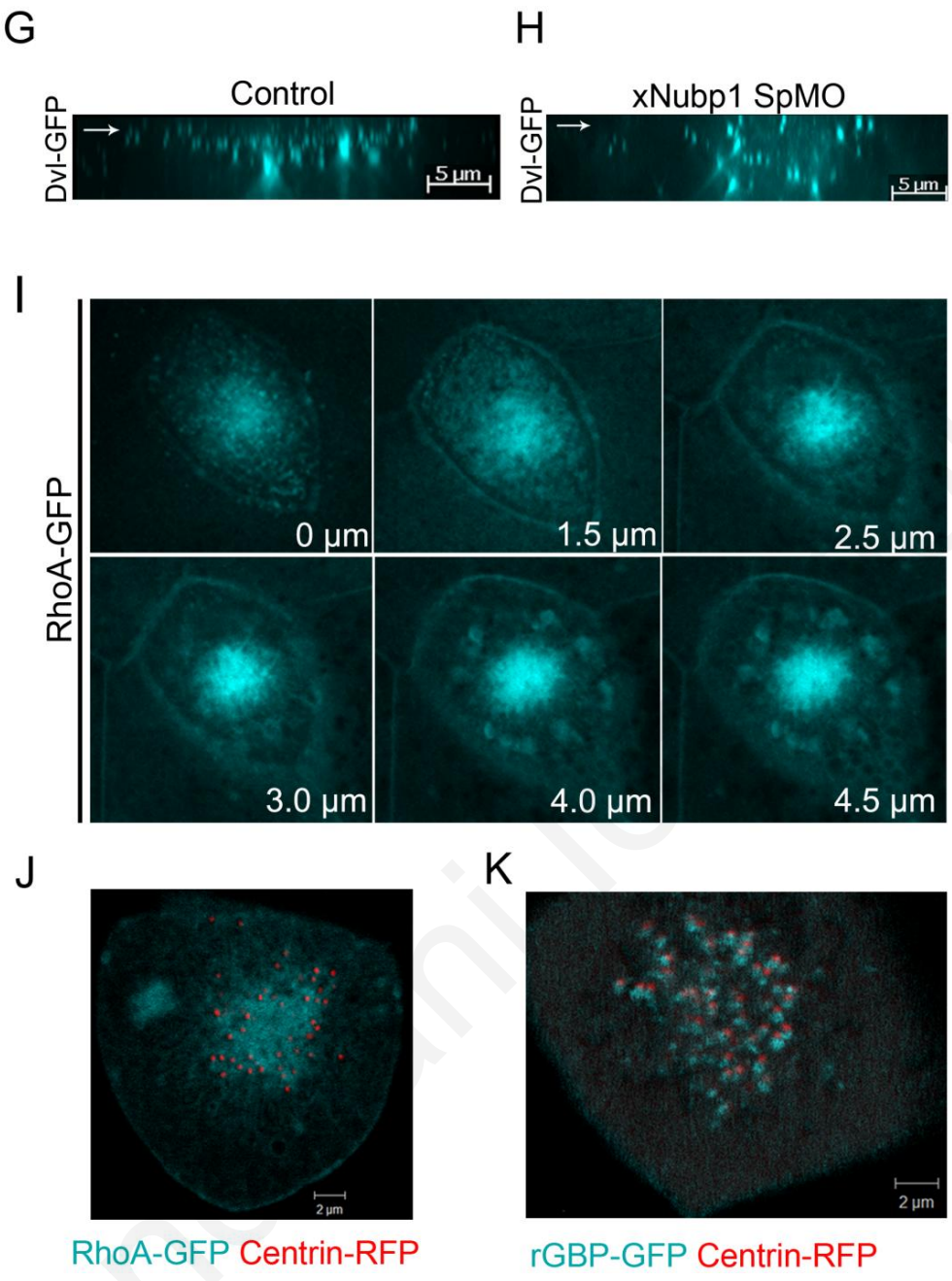
G
H
Control
xNubp1 SpMO
Dvl-GFP
Dvl-GFP
5 µm
5 µm
I
RhoA-GFP
0 µm
1.5 µm
2.5 µm
3.0 µm
4.0 µm
4.5 µm
J
K
2 µm
2 µm
RhoA-GFP Centrin-RFP
rGBP-GFP Centrin-RFP

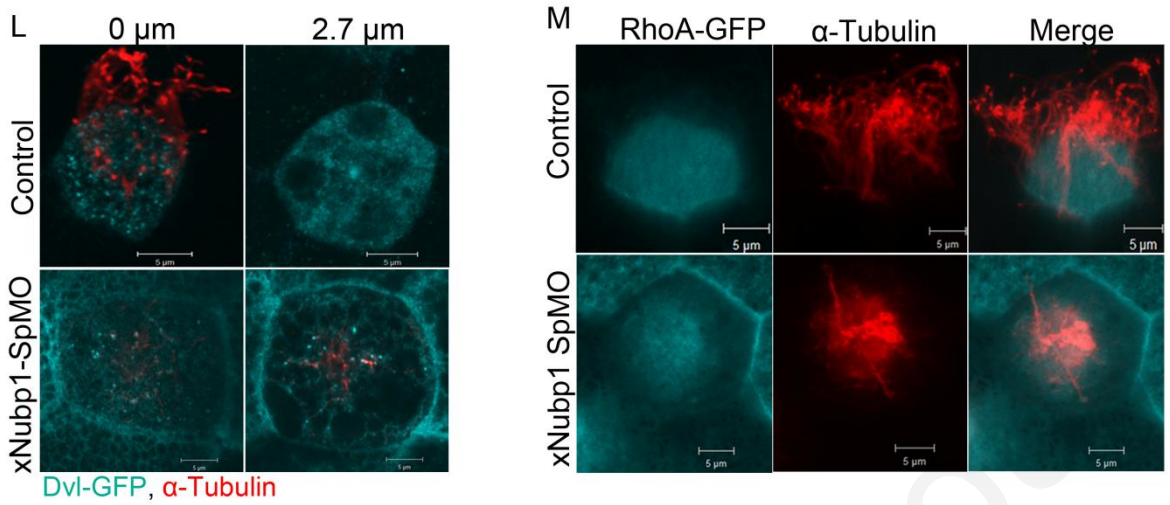

Figure 61. Dvl and RhoA are mislocalized in xNubp1 high-dose morphant multi ciliated epidermal cells with internalized basal bodies.

(A) Dvl-GFP localizes to small foci and larger aggregates at the apical surface of control multi-ciliated cells. (B) xNubp1 morphant ciliated cells have fewer Dvl-GFP foci at the apical surface. (C) RhoA-GFP is enriched at the apical surface of control multi-ciliated cells but apical enrichment is substantially reduced in xNubp1 morphant ciliated epidermal cells (D). (E) Active RhoA (rGBD-GFP) is localized on distinct foci on the apical surface of control multiciliated cells however rGBD-GFP puncta are almost completely absent from the apical surface of xNubp1 morphant ciliated cells (F). (G-H) Serial confocal sections projected in the x-z plane. (G) In Control multi-ciliated epidermal cell Dvl-GFP puncta are mainly localized to the apical surface (depicted by white arrow). (H) Dvl-GFP puncta are not restricted to apical surface (white arrow) in xNubp1 morphants. (I) Optical sectioning through an xNubp1 morphant ciliated epidermal cell shows concentration of RhoA deep within the cell body. (J) Co-expression of RhoA-GFP and Centrin2-RFP reveals that RhoA-GFP co-localizes with internal basal bodies in xNubp1 morphant ciliated cells. (K) RhoA is active deep within the cell body in xNubp1 morphant ciliated cells and is associated with internal basal bodies. (L) Control ciliated epidermal cell with ciliary axonemes extending from the apical surface. Small GFP-Dvl foci are present at the apical surface together with larger Dvl foci. Larger foci are also present below the apical surface, but not deep within the cytoplasm. xNubp1-SpMO multi-ciliated epidermal cell with few Dvl puncta at the apical surface. Small Dvl foci are observed deep within the cell, closely associated with internal acetylated tubulin. (M) In control multi-ciliated cells, RhoA is enriched at the apical surface and ciliary axonemes project outward. In xNubp1-SpMO morphant cells, RhoA is enriched around the internalized acetylated tubulin positive structures below the apical surface.

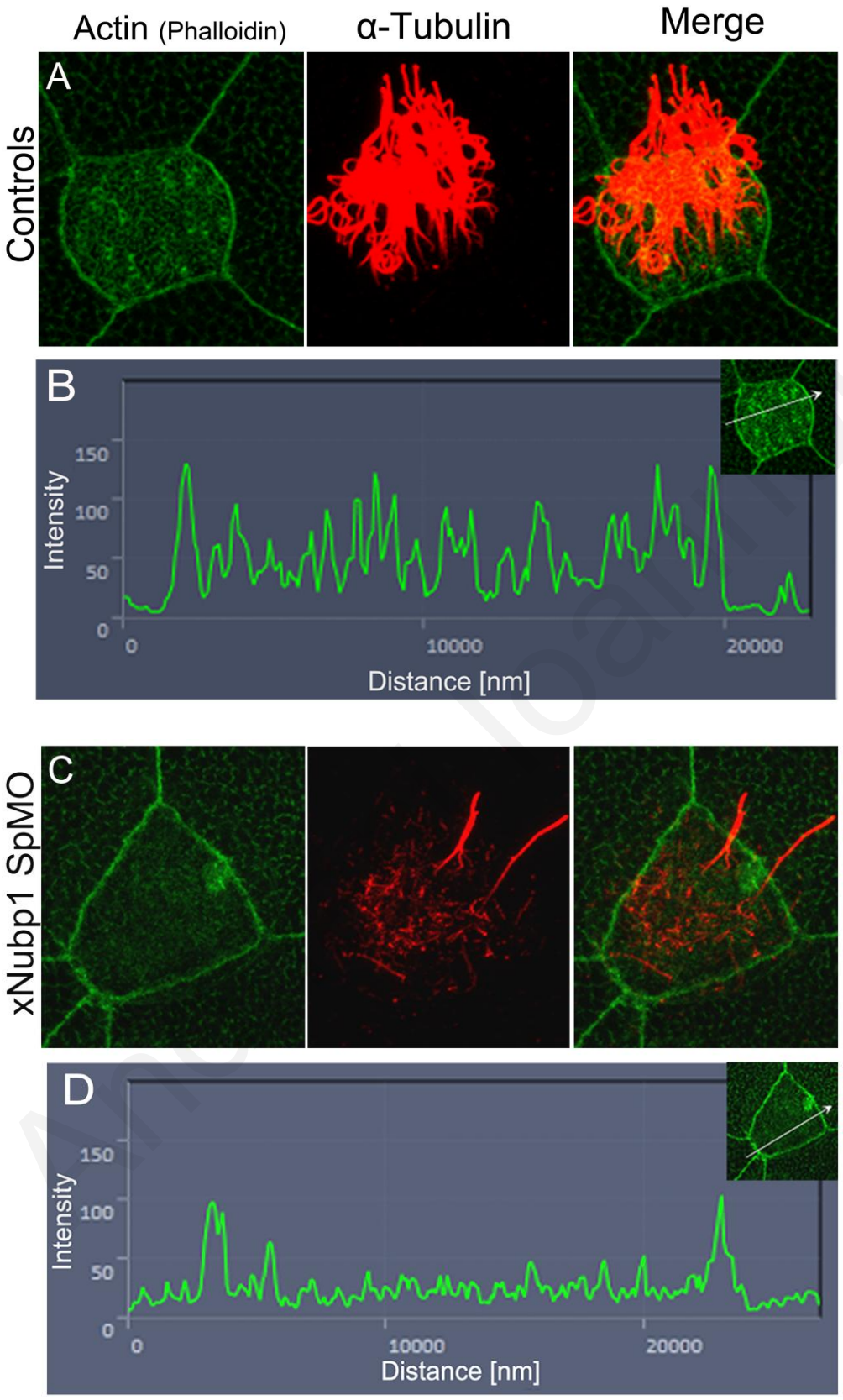
Actin (Phalloidin)
α-Tubulin
Merge
Controls
A
B
Intensity
150
100
50
0
0
10000
20000
Distance [nm]
xNubp1 SpMO
C
D
Intensity
150
100
50
0
0
10000
20000
Distance [nm]

Figure 62. Apical actin is reduced in xNubp1 high-dose morphants.

Immunostaining with phalloidin (actin) and acetylated tubulin (cilia). (A, B) Maximum intensity profile of serial confocal optical sections. (A) Actin filaments are highly enriched at the apical surface of control ciliated cells. (B) The dense actin meshwork is missing from xNubp1 morphant ciliated cells; however, actin at cell boundaries is not affected. (C) Intensity profile showing elevated signal intensity across the entire apical surface of a control ciliated cell. (D) Intensity profile showing elevated actin signal at cell boundaries and low signal intensity across the apical surface of an xNubp1 morphant ciliated cell.

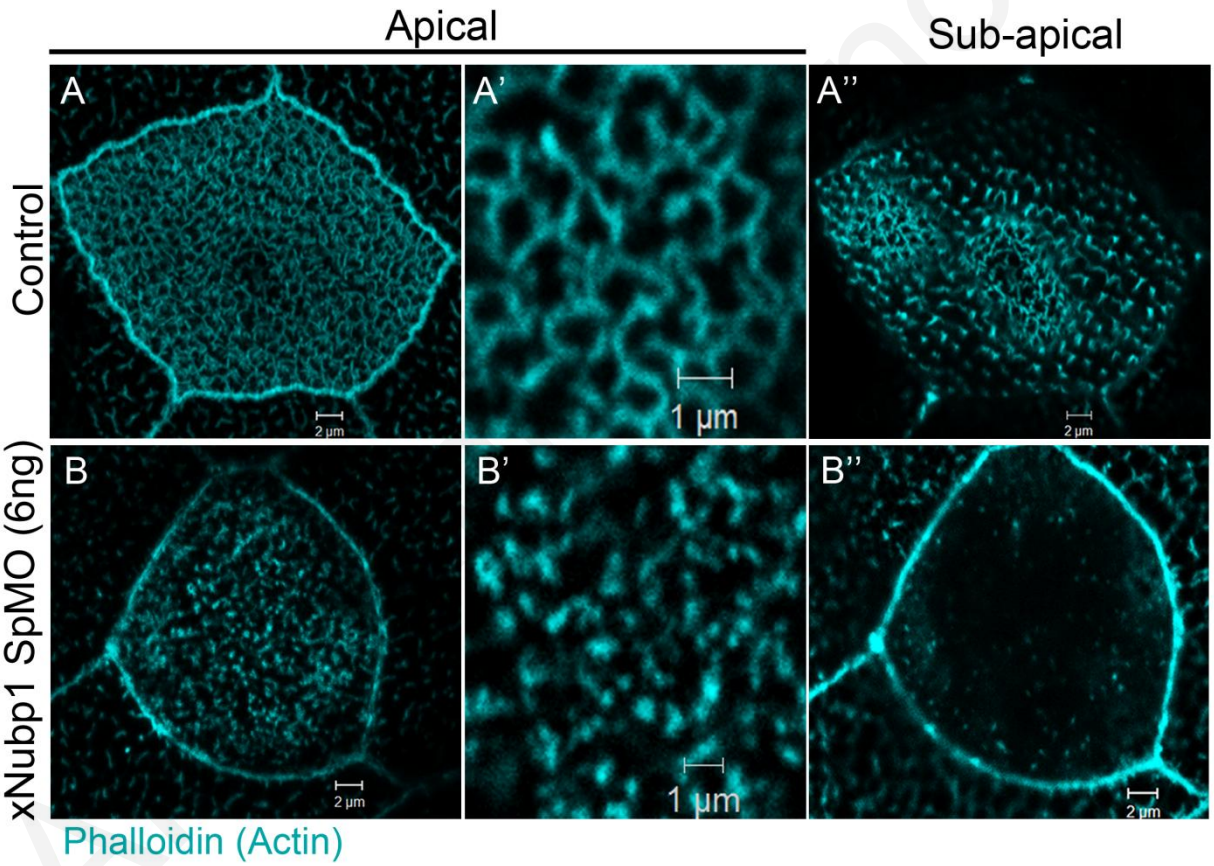

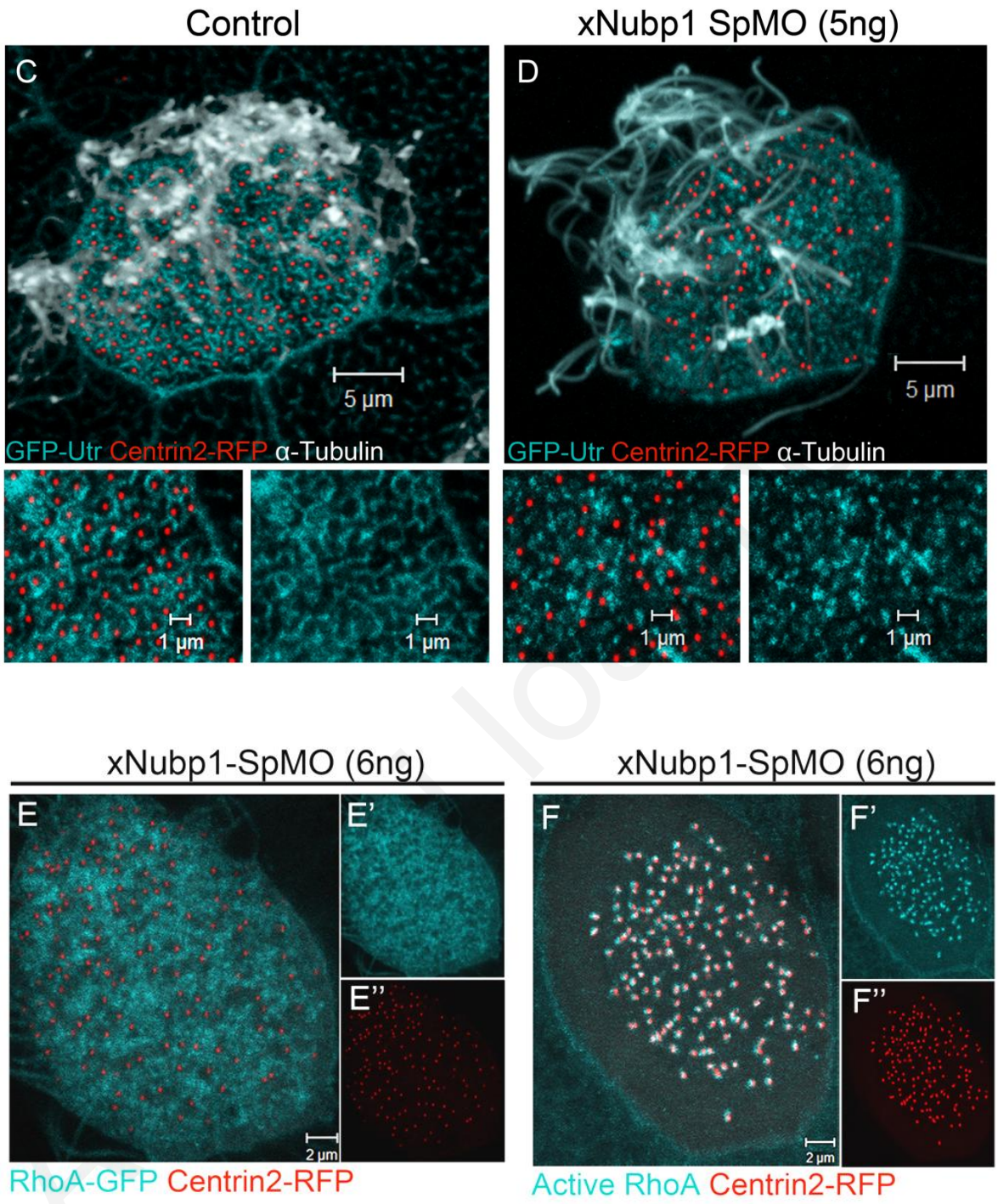

Figure 63. xNubp1 is required for apical actin organization but does not act through RhoA.

(A, A') Apical actin forms an organized enriched meshwork in control multi-ciliated epidermal cells. (A'') Roughly 0.4µm sub-apically a second pool of actin is present. (B, B') The apical actin in xNubp1 morphant multi-ciliated cells is not as enriched as in controls and appears punctate. Cortical actin in ciliated cells and apical actin in neighboring cells is unaffected. (B'') Sub-apical actin is almost entirely absent. (C) Apical actin (GFP-Utrophin) forms an organized enriched meshwork around

docked basal bodies (Centrin2-RFP) in control multi-ciliated cells. Cilia project from the apical surface. (D) Basal bodies in low-dose xnubp1 morphants have migrated and docked to the apical surface and extended cilia. (E) xNubp1 low dose morphants have apically enriched RhoA-GFP and the basal bodies have reached the apical surface (E'). (F) RhoA is active at the apical surface of low-dose morphant ciliated cells with apical basal bodies (F").

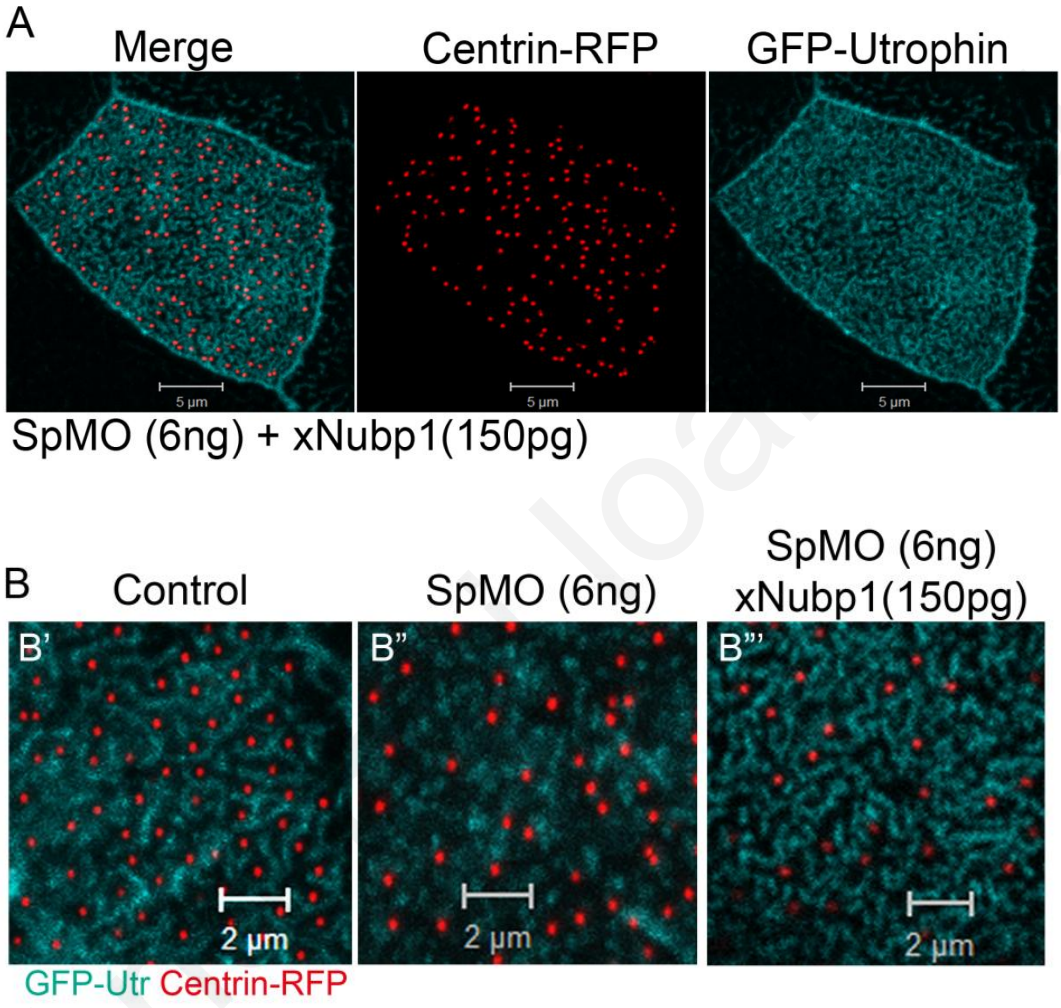

Figure 64. Apical actin phenotype is specific.

(A) Apical actin in rescued multi-ciliated epidermal cell has a more organized apical actin network. The basal bodies still show some spacing issues. (B) Portion of a control, morphant and rescued ciliated cell, showing that the apical actin in rescues resembles control apical actin.

4.6.7 Loss of xNubp1 leads to apical actin destabilization

Despite apical enrichment of RhoA in xNubp1 low-dose morphants, the apical actin failed to organize. Therefore, it is possible that the lack of organization in morphants is stemming from an inability of the cell to stabilize this network in the absence of xNubp1. The co-localization of xNubp1 with the apical actin network in controls is consistent with such a role for xNubp1 in ciliated cells. To examine this possibility, we decided to compare the dynamics of the apical actin network in control and morphant embryos using fluorescence recovery after photobleaching (FRAP) experiments. A small region of the apical actin network was bleached in each cell and the recovery was then monitored. As shown in Figure 65A-B and Figure 66A, the apical actin network in control cells did not fully recover within the acquisition period. In order for control ciliated cells to fully recover, they required roughly five to ten minutes (t1/2 = 86 seconds; data not shown), suggesting that this network is very stable with little polymerization/depolymerisation taking place after it is established. Non-ciliated neighboring cells on the other hand had a highly dynamic apical actin network, with fast recovery rates (data not shown). In low-dose xNubp1 morphants; the recovery rate of apical actin in ciliated cells was much faster (t1/2 of 17.4 seconds), showing full recovery within one minute (Figure 65C, D; Figure 66B). It should be noted that an accurate t1/2 was difficult to obtain as was the immobile fraction in both controls and morphants. In controls, full recovery was too long (at least five minutes and up to ten) and movement of the embryo during this period made accurate measurements very difficult. In low-dose morphants, the actin network was extremely dynamic, again making accurate measurements difficult since the network was remodelled by the time full recovery was reached.

To get a better look at actin dynamics in control and low-dose morphant cells, we also generated time-lapse sequences of adjacent ciliated and non ciliated cells. The apical actin network of control ciliated cells remained unchanged during the acquisition period, while the apical actin of the non-ciliated control cells was quite dynamic and was completely remodeled within the acquisition period (Movie 10). However, in xNubp1 low-dose morphants, the apical actin network of the ciliated cells was quite dynamic and was also completely remodeled within the time frame of the movie (Movie 11). These results suggest that despite apical enrichment and activation of RhoA in the absence of xNubp1, ciliated cells are unable

stabilize the apical actin network. The lack of a stable apical and sub-apical actin network explains both the loss of polarity and irregular spacing of basal bodies in xNubp1 morphants and suggests a role for xNubp1 in stabilizing the apical and sub-apical actin networks of multiciliated cells.

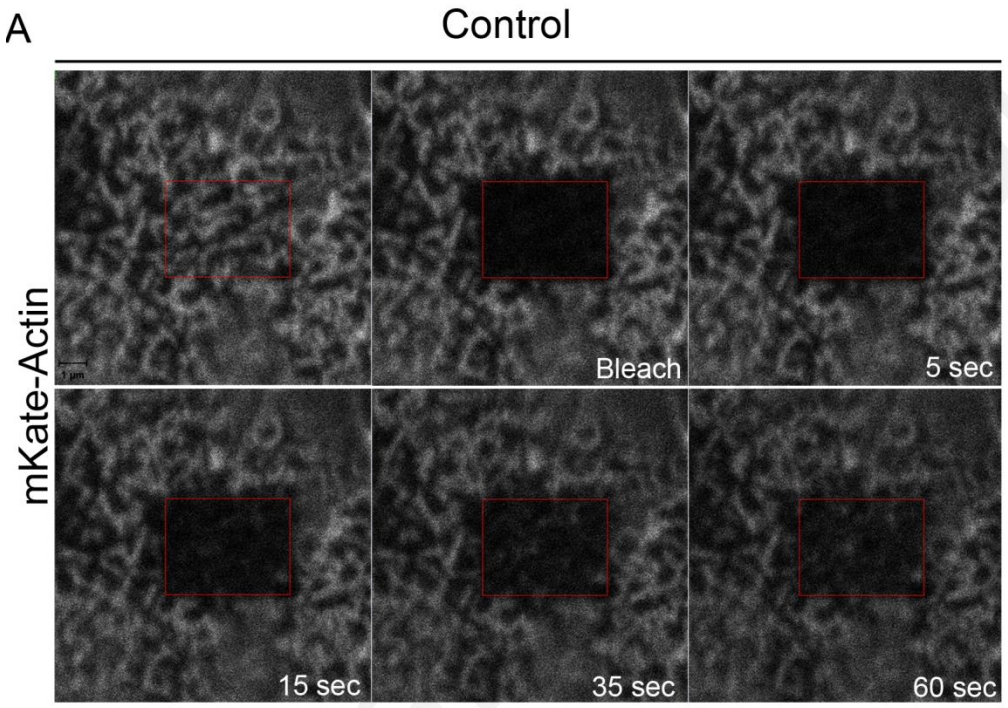

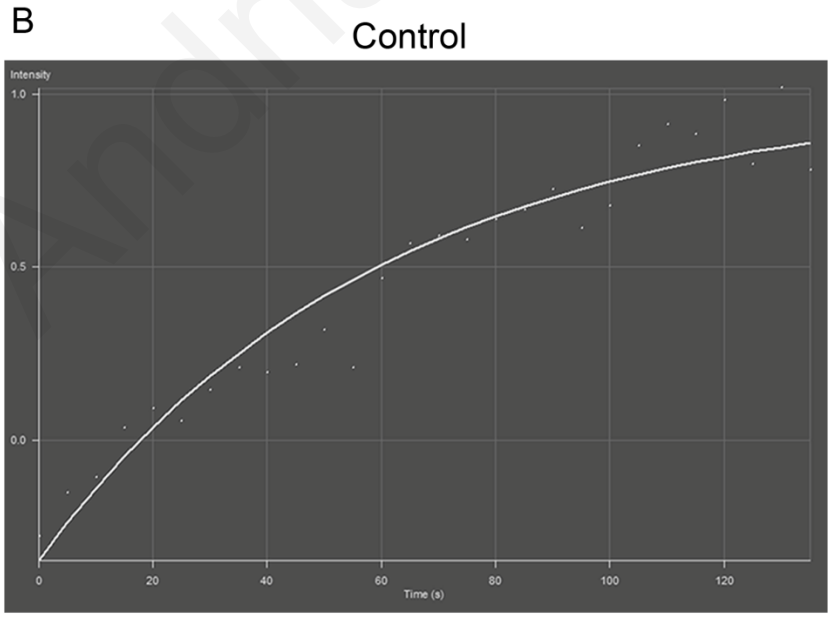

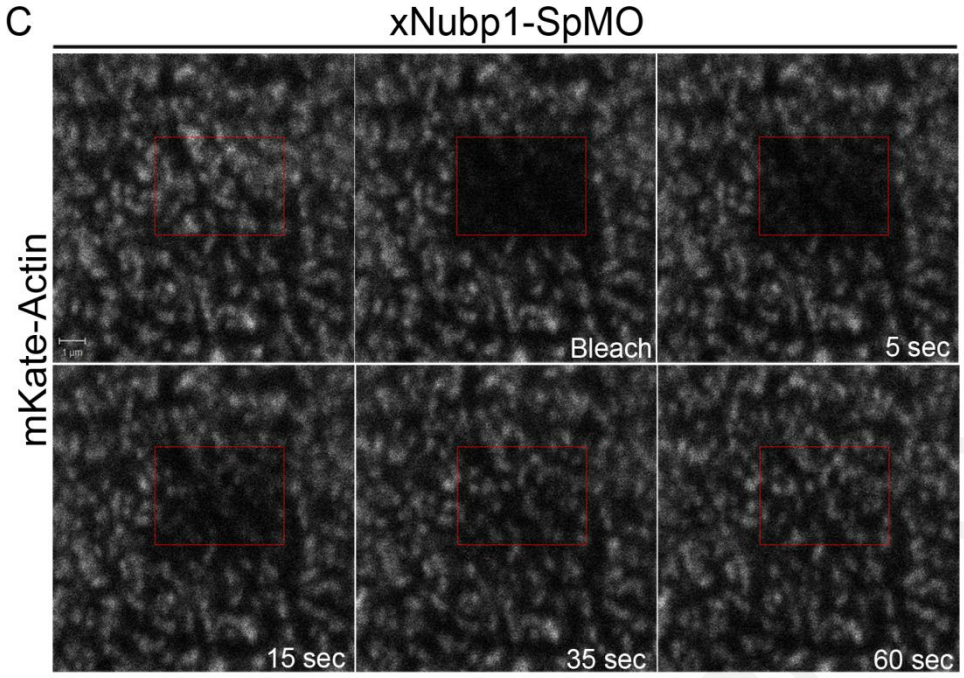

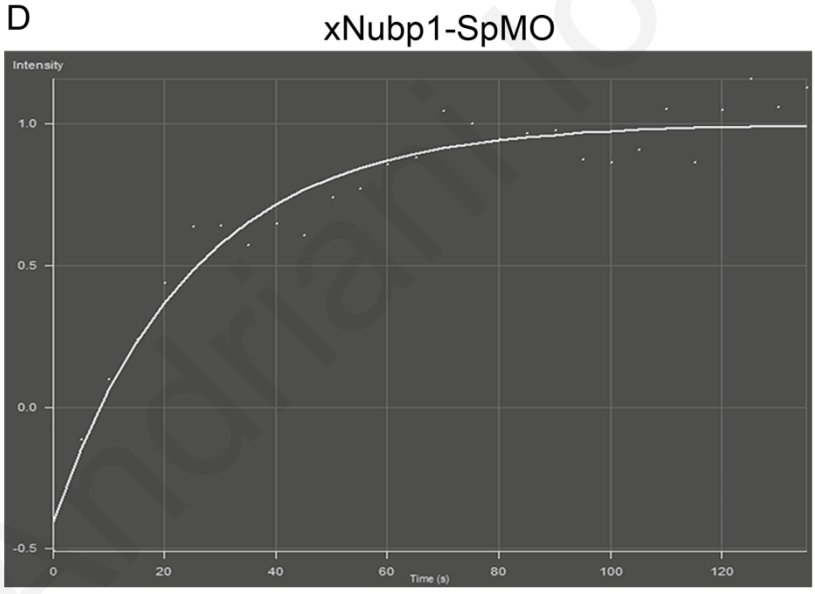

Figure 65. Loss of xNubp1 destabilizes the apical actin network of multiciliated cells.

(A-B) Fluorescence recovery after photobleaching (FRAP) experiment on a stage 29 embryo expressing mKate2-actin. (A) Bleached apical actin region of a control ciliated cell shows little recovery within one minute. (B) Normalized graph of FRAP experiment shows that cell continues recovering after two minutes (B). (C-D) FRAP experiment on stage 29 embryo injected with xNubp1-SpMO and mKate2-actin. (C) Bleached region of morphant ciliated cell recovers fully within one

minute. (D) Normalized graph of FRAP experiment depicting signal intensity of bleached region over time. Graph shows full recovery within the acquisition window.

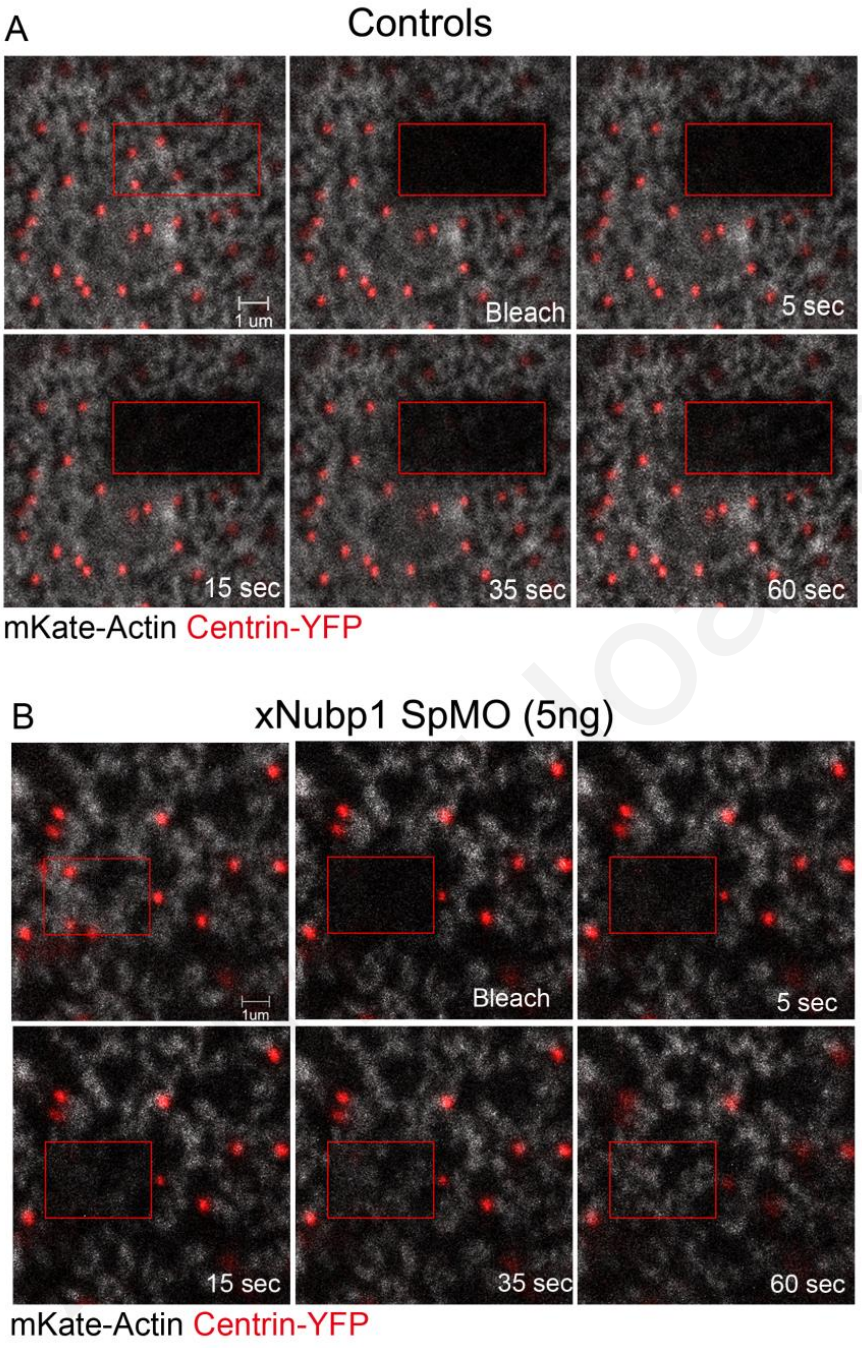

Figure 66. FRAP on cells expressing mKate-Actin and Centrin-YFP to verify the presence of docked basal bodies.

(A, B) FRAP experiments on ciliated cells expressing mKate-actin together with Centrin-YFP. (A) Bleached area in control ciliated cell does not recover within one minute. (B) the apical actin in an xNubp1 morphant ciliated cell with apical basal bodies recovers within one minute.

4.6.8 Live imaging of actin and basal bodies during ciliated cell intercalation

The above data suggest a role for xNubp1 in the generation/maintenance of the apical and sub-apical actin networks of ciliated cells. Since basal body transport is also dependent on acto-myosin (86, 103), these results raised the possibility that problems with basal body transport presented in xNubp1 morphants, may also be due to problems with actin organization and stability. Although the actin cytoskeleton is important for the apical migration of basal bodies, the precise mechanism through which actin is involved in this process is not clear. Therefore, in order to get a better understanding of this process, as well as to determine the temporal relationship between basal body migration and the actin cytoskeleton during ciliogenesis, we decided to image the intercalation of multiciliated epidermal cells live.

Stage 20-22 embryos expressing a GFP tagged form of the F-actin binding domain of Utrophin and Centrin2-RFP were imaged periodically during ciliated cell intercalation. Ciliated cells, which were just beginning to intercalate displayed a dense cortical actin network at their apical region (Figure 67A). Right below the surface of the epidermis, the actin-based protrusive activity of the cortical actin at the apical "neck" region of the intercalating cell was also visible (Figure 67B). At this stage, the basal bodies were observed deep within the cell (Figure 67A, B last panel). From the moment the apical surface of the intercalating cell became visible, apical actin enrichment was also present (Figure 67C'). Some basal bodies were observed at the apical surface from the onset of intercalation and as the diameter of the apical surface increased, basal bodies successively reached and docked at the apical surface. Three-dimensional reconstructions of optical sections taken during intercalation showed that once intercalation began, basal bodies started migrating towards the apical surface en masse (Figure 67C"). Most basal bodies reached the apical region of the cell even before the cell had fully intercalated and remained there until they docked. Although apical actin was enriched very early on during intercalation, it was composed of individual puncta and did not form an organized network. In general, the apical surface of the cell at this early intercalation stage and throughout the intercalation process displayed two distinct pools of actin. The punctate apical actin described above, and the cortical actin network which resembled a "lamellar ring" (Figure 67C' most visible at 37min). Once all the basal bodies

reached the apical surface and the cell had fully intercalated, the apical actin matured into an organized network and the cortical actin no longer resembled a lamellar ring.

Of special interest, was the observation that within the intercalating cell, there was a network of cytoplasmic actin filaments, which surrounded the basal bodies and extended towards the cell periphery, making connections to the cell cortex (Figure 67B last panel, Figure 69B' bottom panel). This internal actin pool surrounded the basal bodies and formed connections between them as they migrated toward the apical surface. When all the basal bodies reached the apical surface, the internal actin spread out just below the apical actin network and appeared to mature into the characteristic sub-apical actin network (Figure 68). These data reveal that apical actin is enriched from the onset of intercalation and becomes organized after the cell intercalates and basal bodies dock. In addition, it is clear that actin forms another network around the internal migrating basal bodies and actin cables project from the actin-basal body cluster toward the cell cortex. This actin network appears to connect the basal bodies, keeping them clustered and at the same time anchoring them to the cell cortex.

In light of these new observations regarding actin cytoskeleton and basal body migration during ciliogenesis, we decided to examine basal body migration and actin organization in xNubp1 low-dose morphants during intercalation. Like controls, xNubp1 morphants showed a dense cortical actin network at the apical surface of ciliated cells just beginning to intercalate (Figure 69A). Early apical actin enrichment with punctate F-actin foci appearing at the apical region of newly intercalating ciliated cells as well as a lamellar ring at the cell periphery was also seen in xNubp1 morphants (Figure 69B'). In fact, the apical actin between control and morphant cells was indistinguishable at this stage. However, the actin network surrounding the migrating basal bodies within the cytoplasm was substantially reduced with few actin cables reaching the cortex in xNubp1 morphants (Figure 69B'' bottom panel), suggesting that the basal body migration defect in morphants may be due to defects in the internal actin network. When the cells had fully intercalated, differences between the apical actin of controls and morphants also became visible, with the controls displaying mature network of apical actin (Figure 69C'), while in morphants this failed to organize and remained as punctate F-actin foci (Figure 69C"). We also observed that when pushed using a coverslip, the apical membrane of control ciliated cells would deform, caving in at places and rarely would the entire cell surface be parallel to the coverslip, presumably due to the apical actin networks stiffness and

resistance to the deforming force. However, in morphants the pressure would cause the apical membrane to become flat all along the coverslip (data not shown), suggesting loss of stiffness and ability to resist deformation. Collectively, these findings suggest that defects in basal body transport, docking and polarity in xNubp1 morphants are likely due to defects in the actin cytoskeleton and provide new insights regarding the mechanism of basal body transport and the involvement of the actin cytoskeleton in ciliogenesis.

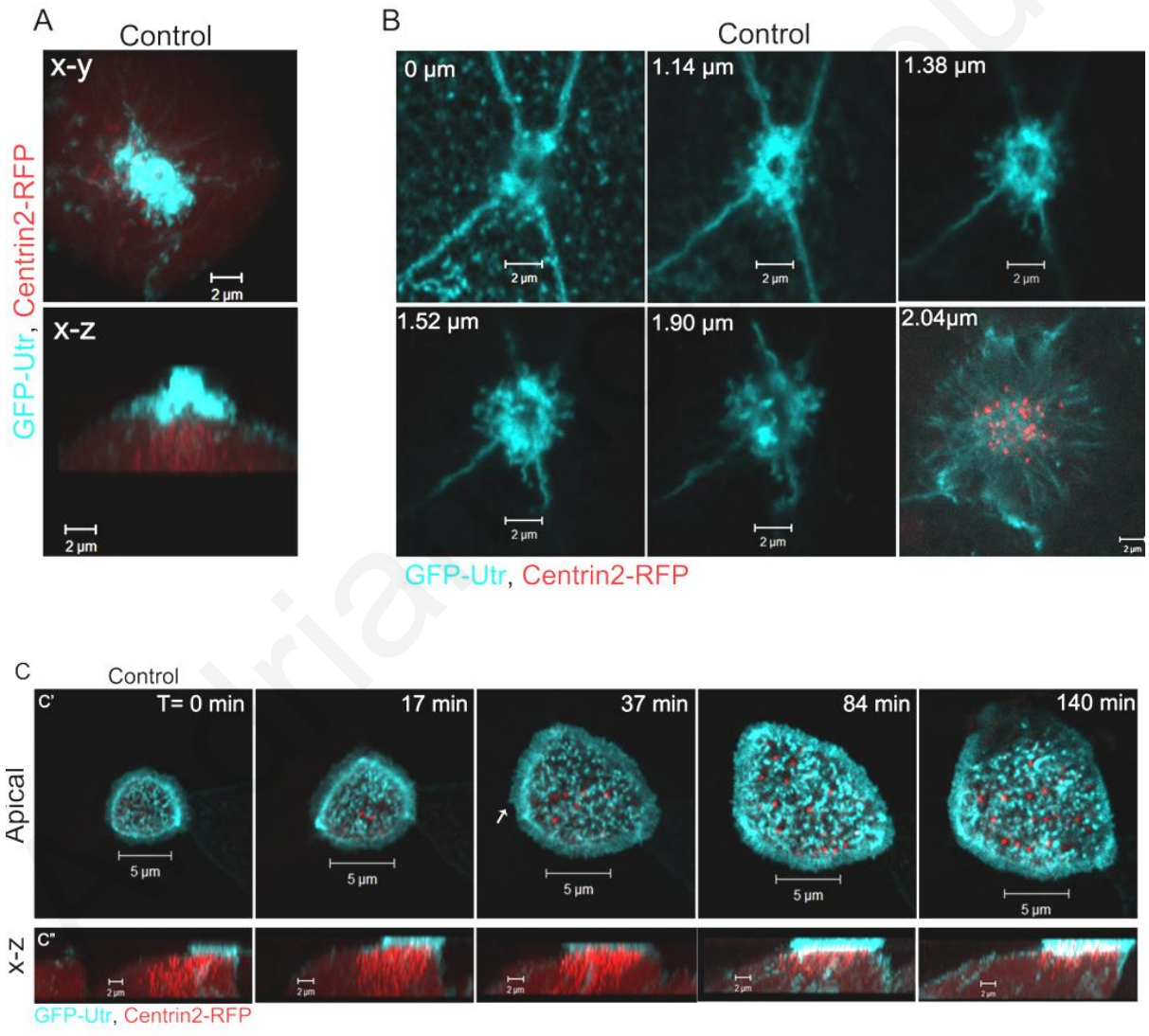

Figure 67. Actin Cytoskeleton during ciliated cell intercalation and basal body migration.

Live confocal imaging of stage 20-30 control and morphant embryos expressing GFP-Utr and Centrin2-RFP. (A) x-y and x-z projections of a stage 20 ciliated cell beginning the intercalation process, showing enrichment of F-actin at the apical region of the cell and internal basal bodies. (B)

Optical z-sections of a newly intercalating ciliated cell. Cortical actin based protrusions are visible at the apical region of the intercalating cells. Within the cell body (2.04μm), an internal actin network surrounds the migrating basal bodies and extends toward the cell cortex. (C') Time points of a stage 21-22 embryo showing the apical surface of an intercalating ciliated cell. The enriched apical actin pool is present from the beginning of intercalation (T=0min). As the cell intercalates, basal bodies sequentially dock at the apical surface. During intercalation we also observe a "lamellar ring" at the apical cortex of the intercalating cell (arrow in T=37min). (C") 3D reconstruction of intercalating cell showing the basal bodies are slowly migrating towards the apical surface. Even before the cell has fully intercalated, most of the basal bodies have reached the apical surface.

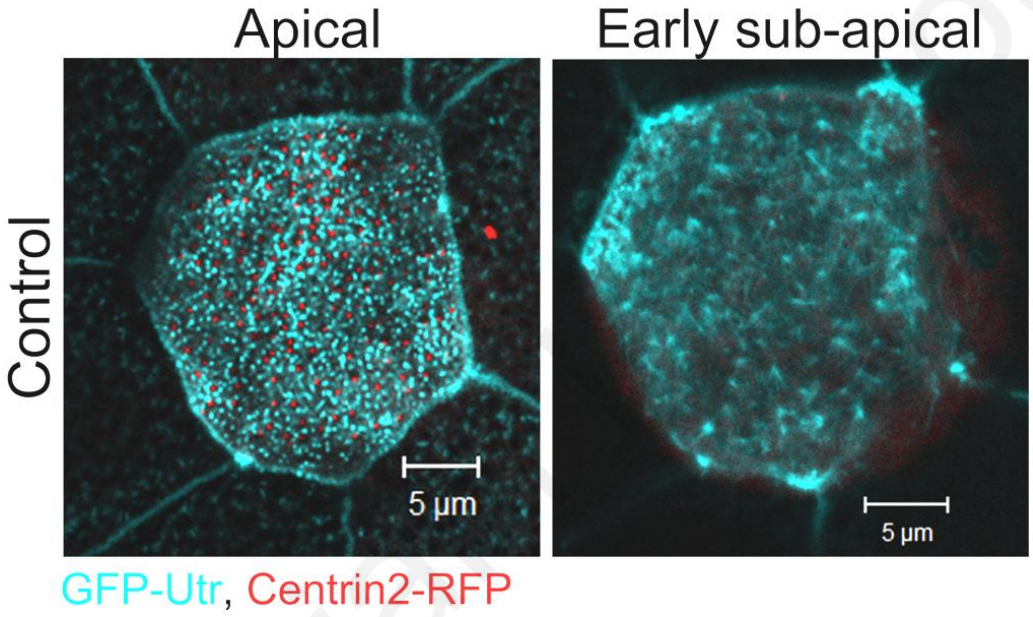

Figure 68. Internal actin forms subapical actin network

Intercalated ciliated cell of a stage 23 embryo. The apical actin pool is still punctate and has not yet organized into a network. The lamellar ring-like cortical actin structure is no longer present. The sub-apical actin network is just beginning to form.

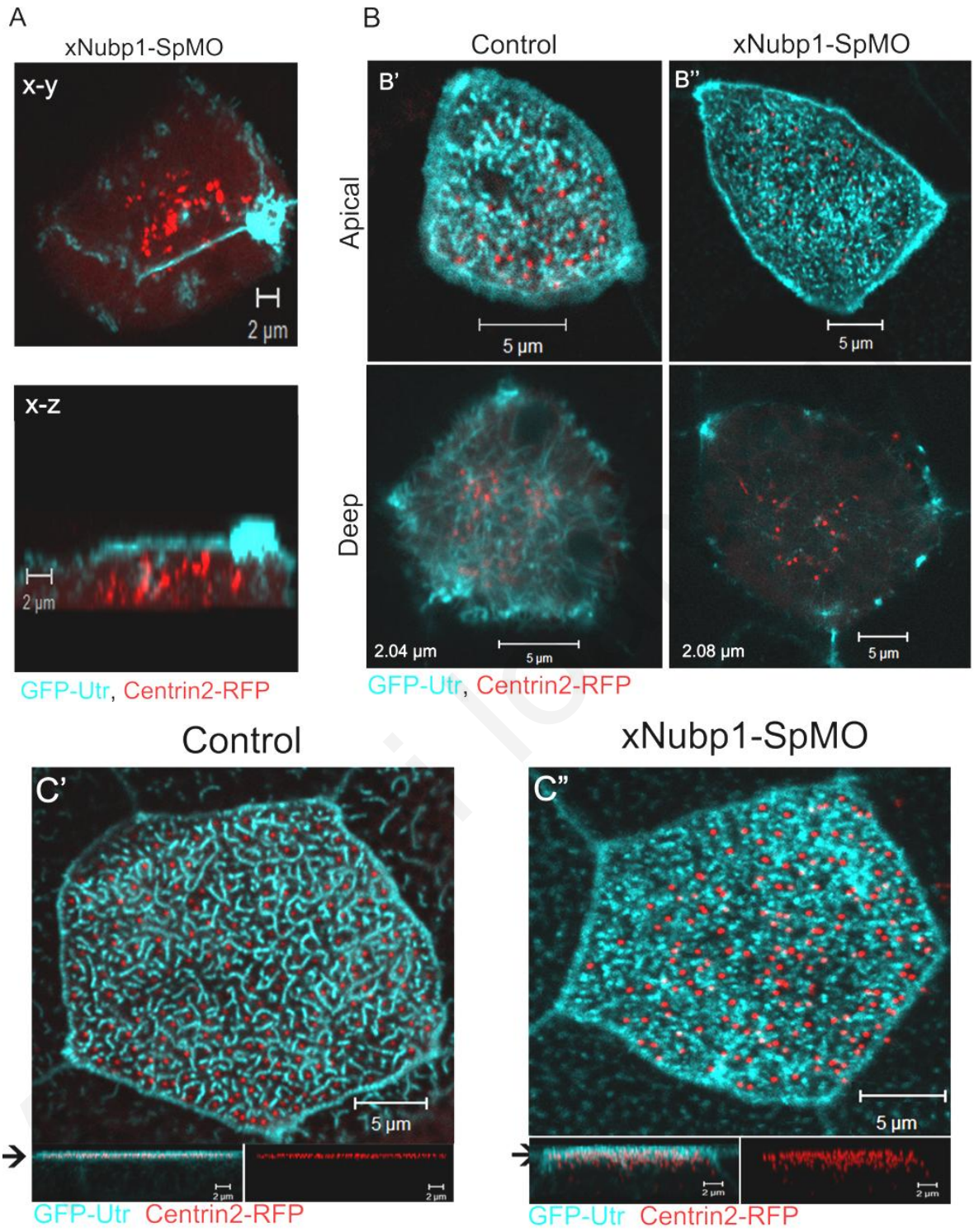

Figure 69. Actin and basal body migration in xNubp1 morphants during ciliated cell intercalation.

(A) x-y and x-z projections of a ciliated cell of a stage 20 xNubp1 low-dose morphant embryo beginning the intercalation process. (B) Intercalating control (B') and xNubp1morphant (B'') ciliated

cell. Deep sections show that the internal actin pool in morphants is severely reduced compared to controls. (C) Fully intercalated control (C') and xNubp1low-dose morphant cell (C") of stage 29-30 embryos. The apical actin pool in control ciliated cell has formed an organized network whereas the apical actin pool of the morphant ciliated cell remains unorganized and punctate. Bottom panels show x-z projections depicting apically localized basal bodies. Black arrows indicate apical surface.

4.7 xNubp1 interacts with xNubp2

Following the same procedure as that for xNubp1, we also cloned Xenopus Nubp2. The sequence of xNubp2 was also identical to that found on Xenbase (XB-Gene- 999233) (129). Since Nubp1 and Nubp2 have been shown to interact in yeast, mice and humans (2, 7, 17, 18), we wanted to examine whether the same held true in *Xenopus laevis.* We co-expressed tagged forms of xNubp1 and xNubp2 in Xenopus embryos and carried out co-immunoprecipitation. FLAG-xNubp2 was brought down by immunoprecipitation and blotted against HA. Our results showed that xNubp2 successfully brought down HA-xNubp1 (Figure 70), indicating that *Xenopus* Nubp proteins do indeed interact. IF on embryos expressing xNubp2 showed that like xNubp1, xNubp2 was also localized at distinct puncta along the ciliary axonemes (Figure 71). It will be interesting to examine the role of xNubp2 alone, and in association with xNubp1, during NTC and Ciliogenesis in more detail.

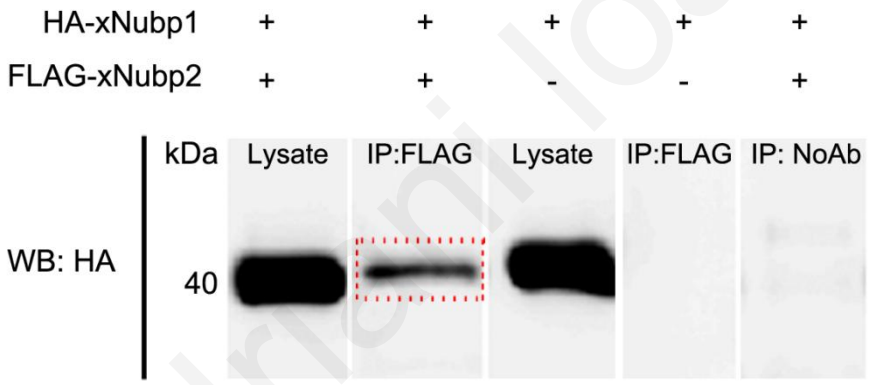

Figure 70. Xenopus Nubp1 and Nubp2 interact.

Western blots of immunoprecipitates (IP) or lysates from tailbud stage embryos expressing Ether HA-xNubp1 (300pg) alone or HA-xNubp1 and FLAG-xNubp2 (300 + 300 pg). xNubp2 brings down xNubp1 (red square). Immunoprecipitation of lysates expressing only HA-Nubp1 served as a negative control and show that xNubp1 is brought down specifically when expressed with FLAG-xNubp2.

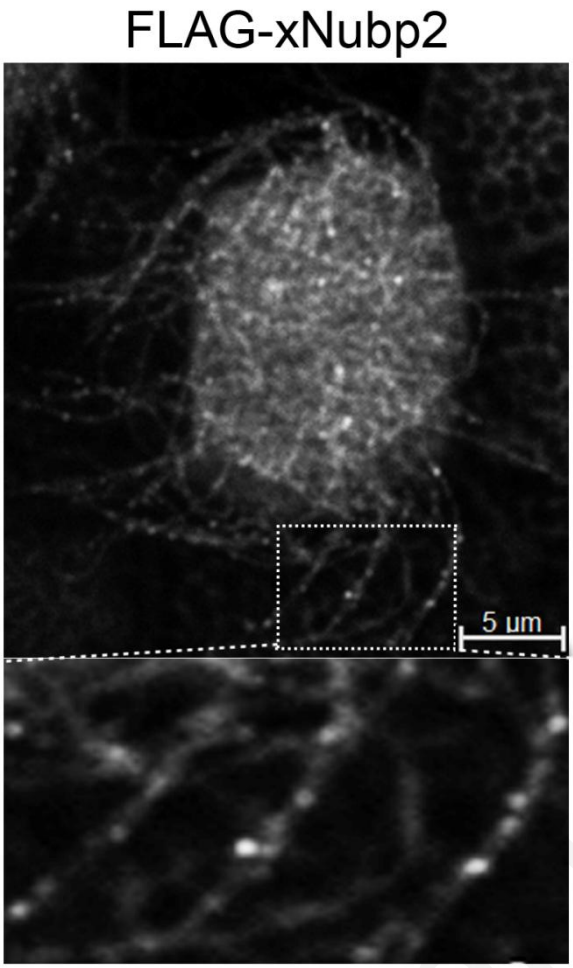

Figure 71. xNubp2 ciliary axoneme localization.

Whole mount IF on stage 31 FLAG-xNubp1 expressing embryos. xNubp1 can be seen at distinct puncta along the ciliary axoneme.

4.8 xNubp1 mutants

In order to gain a better understanding of which regions of the xNubp1 protein are involved in its specific function, we decided to make several mutant forms of xNubp1. The N-terminal cysteine rich domain of Nubp1 has been found to be essential for the iron-sulfur cluster transfer function of Nubp1 (4, 17). Using specifically designed primers (Section 2, Table 2) we created several tagged and untagged xNubp1 mutants. In the first mutant, the N-terminal cysteine rich region was absent (xNubp1- (-)NTerminus). The second Cys rich region mutant included only the N-terminal cysteine rich region (xNubp1- NTerminus-only).

The Walker A motif or P-loop has been shown to be the site for nucleotide binding in many of the P-loop NTPases (1, 2, 140). The conserved lysine in the GXXXXGK(T/S) consensus sequence is crucial for nucleotide binding (140). Mutation of the conserved lysine residue to glutamine (Q) has been shown to abolish ATP binding and render the protein non-functional (4, 13). In addition, in the bacterial homolog ParA, a mutation converting Glycine 16 (Glycine 68 in xNubp1) to Valine abolished ParA dimerization(13). Using site directed mutagenesis we created two xNubp1 P-loop mutants; the $xNubp1_{K72Q}$ and the $xNubp1_{G68V}$ mutants. The mutant constructs have been verified by sequencing and future work will include the testing of each mutant construct separately. We will examine the localization pattern of each construct to determine whether or not it differs from wild type (WT) xNubp1 localization, see whether overexpression of any of the mutant constructs leads to a developmental phenotype and examine mutant xNubp1 dimerization and xNubp1-xNubp2 interaction by co-IP. In addition, we also plan to examine the functionality of the mutants by trying to rescue the various types of phenotype observed by xNubp1 MO knockdown.

5 Discussion

The general aim of this project was the molecular cloning and functional characterization of *Xenopus laevis* Nubp1. Previous research has clearly shown that Nubp1 is indispensible for normal cellular function. However, in order to answer the important questions of how and why is it so important, it is not enough to look only *in vitro* at the cellular level; the role of Nubp1 *in vivo* at the level of the organism must also be examined. To date, only one *in vivo* study (21) has pointed to a potential role of Nubp1 in embryogenesis. By using *Xenopus laevis*, a model organism which has paved the way for the identification of transcription factors, gene regulatory networks and inter- and intracellular signaling pathways that control early development (141), we have been able to observe xNubp1 localization live using sophisticated imaging systems, manipulate xNubp1 expression levels by overexpression and loss-of-function experiments, and have slowly begun to piece together the puzzle of Nubp1 function *in vivo* during vertebrate development.

In this study we have shown that xNubp1 is expressed throughout early development; displaying elevated expression in neural tissues, localization at the mitotic spindle during cell division and to the apical actin network and along ciliary axonemes in multiciliated epidermal cells. Using three distinct morpholino oligonucleotides, which block either translation or splicing, we found that complete loss of Nubp1 is lethal, in agreement with a generalized role of Nubp1 for cell survival. However, at lower amounts of MO, embryos develop to tadpole stages, yet they display neurulation defects suggestive of problems with convergent extension and apical constriction movements during neural tube closure and sensory neuron axon elongation during neurogenesis. Surprisingly, we also found that xNubp1 is required for ciliogenesis in multiciliated epidermal cells and in GRP mono-ciliated cells. Specifically, xNubp1 appears to be important in two processes required for ciliogenesis, basal body transport to the apical surface and regulation of the actin networks which are necessary for basal body migration and docking. Finally, live confocal imaging of the actin cytoskeleton and basal bodies in intercalating multiciliated cells has allowed us to observe the formation of the apical actin network and also to image an internal pool of actin which surrounds the migrating basal bodies. By depleting xNubp1, we have shown that the internal actin network is indeed essential for basal body migration.

5.1 xNubp1 and neurulation

5.1.1 Neural tube closure

The formation of the neural tube from flat neuroepithelial cells is among the most critical steps in the development of the nervous system of vertebrates. If this process fails in any way, neural tube defects (NTDs), which are among the most common birth defects in humans, arise. The identification of genes involved in this process is key to our understanding of these genetic human birth defects. Our results have for the first time, implicated xNubp1 in the process of neural tube closure.

5.1.1.1 Convergent extension

During convergent extension, cells mediolaterally intercalate (48) in order to help close the neural tube and elongate the vertebrate body A-P axis (142). Acto-myosin in cells and tissues has a number of roles and is the driving force behind coordinated cell movements like convergent extension (143-145). In fact, brief exposure to actin destabilizing agents like latrunculin B during Xenopus gastrulation; despite a transient effect on actin stability, leads to long term defects that are strikingly similar to those described by inhibition of the PCP pathway, including shortened anterior posterior axis and curved backs (144, 146). It is possible that loss of xNubp1 leads to a similar destabilization of the acto-myosin cytoskeleton in that context, thus producing a PCP-like phenotype. It is also possible that xNubp1 is a member of a parallel pathway, which regulates the actin cytoskeleton, or is possibly a downstream effector of the PCP pathway. It would be interesting to examine the effects of xNubp1 down regulation on the cytoskeleton, protrusive activity and cell polarity in mesodermal and neural tissues undergoing convergent extension, in order to better understand the mechanism through which loss of xNubp1 inhibits mediolateral intercalation.

5.1.1.2 Apical constriction

The bending of the neural plate is driven largely by cell shape changes in neuroepithelial cells, which undergo apical constriction, and assume a wedge-shaped morphology (43, 147). Apical constriction is tightly linked with apicobasal cell elongation. The molecular control of apical constriction has partially been defined. Several actin binding proteins, their regulators and cell adhesion molecules have been implicated in the process and the long standing notion is that like convergent extension, apical constriction is too an acto-myosin based process (58, 148). In vertebrates, shroom3-mediated activation of ROCKs and myosin II are essential for driving apical constriction (62, 63, 66, 147). Shroom family proteins have all been associated with the actin cytoskeleton (68). Apicobasal elongation on the other hand, is a microtubule driven process and requires the function of certain proteins such as MID1 and MID2 (59, 69, 149). What is intriguing, is the fact that the actin-binding protein Shroom3 has also been shown to govern microtubule architecture in developing epithelia (68). These findings identify a mechanism by which actin and microtubules are coordinating to control certain cell shape changes during development.

Our data has shown that loss of xNubp1 leads to a failure of apical constriction and as a result, elevation of the neural folds is severely compromised. Apical actin fails to accumulate in xNubp1 morphant neuroepithelial cells, suggesting that xNubp1 is required for the formation and/or contraction of the apical actin network.

The use of Cytochalasin D to disrupt actin polymerization during neurulation has shown that actin is necessary for neural tube closure, however, medial hinge point formation remained unaffected (43, 61, 150). This led to the hypothesis that apical constriction in medial hinge point cells was actomyosin independent. However many questions regarding the molecular mechanisms of hinge point formation remain unanswered. Additionally, inhibition of microtubules polymerization prevents apical actin assembly and myosin light chain phosphorylation, thus blocking apical constriction (69, 151). We have shown that xNubp1 is also associated with microtubules. Therefore, it will be very interesting to examine whether loss of xNubp1 also affects microtubule dynamics in neuroepithelial cells undergoing apical constriction.

5.1.2 xNubp1 is involvement in RB sensory neuron axon elongation

During neuronal development, axons emerge from cell bodies, elongate and navigate to target regions guided by a range of environmental cues. During axonal pathfinding, the direction of nerve fiber extension is established by the growth cone at the tip of the growing axon which projects and retracts filopodial and lamelipodial cytoskeletal based membrane protrusions. A large number of guidance cues, receptors and downstream signalling cascades are involved in axon elongation and guidance. However, the ultimate effectors of outgrowth and guidance are the actin and microtubule cytoskeletons (152, 153). We have shown that xNubp1 knockdown leads to a decreased mechanosensory response by affecting the elongation and skin innervations of Rohon-Beard sensory neurons in the Xenopus embryo. We cannot say at present how the loss of xNubp1 affects RB peripheral axon elongation. In Zebrafish several molecules have been found to be involved in RB peripheral axon outgrowth and elongation. Previous studies have demonstrated that the LIM/homeodomain transcription factors Islet1 and Islet2 and the transmembrane co-receptor for class III semaphorins; PlexinA4 affected the outgrowth of peripheral axons (81, 154). Additionally, Semaphorin3d causes a repulsive effect on the growth cone of RB neuron axons which is essential for their exit from the spinal cord (80). xNubp1 may also somehow be acting at the level of the signaling molecules, or perhaps it is acting downstream at the level of the actin and/or microtubule cytoskeleton. Future experiments will focus on examining the actin and microtubule elements of the growth cones of peripheral axons of RB neurons live in xNubp1 morphants. Imaging the growing peripheral axons live will give us the opportunity get a better understanding of how xNubp1 affects this process.

5.2 xNubp1 and ciliogenesis

Understanding the mechanisms and players involved in ciliogenesis is crucial to better understanding the large class human diseases and syndromes, or "ciliopathies"(92, 93), that are associated with defects in ciliary function and development. Studies focusing on mucociliary epithelial development are hampered in mammals due to the inaccessibility of the tissues, especially during early stages of development (89). The *Xenopus* epidermis however, allows for the non-invasive study of the molecular mechanisms of ciliogenesis *in vivo*, thus making it and exceptional model for this type of work.

5.2.1 xNubp1 is required for proper ciliogenesis in multiciliated cells

Although the overall phenotype of xNubp1 knockdown would appear to be related to disruption of PCP signaling, we show that this is not the case. In addition to the long established role of PCP in polarized cell movements like convergent extension (48, 53, 55, 60, 142, 155, 156), there is now mounting evidence that PCP proteins are important for ciliogenesis (88, 93, 106). Core members of the PCP pathway like Dvl; have been clearly linked to both processes (46, 53, 88, 93, 106, 157). The initial evidence of such a connection came from various studies which first found a link between the ciliary protein Inversin and its homologs to known members of the PCP pathway (158-163). Interestingly, proteins such as Inturned and Fuzzy, which are crucial for planar cell polarity in Drosophila (164-167), were found to be more important for ciliogenesis in vertebrates. In Xenopus, knockdown of the PCP proteins Inturned and Fuzzy results in serious defects in ciliogenesis and Hedgehog signaling, but weak convergent extension defects (88, 106). Mutants in the mouse have now confirmed that both have limited roles in vertebrate PCP-mediated processes such as cochlear hair cell alignment and convergent extension, but are essential for ciliogenesis (168-171). Dvl´s role in cell polarity during convergent extension is well documented (51, 55, 142, 172), as is the Dvl-mediated activation of Rho (88, 139, 173). In Xenopus multi-ciliated cells, it has been shown that Dvl is essential for ciliogenesis and that it is required for Rho activation at the apical surface (88). However, unlike Inturned morphants, where apical enrichment of RhoA is lost (106) in multi-ciliated cells, RhoA localization is unaffected in Dvl morphants (88). In both cases though, effects on RhoA activation or localization at the apical membrane result in loss

of the apical actin network (88, 106). Interestingly, although the apical localization of such PCP members is affected in xNubp1 high-dose morphants, most likely due to basal body migration failure, in low-dose morphants, basal body migration to the apical surface is unaffected, and just like Dvl knockdown, RhoA apical enrichments is not affected. Unlike Dvl morphants however, xNubp1 low-dose morphants show normal RhoA activation and in fact, they display enriched apical actin compared to non-ciliated cells, further supporting the conclusion that neither RhoA localization nor its activation are affected by the loss of xNubp1. Even in the presence of apically localized active RhoA, basal body docking is still perturbed, basal body spacing becomes irregular, and drastic effects on the motility and synchronization of cilia are observed in xNubp1 low-dose morphants. In part, the phenotype may arise from rotational polarity issues but these are relatively mild. Unlike Dvl, which leads to randomization in terms of rotational polarity, in xNubp1 morphants rotational polarity is only affected at a distance since adjacent basal bodies maintain similar orientation. Overall, these data suggest that Nubp1 is not acting through Dvl and that despite their similarities, the phenotypes are quite distinct.

A possible explanation of the xNubp1 phenotype emerged when we noted that despite the fact that the apical actin of low-dose morphant ciliated cells was enriched, it appeared disorganized and failed to form an interconnected network. Time lapse sequences as well as FRAP experiments show that the apical actin network of control ciliated cells is extremely stable, with little remodeling taking place once it is set and basal bodies have docked. However, in xNubp1 morphants this network is highly dynamic, being remodeled within a very short time period. This suggests that xNubp1 may have a role in stabilizing the apical actin network in ciliated cells, and this is supported further by the finding that xNubp1 co-localizes with the apical actin cytoskeleton in these cells. However, the exact mechanism through which xNubp1 may be eliciting this effect remains to be elucidated.

Our results point to an additional role of xNubp1 in the transport of basal bodies rather than their maintenance at the apical surface. In high-dose morphants, we observed that nearly all the basal bodies remain deep within the cytoplasm where they form. There, they are associated with Dvl and active Rho and even form internal ciliary axonemes. This shows that apical docking is not required for cilia assembly, which is in agreement with data concerning the Dvl, Celsr2 and Celsr2+3 mutants (88, 138). The presence of active RhoA around these

internal basal bodies, once again shows that xNubp1 does not act through RhoA, and that the defect in basal body transport is consistent with a role of xNubp1 in the regulation of actin dynamics in relation to ciliogenesis.

5.2.2 xNubp1 is important for ciliogenesis on the gastrocoel roof plate

xNubp1 is also involved in ciliogenesis in motile mono-ciliated GRP cells. On the GRP, a single short cilium forms at the center of each cell and subsequently localizes to the posterior of the cell and lengthens in the process. These polarized GRP cilia beat in a circular motion to produce leftward flow which is important for left-right asymmetry (87, 132). PCP has also been linked to the posterior localization of these GRP cilia and for the establishment of L-R asymmetry (95). However, the mechanical process of cilia posteriorization is not completely understood. xNubp1 knockdown leads to a 2.8 fold decrease in cilia length. Some cilia also appear to be more centrally localized. These GRP cilia defects observed consequently lead to a disruption of L-R patterning, which is most likely caused by a decrease or loss of flow across the GRP. In light of the effect of xNubp1 knockdown on apical actin, the lack of polarization and reduced length of the cilia may be due to a mechanical perturbation of basal body posteriorization, since the basal body is able to dock and extend a cilium outward in xNubp1 morphant GRP cells.

5.2.3 Basal body migration and the actin cytoskeleton during multiciliated cell intercalation

During the past decade, a great deal of research has focused on uncovering the mechanisms of ciliogenesis. The mechanical basis of basal body apical migration in multi-ciliated cells and the importance of the actin cytoskeleton in this process however, have not yet been examined thoroughly. A study using the drug Cytochalasin D to perturb the actin cytoskeleton revealed that the migration and docking of basal bodies rely on an intact actin cytoskeleton (103). In Xenopus however, it is difficult to examine the role of the actin cytoskeleton in basal body migration using drugs which target the actin cytoskeleton due to the fact that basal body

migration is concomitant with cell intercalation, and therefore disrupting the actin cytoskeleton will lead to a failure of ciliated cells to intercalate.

Our data lead to several new key observations regarding the formation and importance of the actin cytoskeleton in multi-ciliated cells. We show that the apical actin network, which is a key structural component of multi-ciliated cells, initially manifests as punctate apical actin enrichment at the onset of cell intercalation, and is later organized into an interconnected network. In addition, we show that there is an internal actin network surrounding the migrating basal bodies, making connections between them and the cell cortex. We observed that this internal actin network was still present just below the apical actin once the basal bodies reached the surface. When the basal bodies dock and apical actin matured into a network, the internal actin network was replaced by the sub-apical actin pool. Although we did not directly observe this transition, it is likely that the internal actin network is remodeled into the sub-apical actin network. So it appears that both the apical and the internal actin networks found in ciliated cells are formed independently and are present at the onset of ciliated cell intercalation. In xNubp1 morphants at early stages of intercalation, the internal actin pool surrounding the basal bodies appears very weak and lacks organization compared to controls. The apical actin however is enriched early on and is comparable to controls, but fails to mature into a network later on. The failure of basal bodies to migrate in high-dose cells suggests that loss of xNubp1 at this stage has a preferential effect on the deep actin network without which basal body migration fails.

Overall, this study identifies novel roles for xNubp1 in ciliogenesis, neural tube closure and sensory neuron development. While we cannot say conclusively that the role of xNubp1 in all of these processes stems from its regulation of actin dynamics, from our data, it seems highly likely that this may be the case. It appears that there is a link between xNubp1 function and the actin and microtubule cytoskeleton. Although the role of xNubp1 in some processes, such as convergent extension are likely due to a regulation of the actin cytoskeleton, the function of xNubp1 in other processes like apical constriction and axon elongation/guidance, may be the regulation of both actin and microtubule networks. The precise mechanism through which xNubp1 functions in neurulation and ciliogenesis will be the focus of future studies and we believe that such studies will enable us to determine the exact mechanism by which xNubp1 functions during development.

6 References

1. Leipe, D.D., et al., *Classification and evolution of P-loop GTPases and related ATPases.* Journal of Molecular Biology, 2002. **317**(1): p. 41-72.
2. Hausmann, A., et al., *The eukaryotic P loop NTPase Nbp35: an essential component of the cytosolic and nuclear iron-sulfur protein assembly machinery.* Proc Natl Acad Sci U S A, 2005. **102**(9): p. 3266-71.
3. Walker, J.E., et al., *Distantly related sequences in the alpha- and beta-subunits of ATP synthase, myosin, kinases and other ATP-requiring enzymes and a common nucleotide binding fold.* EMBO J, 1982. **1**(8): p. 945-51.
4. Vitale, G., E. Fabre, and E.C. Hurt, *NBP35 encodes an essential and evolutionary conserved protein in Saccharomyces cerevisiae with homology to a superfamily of bacterial ATPases.* Gene, 1996. **178**(1-2): p. 97-106.
5. Shahrestanifar, M., et al., *Cloning of a human cDNA encoding a putative nucleotide-binding protein related to Escherichia coli MinD.* Gene, 1994. **147**(2): p. 281-285.
6. Nakashima, H., et al., *Two Novel Mouse Genes--Nubp2, Mapped to the t-Complex on Chromosome 17, and Nubp1, Mapped to Chromosome 16-- Establish a New Gene Family of Nucleotide-Binding Proteins in Eukaryotes.* Genomics, 1999. **60**(2): p. 152-160.
7. Christodoulou, A., et al., *Motor protein KIFC5A interacts with Nubp1 and Nubp2, and is implicated in the regulation of centrosome duplication.* J Cell Sci, 2006. **119**(Pt 10): p. 2035-47.
8. Koonin, E.V., *A Superfamily of ATPases with Diverse Functions Containing Either Classical or Deviant ATP-binding Motif.* Journal of Molecular Biology, 1993. **229**(4): p. 1165-1174.
9. Lutkenhaus, J. and M. Sundaramoorthy, *MinD and role of the deviant Walker A motif, dimerization and membrane binding in oscillation.* Mol Microbiol, 2003. **48**(2): p. 295-303.
10. Cabeen, M.T. and C. Jacobs-Wagner, *The bacterial cytoskeleton.* Annu Rev Genet, 2010. **44**: p. 365-92.
11. Shih, Y.L. and L. Rothfield, *The bacterial cytoskeleton.* Microbiol Mol Biol Rev, 2006. **70**(3): p. 729-54.

12. Sakai, N., et al., *The Three-Dimensional Structure of Septum Site-Determining Protein MinD from Pyrococcus horikoshii OT3 in Complex with Mg-ADP*. Structure (London, England : 1993), 2001. **9**(9): p. 817-826.
13. Ptacin, J.L., et al., *A spindle-like apparatus guides bacterial chromosome segregation.* Nat Cell Biol, 2010. **12**(8): p. 791-8.
14. Boyd, J.M., et al., *Archaeal ApbC/Nbp35 homologs function as iron-sulfur cluster carrier proteins.* J Bacteriol, 2009. **191**(5): p. 1490-7.
15. Boyd, J.M., J.L. Sondelski, and D.M. Downs, *Bacterial ApbC protein has two biochemical activities that are required for in vivo function.* J Biol Chem, 2009. **284**(1): p. 110-8.
16. Okuno, T., H. Yamabayashi, and K. Kogure, *Comparison of intracellular localization of Nubp1 and Nubp2 using GFP fusion proteins.* Mol Biol Rep, 2010. **37**(3): p. 1165-8.
17. Netz, D.J.A., et al., *The Cfd1-Nbp35 complex acts as a scaffold for iron-sulfur protein assembly in the yeast cytosol.* Nat Chem Biol, 2007. **3**(5): p. 278-286.
18. Stehling, O., et al., *Human Nbp35 is essential for both cytosolic iron-sulfur protein assembly and iron homeostasis.* Mol Cell Biol, 2008. **28**(17): p. 5517-28.
19. Larkin, M.A., et al., *Clustal W and Clustal X version 2.0.* Bioinformatics, 2007. **23**(21): p. 2947-8.
20. Lill, R. and U. Muhlenhoff, *Iron-sulfur-protein biogenesis in eukaryotes.* Trends Biochem Sci, 2005. **30**(3): p. 133-41.
21. Schnatwinkel, C. and L. Niswander, *Nubp1 Is Required for Lung Branching Morphogenesis and Distal Progenitor Cell Survival in Mice.* PLoS One, 2012. **7**(9): p. e44871.
22. Beck, C.W. and J.M. Slack, *An amphibian with ambition: a new role for Xenopus in the 21st century.* Genome Biol, 2001. **2**(10): p. REVIEWS1029.
23. Sive, H.L., R.M. Grainger, and M.H. Richard, *Early Development of Xenopus laevis: A Laboratory Manual*. 2010, Cold Spring Harbor: Cold Spring Harbor Laboratory Press. 338.
24. Harland, R. and H. Weintraub, *Translation of mRNA injected into Xenopus oocytes is specifically inhibited by antisense RNA.* J Cell Biol, 1985. **101**(3): p. 1094-9.

25. Baker, C., et al., *Effects of oligo sequence and chemistry on the efficiency of oligodeoxyribonucleotide-mediated mRNA cleavage.* Nucleic Acids Res, 1990. **18**(12): p. 3537-43.
26. Heasman, J., *Morpholino oligos: making sense of antisense?* Dev Biol, 2002. **243**(2): p. 209-14.
27. Heasman, J., M. Kofron, and C. Wylie, *Beta-catenin signaling activity dissected in the early Xenopus embryo: a novel antisense approach.* Dev Biol, 2000. **222**(1): p. 124-34.
28. Kenwrick, S., E. Amaya, and N. Papalopulu, *Pilot morpholino screen in Xenopus tropicalis identifies a novel gene involved in head development.* Dev Dyn, 2004. **229**(2): p. 289-99.
29. Nutt, S.L., et al., *Comparison of morpholino based translational inhibition during the development of Xenopus laevis and Xenopus tropicalis.* Genesis, 2001. **30**(3): p. 110-3.
30. Staveley, B.E. *Xenopus Development*. 2007 [cited 2013 April 5]; Available from: www.mun.ca/biology/desmid/brian/BIOL3530/DB_01/DBNHist.html.
31. Smith JC, W.J., *Patterning the Xenopus embryo*. Patterning in Vertebrate Development, ed. Tickle C. 2003: Oxford University Press.
32. Gilbert, S., *Developmental Biology*. Eighth Edition ed. 2006, Sunderland, Massachusetts USA Sinauer Associates, Inc., Puplishers.
33. Gerhart, J., et al., *Cortical rotation of the Xenopus egg: consequences for the anteroposterior pattern of embryonic dorsal development.* Development, 1989. **107**(Supplement): p. 37-51.
34. Heasman, J., *Patterning the early Xenopus embryo.* Development, 2006. **133**(7): p. 1205-1217.
35. Winklbauer, R., *Cell adhesion in amphibian gastrulation.* Int Rev Cell Mol Biol, 2009. **278**: p. 215-75.
36. Leptin, M., *Gastrulation movements: the logic and the nuts and bolts.* Dev Cell, 2005. **8**(3): p. 305-20.
37. Harland, R. and J. Gerhart, *FORMATION AND FUNCTION OF SPEMANN'S ORGANIZER.* Annual Review of Cell and Developmental Biology, 1997. **13**(1): p. 611-667.

38. Niehrs, C., *Wnt Signals and Antagonists: The Molecular Nature of Spemann's Head Organizer*, in *The Vertebrate Organizer*, H. Grunz, Editor. 2004, Springer Berlin Heidelberg. p. 127-149.
39. De Robertis, E.M., et al., *The establishment of Spemann's organizer and patterning of the vertebrate embryo.* Nat Rev Genet, 2000. **1**(3): p. 171-81.
40. Gammill, L.S. and M. Bronner-Fraser, *Neural crest specification: migrating into genomics.* Nat Rev Neurosci, 2003. **4**(10): p. 795-805.
41. Zohn, I.E., C.R. Chesnutt, and L. Niswander, *Cell polarity pathways converge and extend to regulate neural tube closure.* Trends Cell Biol, 2003. **13**(9): p. 451-4.
42. Colas, J.F. and G.C. Schoenwolf, *Towards a cellular and molecular understanding of neurulation.* Dev Dyn, 2001. **221**(2): p. 117-45.
43. Schoenwolf, G.C. and J.L. Smith, *Mechanisms of neurulation: traditional viewpoint and recent advances.* Development, 1990. **109**(2): p. 243-270.
44. Liu, W., et al., *MIM regulates vertebrate neural tube closure.* Development, 2011. **138**(10): p. 2035-47.
45. Wallingford, J.B., et al., *The continuing challenge of understanding, preventing, and treating neural tube defects.* Science, 2013. **339**(6123): p. 1222002.
46. Wallingford, J.B., *Planar cell polarity, ciliogenesis and neural tube defects.* Hum Mol Genet, 2006. **15 Spec No 2**: p. R227-34.
47. Wallingford, J.B., *Neural tube closure and neural tube defects: studies in animal models reveal known knowns and known unknowns.* Am J Med Genet C Semin Med Genet, 2005. **135C**(1): p. 59-68.
48. Wallingford, J.B., S.E. Fraser, and R.M. Harland, *Convergent extension: the molecular control of polarized cell movement during embryonic development.* Dev Cell, 2002. **2**(6): p. 695-706.
49. Keller, R.E., et al., *The function and mechanism of convergent extension during gastrulation of Xenopus laevis.* J Embryol Exp Morphol, 1985. **89 Suppl**: p. 185-209.
50. Shih, J. and R. Keller, *Cell motility driving mediolateral intercalation in explants of Xenopus laevis.* Development, 1992. **116**(4): p. 901-14.
51. Wallingford, J.B. and R.M. Harland, *Xenopus Dishevelled signaling regulates both neural and mesodermal convergent extension: parallel forces elongating the body axis.* Development, 2001. **128**(13): p. 2581-92.

52. Shih, J. and R. Keller, *Patterns of cell motility in the organizer and dorsal mesoderm of Xenopus laevis.* Development, 1992. **116**(4): p. 915-30.
53. Tada, M. and J.C. Smith, *Xwnt11 is a target of Xenopus Brachyury: regulation of gastrulation movements via Dishevelled, but not through the canonical Wnt pathway.* Development, 2000. **127**(10): p. 2227-38.
54. Smith, J.C., et al., *Xwnt11 and the regulation of gastrulation in Xenopus.* Philos Trans R Soc Lond B Biol Sci, 2000. **355**(1399): p. 923-30.
55. Wallingford, J.B., et al., *Dishevelled controls cell polarity during Xenopus gastrulation.* Nature, 2000. **405**(6782): p. 81-5.
56. Strutt, D., *Frizzled signalling and cell polarisation in Drosophila and vertebrates.* Development, 2003. **130**(19): p. 4501-4513.
57. Davidson, L.A. and R.E. Keller, *Neural tube closure in Xenopus laevis involves medial migration, directed protrusive activity, cell intercalation and convergent extension.* Development, 1999. **126**(20): p. 4547-56.
58. Sawyer, J.M., et al., *Apical constriction: a cell shape change that can drive morphogenesis.* Dev Biol, 2010. **341**(1): p. 5-19.
59. Handel, M.A. and L.E. Roth, *Cell shape and morphology of the neural tube: implications for microtubule function.* Dev Biol, 1971. **25**(1): p. 78-95.
60. Ybot-Gonzalez, P., et al., *Convergent extension, planar-cell-polarity signalling and initiation of mouse neural tube closure.* Development, 2007. **134**(4): p. 789-99.
61. Schoenwolf, G.C., D. Folsom, and A. Moe, *A reexamination of the role of microfilaments in neurulation in the chick embryo.* Anat Rec, 1988. **220**(1): p. 87-102.
62. Nishimura, T. and M. Takeichi, *Shroom3-mediated recruitment of Rho kinases to the apical cell junctions regulates epithelial and neuroepithelial planar remodeling.* Development, 2008. **135**(8): p. 1493-502.
63. Haigo, S.L., et al., *Shroom induces apical constriction and is required for hingepoint formation during neural tube closure.* Curr Biol, 2003. **13**(24): p. 2125-37.
64. Morita, H., et al., *Nectin-2 and N-cadherin interact through extracellular domains and induce apical accumulation of F-actin in apical constriction of Xenopus neural tube morphogenesis.* Development, 2010. **137**(8): p. 1315-25.
65. Copp, A.J., N.D. Greene, and J.N. Murdoch, *The genetic basis of mammalian neurulation.* Nat Rev Genet, 2003. **4**(10): p. 784-93.

66. Hildebrand, J.D., *Shroom regulates epithelial cell shape via the apical positioning of an actomyosin network.* J Cell Sci, 2005. **118**(Pt 22): p. 5191-203.
67. Roffers-Agarwal, J., et al., *Enabled (Xena) regulates neural plate morphogenesis, apical constriction, and cellular adhesion required for neural tube closure in Xenopus.* Dev Biol, 2008. **314**(2): p. 393-403.
68. Lee, C., H.M. Scherr, and J.B. Wallingford, *Shroom family proteins regulate gamma-tubulin distribution and microtubule architecture during epithelial cell shape change.* Development, 2007. **134**(7): p. 1431-41.
69. Suzuki, M., et al., *MID1 and MID2 are required for Xenopus neural tube closure through the regulation of microtubule organization.* Development, 2010. **137**(14): p. 2329-39.
70. Wisconsin, U.o. *Gastrulation*. 2002 August 2002; Available from: http://worms.zoology.wisc.edu/urchins/SUgast_primary3.html.
71. Altmann, C.R. and A.H. Brivanlou, *Neural patterning in the vertebrate embryo.* Int Rev Cytol, 2001. **203**: p. 447-82.
72. Dessaud, E., A.P. McMahon, and J. Briscoe, *Pattern formation in the vertebrate neural tube: a sonic hedgehog morphogen-regulated transcriptional network.* Development, 2008. **135**(15): p. 2489-503.
73. Mayor, R. and M.J. Aybar, *Induction and development of neural crest in Xenopus laevis.* Cell Tissue Res, 2001. **305**(2): p. 203-9.
74. Wilson, P.A., et al., *Concentration-dependent patterning of the Xenopus ectoderm by BMP4 and its signal transducer Smad1.* Development, 1997. **124**(16): p. 3177-84.
75. Reversade, B., et al., *Depletion of Bmp2, Bmp4, Bmp7 and Spemann organizer signals induces massive brain formation in Xenopus embryos.* Development, 2005. **132**(15): p. 3381-92.
76. Park, B.-Y., et al., *Xaml1/Runx1 is required for the specification of Rohon-Beard sensory neurons in Xenopus.* Developmental Biology, 2012. **362**(1): p. 65-75.
77. Garcia-Morales, C., et al., *Frizzled-10 promotes sensory neuron development in Xenopus embryos.* Dev Biol, 2009. **335**(1): p. 143-55.
78. Taylor, J.S. and A. Roberts, *The early development of the primary sensory neurones in an amphibian embryo: a scanning electron microscope study.* J Embryol Exp Morphol, 1983. **75**: p. 49-66.

79. Roberts, A. and D. Smyth, *The development of a dual touch sensory system in embryos of the amphibianXenopus laevis.* Journal of comparative physiology, 1974. **88**(1): p. 31-42.
80. Liu, Y. and M.C. Halloran, *Central and peripheral axon branches from one neuron are guided differentially by Semaphorin3D and transient axonal glycoprotein-1.* J Neurosci, 2005. **25**(45): p. 10556-63.
81. Tanaka, H., et al., *Islet1 selectively promotes peripheral axon outgrowth in Rohon-Beard primary sensory neurons.* Developmental Dynamics, 2011. **240**(1): p. 9-22.
82. Lamborghini, J.E., *Disappearance of Rohon-Beard neurons from the spinal cord of larval Xenopus laevis.* J Comp Neurol, 1987. **264**(1): p. 47-55.
83. Roberts, A., *Early functional organization of spinal neurons in developing lower vertebrates.* Brain Res Bull, 2000. **53**(5): p. 585-93.
84. Robles, E. and T.M. Gomez, *Focal adhesion kinase signaling at sites of integrin-mediated adhesion controls axon pathfinding.* Nat Neurosci, 2006. **9**(10): p. 1274-83.
85. Davenport, J.R. and B.K. Yoder, *An incredible decade for the primary cilium: a look at a once-forgotten organelle.* American Journal of Physiology - Renal Physiology, 2005. **289**(6): p. F1159-F1169.
86. Dawe, H.R., H. Farr, and K. Gull, *Centriole/basal body morphogenesis and migration during ciliogenesis in animal cells.* J Cell Sci, 2007. **120**(Pt 1): p. 7-15.
87. Blum, M., et al., *Xenopus, an ideal model system to study vertebrate left-right asymmetry.* Dev Dyn, 2009. **238**(6): p. 1215-25.
88. Park, T.J., et al., *Dishevelled controls apical docking and planar polarization of basal bodies in ciliated epithelial cells.* Nat Genet, 2008. **40**(7): p. 871-9.
89. Hayes, J.M., et al., *Identification of novel ciliogenesis factors using a new in vivo model for mucociliary epithelial development.* Dev Biol, 2007. **312**(1): p. 115-30.
90. Steinman, R.M., *An electron microscopic study of ciliogenesis in developing epidermis and trachea in the embryo of Xenopus laevis.* Am J Anat, 1968. **122**(1): p. 19-55.
91. Hagiwara, H., et al., *Ciliogenesis and ciliary abnormalities.* Med Electron Microsc, 2000. **33**(3): p. 109-14.
92. Baker, K. and P.L. Beales, *Making sense of cilia in disease: the human ciliopathies.* Am J Med Genet C Semin Med Genet, 2009. **151C**(4): p. 281-95.

93. Wallingford, J.B. and B. Mitchell, *Strange as it may seem: the many links between Wnt signaling, planar cell polarity, and cilia.* Genes Dev, 2011. **25**(3): p. 201-13.
94. McGrath, J. and M. Brueckner, *Cilia are at the heart of vertebrate left–right asymmetry.* Current Opinion in Genetics & Development, 2003. **13**(4): p. 385-392.
95. Antic, D., et al., *Planar cell polarity enables posterior localization of nodal cilia and left-right axis determination during mouse and Xenopus embryogenesis.* PLoS One, 2010. **5**(2): p. e8999.
96. Stubbs, J.L., et al., *The forkhead protein Foxj1 specifies node-like cilia in Xenopus and zebrafish embryos.* Nat Genet, 2008. **40**(12): p. 1454-60.
97. deCathelineau, A., B. Short, and R. Williams, *The American Society for Cell Biology, 48th Annual Meeting San Francisco, CA, December 13-17, 2008.* J Cell Biol, 2009. **184**(2): p. 190-5.
98. Phillips, D. *Cilia in the lung bronchiole*. 2012 [cited 2013 April 5]; Available from: http://www.anatomybox.com/tag/cilia/.
99. Werner, M.E. and B.J. Mitchell, *Understanding ciliated epithelia: the power of Xenopus.* Genesis, 2012. **50**(3): p. 176-85.
100. Sorokin, S.P., *Reconstructions of centriole formation and ciliogenesis in mammalian lungs.* J Cell Sci, 1968. **3**(2): p. 207-30.
101. Kobayashi, T. and B.D. Dynlacht, *Regulating the transition from centriole to basal body.* J Cell Biol, 2011. **193**(3): p. 435-44.
102. Anderson, R.G. and R.M. Brenner, *The formation of basal bodies (centrioles) in the Rhesus monkey oviduct.* J Cell Biol, 1971. **50**(1): p. 10-34.
103. Boisvieux-Ulrich, E., M.C. Laine, and D. Sandoz, *Cytochalasin D inhibits basal body migration and ciliary elongation in quail oviduct epithelium.* Cell Tissue Res, 1990. **259**(3): p. 443-54.
104. Klotz, C., et al., *Myosin at the apical pole of ciliated epithelial cells as revealed by a monoclonal antibody.* The Journal of Cell Biology, 1986. **103**(2): p. 613-619.
105. Lemullois, M., C. Klotz, and D. Sandoz, *Immunocytochemical localization of myosin during ciliogenesis of quail oviduct.* Eur J Cell Biol, 1987. **43**(3): p. 429-37.

106. Park, T.J., S.L. Haigo, and J.B. Wallingford, *Ciliogenesis defects in embryos lacking inturned or fuzzy function are associated with failure of planar cell polarity and Hedgehog signaling.* Nat Genet, 2006. **38**(3): p. 303-11.
107. Pan, J., et al., *RhoA-mediated apical actin enrichment is required for ciliogenesis and promoted by Foxj1.* J Cell Sci, 2007. **120**(Pt 11): p. 1868-76.
108. Huang, T., et al., *Foxj1 is required for apical localization of ezrin in airway epithelial cells.* J Cell Sci, 2003. **116**(Pt 24): p. 4935-45.
109. Gomperts, B.N., X. Gong-Cooper, and B.P. Hackett, *Foxj1 regulates basal body anchoring to the cytoskeleton of ciliated pulmonary epithelial cells.* J Cell Sci, 2004. **117**(Pt 8): p. 1329-37.
110. Werner, M.E., et al., *Actin and microtubules drive differential aspects of planar cell polarity in multiciliated cells.* J Cell Biol, 2011. **195**(1): p. 19-26.
111. Hall, A., *Rho GTPases and the actin cytoskeleton.* Science, 1998. **279**(5350): p. 509-14.
112. Mitchell, B., et al., *The PCP pathway instructs the planar orientation of ciliated cells in the Xenopus larval skin.* Curr Biol, 2009. **19**(11): p. 924-9.
113. Boisvieux-Ulrich, E., M.C. Laine, and D. Sandoz, *The orientation of ciliary basal bodies in quail oviduct is related to the ciliary beating cycle commencement.* Biol Cell, 1985. **55**(1-2): p. 147-50.
114. Frisch, D. and A.I. Farbman, *Development of order during ciliogenesis.* Anat Rec, 1968. **162**(2): p. 221-32.
115. Mitchell, B., et al., *A positive feedback mechanism governs the polarity and motion of motile cilia.* Nature, 2007. **447**(7140): p. 97-101.
116. Frisch, D. and A.I. Farbman, *Development of order during ciliogenesis.* The Anatomical Record, 1968. **162**(2): p. 221-231.
117. Boisvieux-Ulrich, E., D. Sandoz, and J.-P. Allart, *Determination of ciliary polarity precedes differentiation in the epithelial cells of quail oviduct.* Biology of the Cell, 1991. **72**(1–2): p. 3-14.
118. Hagiwara, H., N. Ohwada, and K. Takata, *Cell Biology of Normal and Abnormal Ciliogenesis in the Ciliated Epithelium*, in *International Review of Cytology*. 2004, Academic Press. p. 101-141.

119. Godfrey, E.W. and G.E. Sanders, *Effect of water hardness on oocyte quality and embryo development in the African clawed frog (Xenopus laevis).* Comp Med, 2004. **54**(2): p. 170-5.
120. Sive, H.L., R.M. Grainger, and R.M. Harland, *Early Development of Xenopus laevis. A Laboratory Manual*. first ed ed, ed. S. Curtis. 2000, Cold Spring Harbor, New York.: Cold Spring Harbor Laboratory Press, New York.
121. Hilken, G., J. Dimigen, and F. Iglauer, *Growth of Xenopus laevis under different laboratory rearing conditions.* Lab Anim, 1995. **29**(2): p. 152-62.
122. Ubbels, G.A., et al., *Evidence for a functional role of the cytoskeleton in determination of the dorsoventral axis in Xenopus laevis eggs.* J Embryol Exp Morphol, 1983. **77**: p. 15-37.
123. Smith, W.C. and R.M. Harland, *Injected Xwnt-8 RNA acts early in Xenopus embryos to promote formation of a vegetal dorsalizing center.* Cell, 1991. **67**(4): p. 753-65.
124. Nieuwkoop, P.D.a.F., J., *Normal Table of Xenopus laevis (Daudin).* 1 ed. 1994, New York: Garland.
125. Piccolo, S., et al., *Dorsoventral patterning in Xenopus: inhibition of ventral signals by direct binding of chordin to BMP-4.* Cell, 1996. **86**: p. 589-98.
126. Smith, W.C. and R.M. Harland, *Injected Xwnt-8 RNA acts early in Xenopus embryos to promote formation of a vegetal dorsalizing center.* Cell, 1991. **67**(4): p. 753-765.
127. Kragtorp, K.A. and J.R. Miller, *Regulation of somitogenesis by Ena/VASP proteins and FAK during Xenopus development.* Development., 2006. **133**: p. 685-95.
128. Hellsten, U., et al., *Accelerated gene evolution and subfunctionalization in the pseudotetraploid frog Xenopus laevis.* BMC Biol, 2007. **5**: p. 31.
129. Bowes, J.B., et al., *Xenbase: gene expression and improved integration.* Nucleic Acids Res, 2010. **38**(Database issue): p. D607-12.
130. Glotzer, M., *The 3Ms of central spindle assembly: microtubules, motors and MAPs.* Nat Rev Mol Cell Biol, 2009. **10**(1): p. 9-20.
131. Roberts, A. and B.P. Hayes, *The Anatomy and Function of 'Free' Nerve Endings in an Amphibian Skin Sensory System.* Proceedings of the Royal Society of London. Series B. Biological Sciences, 1977. **196**(1125): p. 415-429.
132. Schweickert, A., et al., *Cilia-Driven Leftward Flow Determines Laterality in Xenopus.* Current biology : CB, 2007. **17**(1): p. 60-66.

133. Chung, M.-I., et al., *RFX2 is broadly required for ciliogenesis during vertebrate development.* Developmental Biology, 2012. **363**(1): p. 155-165.
134. Sandoz, D., et al., *Organization and functions of cytoskeleton in metazoan ciliated cells.* Biol Cell, 1988. **63**(2): p. 183-93.
135. Gordon, R.E., *Three-dimensional organization of microtubules and microfilaments of the basal body apparatus of ciliated respiratory epithelium.* Cell Motil, 1982. **2**(4): p. 385-91.
136. Boisvieux-Ulrich, E., M.C. Laine, and D. Sandoz, *In vitro effects of colchicine and nocodazole on ciliogenesis in quail oviduct.* Biol Cell, 1989. **67**(1): p. 67-79.
137. Nishikawa, S., J. Hirata, and F. Sasaki, *Fate of ciliated epidermal cells during early development of <i>Xenopus laevis</i> using whole-mount immunostaining with an antibody against chondroitin 6-sulfate proteoglycan and anti-tubulin: transdifferentiation or metaplasia of amphibian epidermis.* Histochemistry and Cell Biology, 1992. **98**(6): p. 355-358.
138. Tissir, F., et al., *Lack of cadherins Celsr2 and Celsr3 impairs ependymal ciliogenesis, leading to fatal hydrocephalus.* Nat Neurosci, 2010. **13**(6): p. 700-7.
139. Habas, R., Y. Kato, and X. He, *Wnt/Frizzled activation of Rho regulates vertebrate gastrulation and requires a novel Formin homology protein Daam1.* Cell, 2001. **107**(7): p. 843-54.
140. Ramakrishnan, C., V.S. Dani, and T. Ramasarma, *A conformational analysis of Walker motif A [GXXXXGKT (S)] in nucleotide-binding and other proteins.* Protein Eng, 2002. **15**(10): p. 783-98.
141. Blitz, I.L., G. Andelfinger, and M.E. Horb, *Germ layers to organs: using Xenopus to study "later" development.* Semin Cell Dev Biol, 2006. **17**(1): p. 133-45.
142. Wallingford, J.B. and R.M. Harland, *Neural tube closure requires Dishevelled-dependent convergent extension of the midline.* Development, 2002. **129**(24): p. 5815-25.
143. Skoglund, P., et al., *Convergence and extension at gastrulation require a myosin IIB-dependent cortical actin network.* Development, 2008. **135**(14): p. 2435-44.
144. Kim, H.Y. and L.A. Davidson, *Punctuated actin contractions during convergent extension and their permissive regulation by the non-canonical Wnt-signaling pathway.* J Cell Sci, 2011. **124**(Pt 4): p. 635-46.

145. Rauzi, M. and P.F. Lenne, *Cortical forces in cell shape changes and tissue morphogenesis.* Curr Top Dev Biol, 2011. **95**: p. 93-144.
146. Zhou, J., H.Y. Kim, and L.A. Davidson, *Actomyosin stiffens the vertebrate embryo during crucial stages of elongation and neural tube closure.* Development, 2009. **136**(4): p. 677-88.
147. Rolo, A., P. Skoglund, and R. Keller, *Morphogenetic movements driving neural tube closure in Xenopus require myosin IIB.* Developmental Biology, 2009. **327**(2): p. 327-338.
148. Lee, J.-Y. and R.M. Harland, *Actomyosin contractility and microtubules drive apical constriction in Xenopus bottle cells.* Developmental Biology, 2007. **311**(1): p. 40-52.
149. BURNSIDE, B., *Microtubules and Microfilaments in Amphibian Neurulation.* American Zoologist, 1973. **13**(4): p. 989-1006.
150. Ybot-Gonzalez, P. and A.J. Copp, *Bending of the neural plate during mouse spinal neurulation is independent of actin microfilaments.* Developmental Dynamics, 1999. **215**(3): p. 273-283.
151. Rogers, S.L., et al., *Drosophila RhoGEF2 Associates with Microtubule Plus Ends in an EB1-Dependent Manner.* Current biology : CB, 2004. **14**(20): p. 1827-1833.
152. Dent, E.W., S.L. Gupton, and F.B. Gertler, *The growth cone cytoskeleton in axon outgrowth and guidance.* Cold Spring Harb Perspect Biol, 2011. **3**(3).
153. Challacombe, J.F., D.M. Snow, and P.C. Letourneau, *Role of the cytoskeleton in growth cone motility and axonal elongation.* Seminars in Neuroscience, 1996. **8**(2): p. 67-80.
154. Miyashita, T., et al., *PlexinA4 is necessary as a downstream target of Islet2 to mediate Slit signaling for promotion of sensory axon branching.* Development, 2004. **131**(15): p. 3705-3715.
155. Sokol, S.Y., *Analysis of Dishevelled signalling pathways during Xenopus development.* Curr Biol, 1996. **6**(11): p. 1456-67.
156. Heisenberg, C.P., et al., *Silberblick/Wnt11 mediates convergent extension movements during zebrafish gastrulation.* Nature, 2000. **405**(6782): p. 76-81.
157. Wallingford, J.B., *Planar cell polarity signaling, cilia and polarized ciliary beating.* Curr Opin Cell Biol, 2010. **22**(5): p. 597-604.

158. Ross, A.J., et al., *Disruption of Bardet-Biedl syndrome ciliary proteins perturbs planar cell polarity in vertebrates.* Nat Genet, 2005. **37**(10): p. 1135-40.

159. Otto, E.A., et al., *Mutations in INVS encoding inversin cause nephronophthisis type 2, linking renal cystic disease to the function of primary cilia and left-right axis determination.* Nat Genet, 2003. **34**(4): p. 413-20.

160. Simons, M., et al., *Inversin, the gene product mutated in nephronophthisis type II, functions as a molecular switch between Wnt signaling pathways.* Nat Genet, 2005. **37**(5): p. 537-43.

161. Das, G., et al., *Diego interacts with Prickle and Strabismus/Van Gogh to localize planar cell polarity complexes.* Development, 2004. **131**(18): p. 4467-76.

162. Jenny, A., et al., *Diego and Prickle regulate Frizzled planar cell polarity signalling by competing for Dishevelled binding.* Nat Cell Biol, 2005. **7**(7): p. 691-7.

163. Feiguin, F., et al., *The ankyrin repeat protein Diego mediates Frizzled-dependent planar polarization.* Dev Cell, 2001. **1**(1): p. 93-101.

164. Park, W.J., et al., *The Drosophila tissue polarity gene inturned acts cell autonomously and encodes a novel protein.* Development, 1996. **122**(3): p. 961-9.

165. Lee, H. and P.N. Adler, *The function of the frizzled pathway in the Drosophila wing is dependent on inturned and fuzzy.* Genetics, 2002. **160**(4): p. 1535-47.

166. Adler, P.N., C. Zhu, and D. Stone, *Inturned localizes to the proximal side of wing cells under the instruction of upstream planar polarity proteins.* Curr Biol, 2004. **14**(22): p. 2046-51.

167. Collier, S. and D. Gubb, *Drosophila tissue polarity requires the cell-autonomous activity of the fuzzy gene, which encodes a novel transmembrane protein.* Development, 1997. **124**(20): p. 4029-37.

168. Gray, R.S., et al., *The planar cell polarity effector Fuz is essential for targeted membrane trafficking, ciliogenesis and mouse embryonic development.* Nat Cell Biol, 2009. **11**(10): p. 1225-32.

169. Heydeck, W. and A. Liu, *PCP effector proteins inturned and fuzzy play nonredundant roles in the patterning but not convergent extension of mammalian neural tube.* Dev Dyn, 2011. **240**(8): p. 1938-48.

170. Heydeck, W., H. Zeng, and A. Liu, *Planar cell polarity effector gene Fuzzy regulates cilia formation and Hedgehog signal transduction in mouse.* Dev Dyn, 2009. **238**(12): p. 3035-42.
171. Zeng, H., A.N. Hoover, and A. Liu, *PCP effector gene Inturned is an important regulator of cilia formation and embryonic development in mammals.* Dev Biol, 2010. **339**(2): p. 418-28.
172. Wallingford, J.B. and R. Habas, *The developmental biology of Dishevelled: an enigmatic protein governing cell fate and cell polarity.* Development, 2005. **132**(20): p. 4421-36.
173. Schlessinger, K., A. Hall, and N. Tolwinski, *Wnt signaling pathways meet Rho GTPases.* Genes Dev, 2009. **23**(3): p. 265-77.

7 Annexes

7.1 Abbreviations

Ab: Antibody

A-P: Anterior -Posterior

ATPase: Adenosine TriPhosphatase

A-V: Animal-Vegetal

BB:BA: Benzyl Benzoate Benzyl Alcohol

CE: Convergent extension

CNS: Central Nervous System

CoMO: Control Morpholino

DV: Dorsal-Ventral

FRAP: Fluorescence Recovery After Photobleaching

GRP: Gastrocoel Roof Plate

IF: Immunofluorescence

IP: Immunoprecipitation

MAB: Maleic Acid Buffer

MBT: Mid Blastula Transition

MIP: Maximum Intensity Projection

MOs: Morpholino Oligos

MMR: Marc's Modified Ringers

mRNA: messenger RNA

MTOC: Microtubule Organizing Center

NPB: Neural Plate Border

NTC: Neural Tube Closure

NTDs: Neural Tube Defects

Nubp1: Nucleotide Binding Protein 1

Nubp2: Nucleotide Binding Protein 2

NTPase: Nucleoside TriPhosphatase

PFA: Paraformaldehyde

P-loop: Phosphate loop

PCP: Planar Cell Polarity

RNAi: RNA interference

RB: Rohon-Beard

RT: Room Temperature

RT-PCR: Reverse Transcription Polymerase Chain Reaction

TEO: Triethanolamine

WT: Wild Type

WISH: Whole-Mount *In Situ* Hybridization

7.2 Buffers, solutions and media

10X Marc's Modified Ringers (MMR)
0.1M NaCl
1.8mM KCl
2.0 mM $CaCl_2$
1mM $MgCl_2$
5mM HEPES
Adjust pH to 7.4 with NaOH.
Add Gentamycin gel to a final concentration of 0.05mg/mL.
Before use, dilute 1:10 (1x MMR).

1x PBDT
1x PBS
0.5% Triton-x
1% DMSO

IF Block and Ab incubation solution
1x PBDT
10% Normal goat or donkey serum

1x MEMFA (100ml)
0.1M MOPS (pH 7.4)
2mM EGTA
1mM $MgSO_4$
3.7% Formaldehyde
Prepare 10X solution of MEM and autoclave (turns yellow)
Before use add formaldehyde and dilute 1:10 (1x MEMFA)

4% Ficoll (100ml)
4g Ficoll dissolved in 0.33xMMR

2%Cysteine (100ml)
2g L-Cysteine diluted in 0.33 MMR, adjust pH to 7.8

1x PBTw
1x PBS
0.1% Tween-20

1x Alkaline Phosphatase Buffer (1L)
100ml TRIS (pH 9.5, 1M)
20ml NaCl (5M)
50ml MgCl2 (1M)
Adjust pH to 9.5, add DDW to 1L

1x Maleic Acid Buffer (MAB, 1L)

11.61g Maleic Acid (100mM)
30ml NaCl (5M)
800ml DDW
Adjust pH to 7.5, add DDW to 1l, autoclave

Hybridization solution (1L)
10g Boehringer Block
500ml Formamide
250ml SSC (20x)
Heat to 65°C for 1 hour
120ml DDW
100ml Torula RNA (10mg/ml in DDW, dissolved at 65°C; filtered)
2ml Heparin (50mg/ml in 1xSSC pH 7)
5ml Tween20 (20%)
10ml CHAPS (10%)
10ml EDTA (0.5M)
Filter (5μm)

2% WISH Antibody Blocking Buffer
10g BMB block in 1xMAB (100ml final)
Autoclave
2ml 10xBMB in 1xMAB (final 10ml)

Bleaching solution (50ml)
1.25ml 20xSSC
2.5 ml formamide
2 ml 30% peroxide
45 ml distilled water

MK's modified lysis buffer
50 mM Tris HCl pH8
150 mM NaCl
1 mM EGTA
0.5% NP-40
0.5% Triton-X100
5mM NaF
5mM phosphatase inhibitors (Na_3VO_4)
1mM protease inhibitors (PMSF, Sigma)

7.3 Publications

7.3.1 Journal articles

1. ***Andriani Ioannou,** Niovi Santama and Paris A. Skourides. *Xenopus laevis* Nucleotide binding protein 1 (xNubp1) is important for convergent extension movements and controls ciliogenesis via regulation of the actin cytoskeleton. *Developmental Biology* (In Press).
2. ***Andriani Ioannou**, Iro Eleftheriou, Andrea Lubatti, Anna Charalambous and Paris A. Skourides. High Resolution Whole Mount *in Situ* Hybridization Using Quantum Dot Nanocrystals. *Journal of Biomedicine and Biotechnology* Volume 2012 (January 2012), Article ID 627602.
3. *Eleonora Muro, Alexandra Fragola, Thomas Pons, Nicolas Lequeux, **Andriani Ioannou**, Paris Skourides and Benoit Dubertret. Comparing Intracellular Stability and Targeting of Sulfobetaine Quantum Dots with Other Surface Chemistries in Live Cells. *Small.* February 2012, DOI: 10.1002/smll.201101787)
4. *Muro E, Vermeulen P, **Ioannou A**, Skourides P, Dubertret B, Fragola A, Loriette V. Single-shot optical sectioning using two-color probes in HiLo fluorescence microscopy. *Biophysical Journal* (Volume 100, Issue 11, 8 June 2011, Pages 2810-2819)
5. Maria Andreou, Iro Eleftheriou, Anna Eleftheriou, Neophytos Christodoulou, Ioanna Antoniadou, **Andriani Ioannou**, Nicoletta Petridou, Panayiota Stylianou, Paris Skourides. Evaluation of total toxicity of effluents from several waste water treatment stations and major water sources of Cyprus using *Xenopus laevis* as a model organism. *Journal of Environmental Research and Development* Vol. 6 No. 1, July-September 2011

7.3.2 Book contributions

- ****In Situ* Hybridization Methods, Methods and protocols, Springer Protocols, Neuromethods, Springer Science +Business Media. Chapter on: Multiplexed fluorescent in situ hybridization using Quantum Dots Nanocrystals in Xenopus. **Andriani Ioannou**, Iro Eleftheriou, Anna Charalambous and Paris A. Skourides (Submitted).

***Copy of papers and book chapter attached**

7.4 Conferences/Special Courses

- **March 2013 -** Joint Meetings of the British Societies for Cell Biology and Developmental Biology, Spring Conference. **Poster**: A. Ioannou, N. Santama and P.Skourides. *Xenopus laevis* Nucleotide binding protein 1 (xNubp1) is important for convergent extension movements and controls ciliogenesis via regulation of the actin cytoskeleton.
- **November 2012 -** University of Cyprus – Workshop for the presentation of Post-graduate research. **Talk:** Role of *Xenopus laevis* Nucleotide Binding protein 1 (xNubp1) in motile ciliogenesis
- **September 2012 -** 14th International Xenopus Conference. **Poster:** A. Ioannou, N. Santama and P.Skourides. Molecular cloning and functional characterization of *Xenopus laevis* Nucleotide Binding protein 1 (xNubp1).
- **August 2012 -** Santa Cruz Developmental biology meeting 2012. **Poster:** A. Ioannou, N. Santama and P.Skourides. Molecular cloning and functional characterization of *Xenopus laevis* Nucleotide Binding protein 1 (xNubp1).
- **April 2011 -** Accepted (with partial scholarship) into and attended the Cold Spring Harbor Cell & Developmental Biology of Xenopus **Course**. Received the Xenopus One 2011 Cold Spring Harbor Photo Competition **First prize** for the best science photo taken during the course.
- **April 2010 -** Nanotheranostics: Fabrication and Safety Concerns International **Poster:** A. Ioannou, B. Dubertret and P.Skourides. Biocompatible Sulfobetaine Zwitterionic Quantum Dots for *in vivo* Imaging.